Earth, Environmental and Life Sciences
Princetonlaan 6
3584 CB Utrecht
P.O. Box 80015
3508 TA Utrecht
The Netherlands

www.tno.nl

T +31 88 866 42 56
F +31 88 866 44 75

TNO report

TNO 2017 R10166 | Final report

Conceptual diagenetic models for cementation in Rotliegend sandstones

Date	25 April 2017
Author(s)	Tanya Goldberg, Marielle Koenen, Susanne Nelskamp, Vincent Vandeweijer
Copy no	
No. of copies	
Number of pages	125 (incl. appendices)
Number of appendices	
Sponsor	TOTAL E&P Nederland EBN RVO (public subsidy provider via reference TEG0114003)
Project name	A conceptual diagenetic model for cementation in the Rotliegend sandstones (NL) – targeting reservoir sweetspots
Project period	September 2016 – April 2017
Project number	060.16733 (TEG0114003)

Het project is uitgevoerd met subsidie van het Ministerie van Economische Zaken, Nationale regelingen EZ-subsidies, Topsector Energie uitgevoerd door Rijksdienst voor Ondernemend Nederland."

Executive summary

Porosity and permeability determine to a large extent the reservoir quality and the success of gas production. The growth of cements (= diagenetic minerals) can lead to severe reservoir quality reduction locally. This study is aimed at the understanding of processes that influence cement diagenesis in relation to porosity and permeability loss in the Upper Rotliegend sandstones.

A detailed, quality controlled petrographic database was compiled and built the foundation for the study. The data was sourced from publicly available reports from the Geological Survey of the Netherlands, literature and confidential reports supplied by Total E&P Netherlands. The database contains thin section petrography data, X-ray Diffraction and Mineralog data, and sedimentological and conventional core analysis data. Cements and detrital components were combined according to hierarchical categories and statistical and cluster analyses (using SPSS) were performed on cement groups in relation to porosity and permeability. Thin-section and scanning electron microscopy images were screened to understand mineral relationships and paragenetic sequences.

For single well locations basin modeling was performed using the software PetroMod 2015 to determine burial history, including the temperature and pressure history of the studied location based on calibrated 1D models. The 1D and the TNO-produced temperature, maturity, and pressure 3D basin models were combined with petrography to establish locally dominant mechanisms of cementation. For a selected area (K5, K6, L5 and L6 blocks), paragenetic sequences of events were reconstructed. Additionally, fault modelling, differentiation of gas/water wells and contacts, overpressure, gas compositions and clay volume calculation was undertaken for the case study area.

Although mechanical compaction has a major impact on the reservoir quality, particularly in clay matrix/clay laminae rich sediments, reservoir quality is also clearly reduced by cementation. Aeolian deposits have generally a lower detrital clay content, better soring and better reservoir quality than fluvial and sabkha/lacustrine deposits. Overall, the main cements that decrease porosity and permeability are carbonates (particularly ankerite) and to a lesser degree sulphates (mainly anhydrite). High contents of illite cement are responsible for permeability reduction.

The illite/kaolinite ratio does not increase with depth, as previously assumed. Instead, prolonged deep burial likely lead to significant illite formation. This is preferred in fluvial environments, particularly in proximal alluvial unconfined and overbank deposits where high detrital clay contents could be converted to authigenic illite.

The acidic fluids from the coal-bearing Carboniferous strata are responsible for significant dissolution and precipitation of a variety of minerals. They promote the dissolution of feldspar, early carbonate cements (calcite and dolomite) and Fe-oxides. On the other hand they encourage the growth of kaolinite, illite, ankerite, siderite and barite. The dissolution of feldspar delivers significant amounts of

aluminium and silica for kaolinite and a quartz formation. The original feldspar content may thus have been central to kaolinite, quartz (and partly illite) formation. The influx of the acidic Carboniferous fluids tends to cause a zonation in the authigenic mineralogy (up to a few 10-100m vertically and few km laterally). A kaolinite zone is followed by an illite zone and an ankerite zone is followed by a dolomite zone.

Evaporitic conditions towards the Silverpit and the Zechstein strata promoted the precipitation of sulphates and carbonates (initially as gypcretes, calcretes and dolocretes). Also the Slochteren sandstones experienced an increase in anhydrite, ankerite, barite and dolomite cements towards the Zechstein and Silverpit. The formation of these minerals was either synsedimentary or by fluid expulsion from the Silverpit playa lake towards the adjacent Slochteren sandstones during early burial. Upon further burial, P/T increase lead to conversion of gypsum to anhydrite and calcite to dolomite or ankerite (depending on Fe^{2+} activity). In evaporative environments the burial resulted in further saturation and precipitation of dolomite that was transferred to ankerite by continuous solid solution during intermediate and late diagenesis.

A further impact on sulphate (mainly anhydrite) cementation also likely occurred during the late Jurassic inversion. The elevation of the Silverpit and Zechstein evaporites to the ground-water level led to dissolution of sulphates via meteoric fluid interaction. However, to facilitate the fluid transport to and precipitation of anhydrite in the Slochteren sandstones an fracture network or tectonic juxtapositioning with Zechstein/Silverpit evaporites is required. The juxtapositioning of the Carboniferous, Silverpit and Zechstein against the Slochteren deposits did have an impact on cementation, however a more rigorous fault study is necessary to identify the locations.

The diagenetic models can be used to predict locations of enhanced cementation of a particular cement or cement combination and the related porosity/permeability loss. The conceptual diagenetic models presented in this study may vary locally and therefore regional effects (e.g. magmatic activity) need to be considered before applying the models for reservoir quality prediction.

The results exemplify that the research on a multi-vintage and multi-source petrographic data can deliver an understanding of diagenetic processes that are related to reservoir quality. The study of cementational reservoir quality reduction could be greatly improved by accessing more (currently confidential) petrographic data and including new analyses on more (already existing) core material. To be able to reconstruct the paragenetic sequences with more certainly a good cement dating procedure is required. Facies and sub-environment interpretation needs to be improved and extended, as it may provide more information than revealed in this study. Consequently, a detailed geological subsurface model is essential to propagate cementational trends and trace fluid flow pathways.

Contents

1 Introduction

1.1 Research objectives

Porosity and permeability determine to a large extent the success of gas production. As the most high-productivity fields in the Netherlands are largely explored and produced we are left with tighter and less prolific areas. Different types of cements are generally not equally distributed in sandstone reservoirs. Cementational porosity/permeability loss can have a strong influence on the total reservoir quality reduction in some intervals or locations. This study is ultimately aimed at increasing the ability to predict the quality of the sandstone reservoirs at unexplored locations by understanding the cementation within the Upper Rotliegend reservoirs of the Dutch subsurface. The prediction of the mineralogy at a location with more certainty may also allow a better approach to well design and production/injection procedures.

State of knowledge on sandstone reservoir quality prediction has been summarized in recent studies (Ajdukiewicz and Lander, 2010; Gaupp and Okkerman 2011). Local model input generally tries to combine sediment composition, sediment texture, burial history, changes in effective stress and changes in temperature, as well as interaction of depositional and diagenetic processes. There are still many unknowns, and the amount and detail of data required is often not available. The knowledge of local diagenetic processes is crucial but only if the local diagenetic models are combined would they lead to a global understanding of the reservoir systems in the Rotliegend (Mijnlieff et al., 2014).

A considerable amount of core analyses and petrological data is available on the publically accessible NLog database. In an MSc study by Stahl (2011), performed at TNO, mineralogy, microtexture and porosity in the Upper Rotliegend was screened for a number of wells and documented in a database. Statistical analyses from the study indicated distinct correlations between reservoir quality and clay mineralogy as well as particular distribution of the cements according to formation (Figure 1-1). This pre-study encouraged us to devise this project and build upon the initial database and findings.

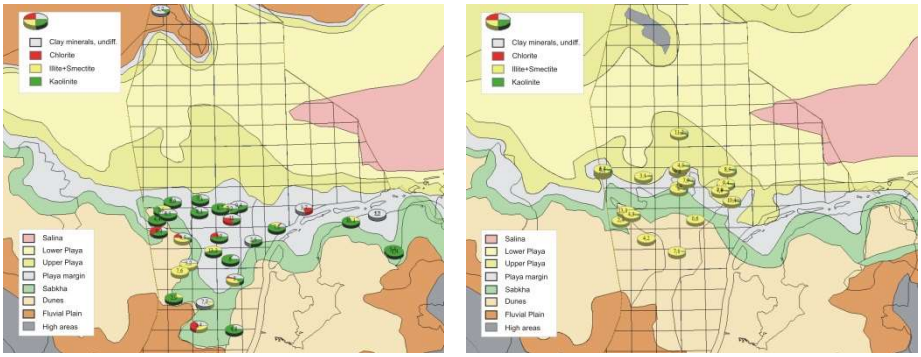

Figure 1-1 Distribution of clay minerals in the Upper Slochteren Member (left) and Lower Slochteren Member (right), from Stahl (2011).

The key questions in this study are:

a) Do certain cements (clay, carbonate, sulphate, quartz) cluster in particular intervals both laterally and vertically and how does this impact the reservoir porosity and permeability?

b) How does the occurrence of authigenic minerals relate to the subsurface architecture, burial history and fluid flow?

c) Can local diagenetic models be connected to achieve a conceptual model for the Rotliegend cements?

1.2 The Rotliegend in the Netherlands

Following the long period of Late-Carboniferous inversion and Early to middle Late Permian uplift and erosion resulting in the Saalian unconformity (also referred to the Base Permian Unconformity = BPU) deposition was reinitiated sometime during the Tartarian (Glennie, 1997). The Southern Permian Basin, that had formed much earlier in Germany and progressively widened westward, extended into the Netherlands, Southern North Sea and eastern U.K. under a transtensional strike-slip regime (e.g., Geluk, 2007; Gast et al., 2010).

In the Netherlands on- and offshore the Rotliegend sequences reach up to 300 metres within a wide band of fluvial sands and (reworked) aeolian sands along the southern basin margin. Marginal-lake deposits and desert-lake shales/evaporites were deposited towards the north. In the NE of the Dutch offshore, the lake sequence thickens to more than 600 m (Geluk, 2007; Gast et al., 2010; Van den Belt and Van Hulten, 2011). The sandy facies were primarily derived from the Variscan orogen in the south, and to a lesser extent from highs in the U.K. (Geluk, 2007; Glennie, 1998; Verdier, 1996).

The Permian comprises three lithostratigraphic groups in the Netherlands: The Lower Rotliegend, the Upper Rotliegend and the Zechstein Group (e.g. van Adrichem Boogaert, 1993). The Lower Rotliegend strata consists of syn-rift volcanics and siliciclastics. In the Netherlands Permian volcanics are restricted in their geographic distribution and are only found as thin sequences. In most parts of the Netherlands the Rotliegend was deposited unconformably on top of the Carboniferous, starting with the Upper Rotliegend Group.

The sediments of the Upper Rotliegend were deposited in arid to semi-arid climatic conditions in intracontinental basins (Glennie, 1983). The climate, driven mainly by Milankovich cycles, was characterised by interchanging wet and dry periods. This cyclcity led to a periodic expansion and retreat of the lacustrine facies belt, resulting in an alternation of fluvial and aeolian deposition at the lake margin (Geluk, 2007).

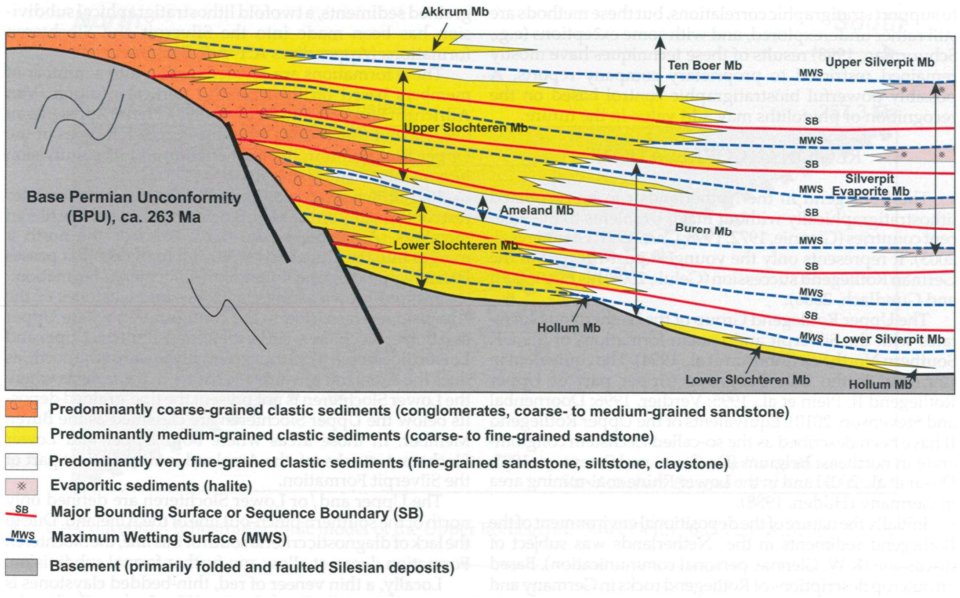

Figure 1-2 Lithostratigraphic successions illustrating the distribution of prime lithologies (Ojik et al., 2011).

The Upper Rotliegend in the Netherlands includes the Slochteren Formation, divided into the Lower Slochteren and Upper Slochteren Members, and the Silverpit Formation. The Silverpit Formation, comprising the Ten Boer, Ameland and Hollum Members, contains mostly fine-grained red sediments, evaporitic layers and intercalated sandstones (Figure 1-2). Deposited in and around the edge of the playa lake (in the centre of the Southern Permian basin) these lacustrine playa sediments make up the main part of the Silverpit Formation (Ojik et al., 2011). The water and sediment supply into the basin was commonly introduced by ephemeral streams (Glennie, 1972). The sediments of the Upper and Lower Slochteren Members comprise coarser-grained aeolian and finer-grained fluvial sandstones and conglomerates (Brouwer, 1972). Towards the south, along the fringe of the playa lake, large aeolian dune fields developed (Figure 1-2). A major fluvial axis, that was active particularly during deposition of the Lower Slochteren, was recognised along a SE-NW to N-S trend across the Dutch offshore (Van den Belt and Van Hulten, 2011).

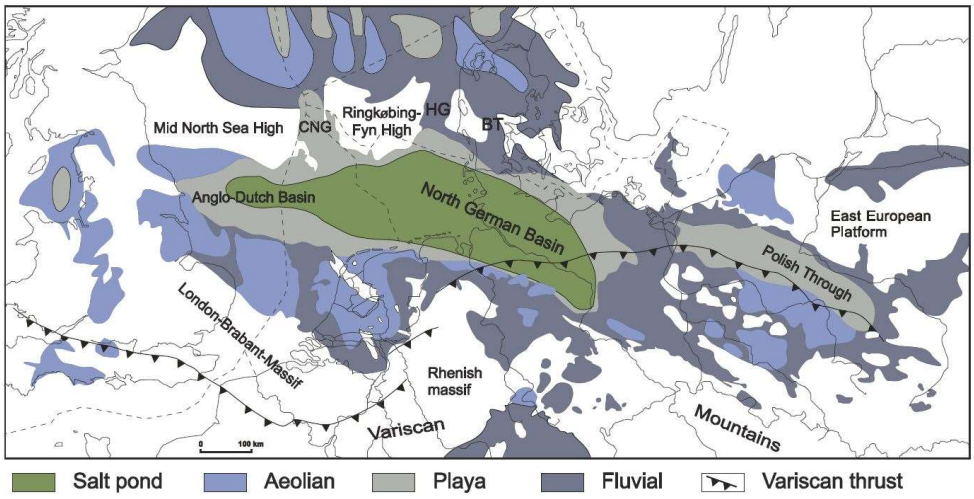

Figure 1-3 Present-day distribution map of Upper Rotliegend sediments attributed to late Middle to early Late Permian in the Southern Permian Basin (from Geluk, 2005).

The Permian basin was first flooded around 258 Ma, creating the saline Zechstein Sea (Burri, et al., 1993). Until the end of the Permian, up to 1500m of cyclic Zechstein evaporitic sequences were deposited. The basal Zechstein deposits are mostly marine evaporite deposits, beginning with a marine, bituminous claystones followed by carbonates and evaporites (anhydrite and halite).

1.3 Cement diagenesis in siliciclastic rocks

Cementation is the in-situ growth of minerals in pore spaces of sediments. The genesis of authigenic minerals (= cements) can be divided roughly into early and late diagenesis. Early diagenesis is also referred to as eodiagenesis. This stage includes all processes that occur at or near the surface (Worden & Burley, 2003). The pore-water chemistry is mainly influenced by the depositional environment. The eodiagenetic domain can extend from only a few meters in low permeable sediments to over a thousand meters in coarse grained porous sandstones. Mesodiagenesis (also referred to as late diagenesis) involves all processes which occur during burial once the sediment has passed the influence of meteoric waters (Worden & Burley, 2003). The boundaries between diagenesis are not sharp and vary locally. Telodiagenesis is also late diageneic process connected to the renewed contact to meteoric waters due to uplift and/or inversion. In this study we refer to telodiagenesis also as late diagenesis.

The formation of authigenic minerals requires a fluid phase and arises due to changes in fluid chemistry, temperature and pressure. During early diagenesis in arid environments evaporative processes of meteoric pore-water are largely responsible for cementation (Worden & Burley, 2003). Typically, eodiagenesis drives the formation of calcretes, dolocretes, gypcretes and smectite clays. These early cements often show a depositional environmental control.

During burial, temperature and pressure increases leading to mineral dissolution and re-precipitation. Both detrital components and early cements are influenced by the thermodynamic changes in the pore-waters. With increasing burial depth

hydrous minerals are the first to dissolve and convert to a more stable (water-free) mineral phases. Dioctahedral smectite is replaced by illite at higher temperatures (McKinley et al., 2003). Illitisation of smectite will result in excess silica and lead to quartz precipitation. Between ~50 and 120°C gypsum can dehydrate to anhydrite.

The dissolution of feldspars and lithic fragments is a common mesodiagenetic process that creates secondary porosity and/or the precipitation of other mineral phases. Dissolution of K-feldspar and plagioclase could lead to formation of illite, kaolinite and/or quartz (Ziegler, 2006; Bertier et al, 2006). Feldspar can also react with existing kaolinite to form illite and quartz (Worden & Burley, 2003). Examples of reactions featuring feldspar are:

$$KAlSi_3O_8 + 2NaAlSi_3O_8 + H^+ \rightarrow KAl_3Si_3O_{10}(OH)_2 + 6SiO_2 + 2Na^+ \quad (1)$$

$$2KAlSi_3O_8 + H_2O + 2H^+ \rightarrow Al_2Si_2O_5(OH)_4 + 4SiO_2 + 2K^+ \quad (2)$$

$$Al_2Si_2O_5(OH)_4 + KAlSi_3O_8 \rightarrow KAl_3Si_3O_{10}(OH)_2 + 2SiO_2 + H_2O \quad (3)$$

For these reactions to occur not only a favourable temperature and fluid chemistry are crucial but also pH and salinity. Whereas chlorite requires alkaline conditions (conversion of smectite to corrensite to chlorite), kaolinite favours an acidic environment with positive eH but low salinity (e.g. Ziegler, 2006). Illite requires a high K+/H+ activity ratio but can handle high salinity and low pH. Illitisation can occur via recrystallisation of infiltrated clay coatings, recrystallisation of authigenic illite/smectite or by grain (mainly feldspar) dissolution. Kaolinite was postulated to be dominant in shallow buried (platform) settings and experience progressive illitisation with burial depth (Figure 1-4; Gaupp & Okkerman, 2011).

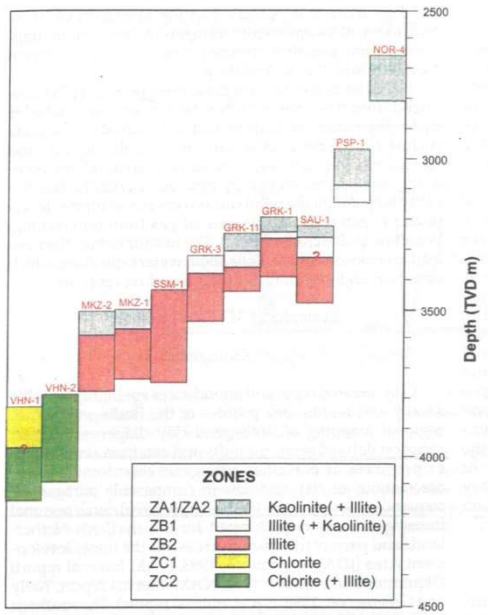

Figure 1-4 Vertical distribution of clay minerals in wells from the Lauwerzee Trough (from Gaupp & Okkerman, 2011).

K-Ar dating of illites showed that illite can form over a wide range of temperatures from 20 to 220°C (Lee et al., 1989; Ziegler, 2006). One of the controlling factors on illite generation is considered to be the duration of deep burial, provided favourable

conditions for illite formation are in place (Figure 1-5). Deep kaolinite was explained by either fast reaction kinetics or by transformation of kaolinite to blocky dickite crystals (Ehrenberg et al., 1993). It was also brought to attention that illite precipitation was prone to deeper seated basins than structural highs, which were more dominated by kaolinite clays (Ziegler, 2006 and refs therein)

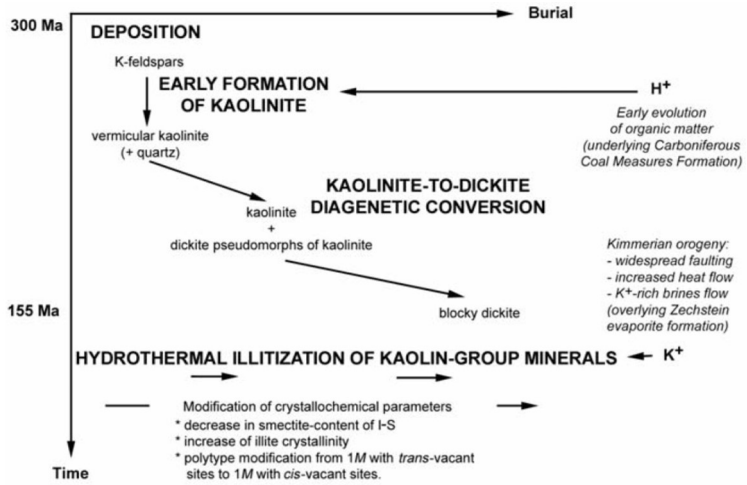

Figure 1-5 Diagram of the reactions of clay minerals occurring during burial diagenesis in the Rotliegend of the Broad Fourteens Basin (from Ziegler, 2006)

Carbonates are quite common cements in sandstones. Whereas calcite [$CaCO_3$] is a pure calcium-carbonate it often occurs as the Fe-containing ferroan-calcite cement. Dolomite [$Mg,Ca(CO_3)_2$] is a Mg-rich carbonate. Ankerite [$Ca(Fe,Mg)(CO_3)_2$] is often referred to as ferroan-dolomite, due to its major ions being calcite, magnesium and iron. However, ankerite can also contain Mn as major element. Siderite [$FeCO_3$] is an iron-carbonate that can also contain minor amounts of Mn and Mg.

A common source for mesodiagenetic carbonates is the redistribution of eodiagenetic carbonate cements (Platt, 1994). Calcite becomes progressively unstable with depth and depending on the activity of Mg^{2+}, Fe^{2+} and Mn^{2+} will transform to dolomite, ferroan calcite, ankerite or siderite. Siderite and ankerite are less soluble than calcite and dolomite and thus less sensitive to re-crystallisation (Morad, 1998).

Fe-carbonates (ankerite, siderite) can precipitate in reducing fluids, carrying ferrous iron. Formation of siderite requires a high Fe^{2+}/Ca^{2+} ratio as well as low CO_2 partial pressure (Curtis, 1967). The source of Fe^{2+} can be either external or from the dissolution of early formed Fe-oxides.

1.4 Influence of fluid flow on cementation

The Rotliegend sediment diagenesis was influenced by the following types of fluids:

- Connate, meteoric Rotliegend fluids
- Alkaline fluids from Rotliegend shales
- Acidic fluids from the Carboniferous
- Zechstein brines

The rise and fall of the groundwater level and successive evaporation of meteoric fluids steers the formation of precipitates, such as calcretes, dolocretes and gypcretes during early diagenesis. Cements related to this meteoric (eodiagenetic) fluids are carbonate, sulphates, halite and minor quartz. Fe-oxide coatings can be inherited from oxic weathering processes at the surface, often combined with the formation of infiltrated clay coatings (Gaupp, 1996). Precipitation of Fe-oxides in semi-arid environments intrastratal weathering of iron-bearing minerals, such as detrital ferromagnesian silicates and iron-bearing clays (e.g., Walker, 1967). Illites and smectites can infiltrate the porous sands through the falling groundwater level.

During early burial compaction of the Rotliegend playa shales released saline fluids into the adjacent sandstones. The expulsion of the alkaline brines from the basin centre is responsible for early chlorite, dolomite and sulphate cements. The influx of these alkaline fluids into the Slochteren sandstones may have also occurred during Zechstein transgression (Platt, 1994).

The hydrocarbon charge lead to the introduction of reactive organic components that generated a number of diagenetic reactions. The fluids, originating from the Carboniferous source rocks, were both acidic and reducing due to their organic acid and CO_2-content. They lead to the crystallisation of kaolinite, illite, quartz, late chlorite, dolomite, ankerite and siderite at the expense of feldspar and calcite. Bleaching of the red beds was also related to the reducing fluid interaction (Gaupp et al., 1993). The formation of the Fe- and Mn-rich carbonates can be related to reducing fluids carrying Fe^{2+} that is provided by the reduction of Fe-oxides.

Distinct clay zoning was observed in near fault zones, where the Rotliegend was juxtaposed against the coal-bearing Carboniferous (Figure 1-6). Adjacent to the faults (few 100 meters) acidic fluids can lead to the complete dissolution of feldspar and partially carbonate. In this zone kaolinite cementation is favoured, together with minor ankerite and siderite cement. Further away from the fault zone (> 1 km) the dissolution of feldspar is incomplete with less carbonate dissolution. This results in a second cement generation of predominantly illite. Vertical flow from the coal-bearing Carboniferous at the BPU contact to the Slochteren can result in kaolinite and illite zonation. The distance will depend on the vertical permeability, which is generally lower than the lateral permeability along a sandstone bed. The kaolinite and illite zones will likely be a magnitude lower vertically (a few hundreds of meters in total) than horizontally.

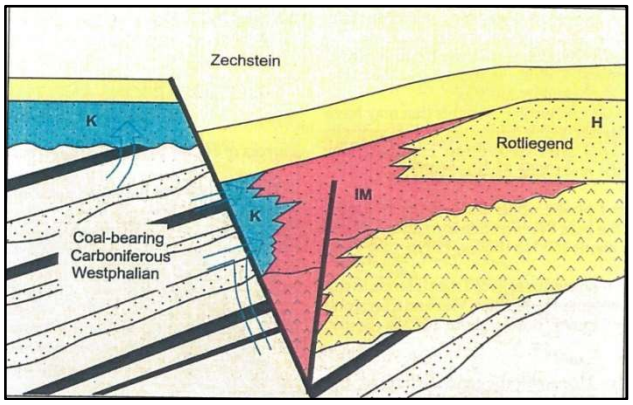

Figure 1-6 (from Gaupp & Okkerman, 2011)

The percolation of hydrocarbons also resulted in solid bitumen coating of the pore spaces and may have led to further cement inhibition (e.g., Marchard et al., 2002). A further, reservoir quality retaining effect was suggested to be the gas emplacement, which displaced the formation waters and preventing further mineral growth (Taylor et al., 2010). This was only relevant to permanent gas pockets restricted to structural highs (hydrocarbon gas pockets).

Telodiagenetic influence of meteoric fluids can cause an alteration of feldspars to kaolinite (and quartz). Meteoric waters are dilute and oxidising, which can lead to the oxidation of Fe-bearing cements, such as ankerite, siderite and chlorite (Worden and Morad, 2003). Exhumed structural highs allowed the infiltration of meteoric waters into the Rotliegend sandstones close to the highs but much less in the deeper structural lows (Figure 1-7). Halite, gypsum and anhydrite are highly soluble (Purvis, 1992). The ingression of meteoric water would have led to dissolution of Zechstein and Silverpit evaporites. Transport towards the Rotliegend sandstones was operated by diffusion and density driven flow (Gaupp, 2008).

Lateral flow of fluids from Zechstein into the Rotliegend occurred on or near uplifted blocks (Platt, 1994). At major faults where Zechstein was juxtaposed against the Rotliegend, alkaline Zechstein brines entering the Rotliegend sandstones delivering anhydrite (and carbonate) saturated water that precipitated in the Rotliegend sandstones (Gaupp, 1993; Platt, 1994). This was evidenced by a similar S isotope composition between the Rotliegend anhydrite cements and the Zechstein sulphates and was proposed to have occurred at the beginning of the structural inversion period in the Lower Creatceous to Early Tertiary (Sullivan et al., 1994).

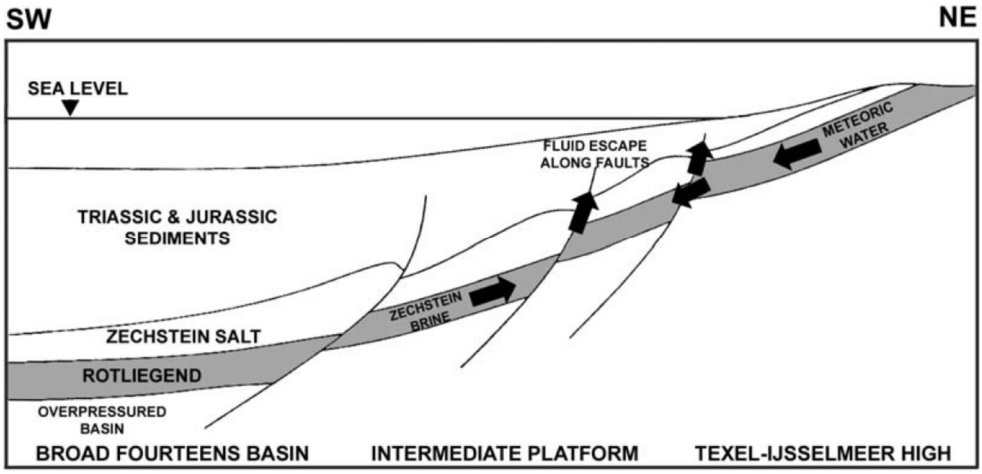

Figure 1-7 Schematic drawing of Zechstein fluid interaction with meteoric fluids in the Southern North Sea (from Ziegler, 2006).

1.5 Impact of cementation on reservoir quality

The main authigenic minerals found in Rotliegend siliciclastics are carbonates (dolomite, ankerite, siderite), sulphates (anhydrite, barite), quartz, clay minerals (kaolinite, illite-smectite, chlorite), Fe-oxides, halite and pyrite (Gaupp & Okkermann). The growth of these cements leads mostly to loss of porosity and/or permeability but in some cases it can also stabilise the sediment framework and reduce further compaction.

Early grain-rimming chlorite has been proposed to reduce compaction and the dissolution of feldspar, thus retaining high intergranular pore space (Gaupp & Okkerman 2011, Gaupp 1993). Chlorite grain rims can also inhibit quartz overgrowth (Adjukiewicz et al, 2000; Ziegler, 2006). Late chlorite does not seem to have a strong effect on reservoir quality. Mg^{2+} is needed for the formation of chlorite and dolomite. Consequently, their formational processes compete with each other, which can be in favour of the dolomite formation resulting in porosity reducing dolomite cement (Gaupp & Okkerman 2011).

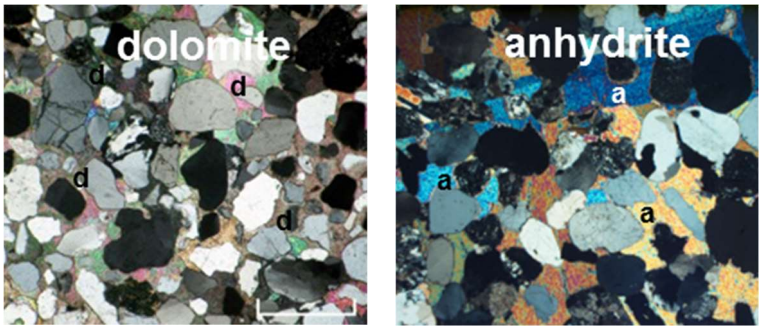

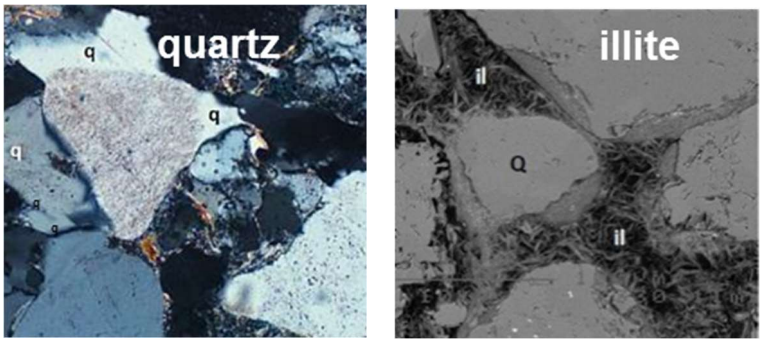

Figure 1-8 Thin-section images and an SEM image (illite) of sandstones.

The clay mineral kaolinite has been observed to lower porosity but not influence permeability in any way. Illite (and mixed layer illite-smectite) is a clay mineral that has the most detrimental effect on reservoir quality with regard to permeability. The mere presence of illite does not guarantee permeability reduction. This largely depends on the type of illite, whether grain replacive, grain-rimming, or (fibrous) pore-filling (Figure 1-8). Early grain-rimming illite may even inhibit quartz precipitation (Worden & Morad, 2003) but can also grow radially in a fibrous texture and reduce permeability. Whereas grain replacive illite can enhance rather than reduce permeability, pore-filling illite will reduced it.

A further problematic aspect of clays is fines migration. Upon improving high pressure difference during well production on a sediment containing clay, illite, smectite, chlorite and kaolinite may be mobilised causing pore-throat plugging.

Quartz cementation can also have a reservoir quality reducing effect (Worden & Morad, 2000). On the other hand, early quartz overgrowths have also been seen to stabilise the sediment grain-framework and thus reduce compaction.

Both carbonates and sulphates can cause severe pore plugging in the Rotliegend (e.g. Gaupp & Okkerman, 2011). If carbonate cementation is early and minor a framework stabilising effect can be achieved to prevent further compaction (Morad, 1998).

2 Petrographic Database

2.1 Database compilation and quality control

The petrographic database consists of 2257 samples from a total of 104 wells in the Rotliegend of the Netherlands. The petrographic dataset comprises analysis results of three different techniques:

1. Point-count analysis, including textural description
2. XRD analysis (whole rock and clay XRD)
3. MINERALOG analysis

The data was compiled mainly from reports from the NL Olie- en Gasportaal (http://nlog.nl/nl/home/NLOGPortal.html) and partially from literature (Petrographic Atlas, 1991). Additionally, petrographic and mineralogical data (from 16 wells) was kindly provided by TOTAL E&P Netherlands for the project and will remain confidential.

Each sample has an administrative attribute, such as well name and depth in m (MD = measured depth in meters and TVD-NAP = true vertical depth referenced to NAP) as well as UWI (Unique Well Code) and co-ordinates of the well (as UTM31_ED50). If the loggers depth was available it was entered, however for many wells it is not certain whether the measured depths represent the log depths. TVD-NAP depth reference was taken from the DINO deviation surveys. The TVD_report depth was taken from the respective reports, if available. Supporting information was added to the database such as depositional environment, core analysis (porosity, permeability, grain density) and lithostratigraphic unit. Not all data was available for each well. Measured depths were taken from the reports and datasheets.

Point-count analyses are performed with an Optical Polarisation Microscope on thin-sections. Quantification of the mineralogical composition is achieved by counting generally 300 points, using a mechanical interval displacer. The mineralogical composition obtained from point-count-analysis and its accuracy is dependent on the analyst. Not all analyses have the same level of detail. Some datasets only contain approximate concentrations of minerals.

Whole rock X-ray diffraction spectroscopy (XRD) is performed on a powdered rock sample. The samples are scanned with an X-ray spectrometer that provides an X-ray spectra of the crystalline phases in the sample. The spectra are achieved by emitting X-rays that diffract from the crystal planes. The spectra is then evaluated by an analyst who uses a specialist program to allocate the peaks of a spectra to individual minerals. The quantification of the minerals is performed either by using an RIR (Reference intensity ratio) that has been calibrated internally to pure mineral phase standards or by Rietveld Refinement software. Note that XRD is a semi-quantitative technique, meaning that the uncertainty is not known or may be unreasonably large, although the precision may be very good (Hiller, 2003).

Clay XRD essentially follows the same principals as whole rock XRD. The difference is that the “clay fraction” consists of particles less than 2µm. A total of 4 spectral analyses are ran with different sample treatment (dry, glyconated, heated at different temperatures) to be able to differentiate between certain clay minerals (e.g. kaolinite and chlorite).

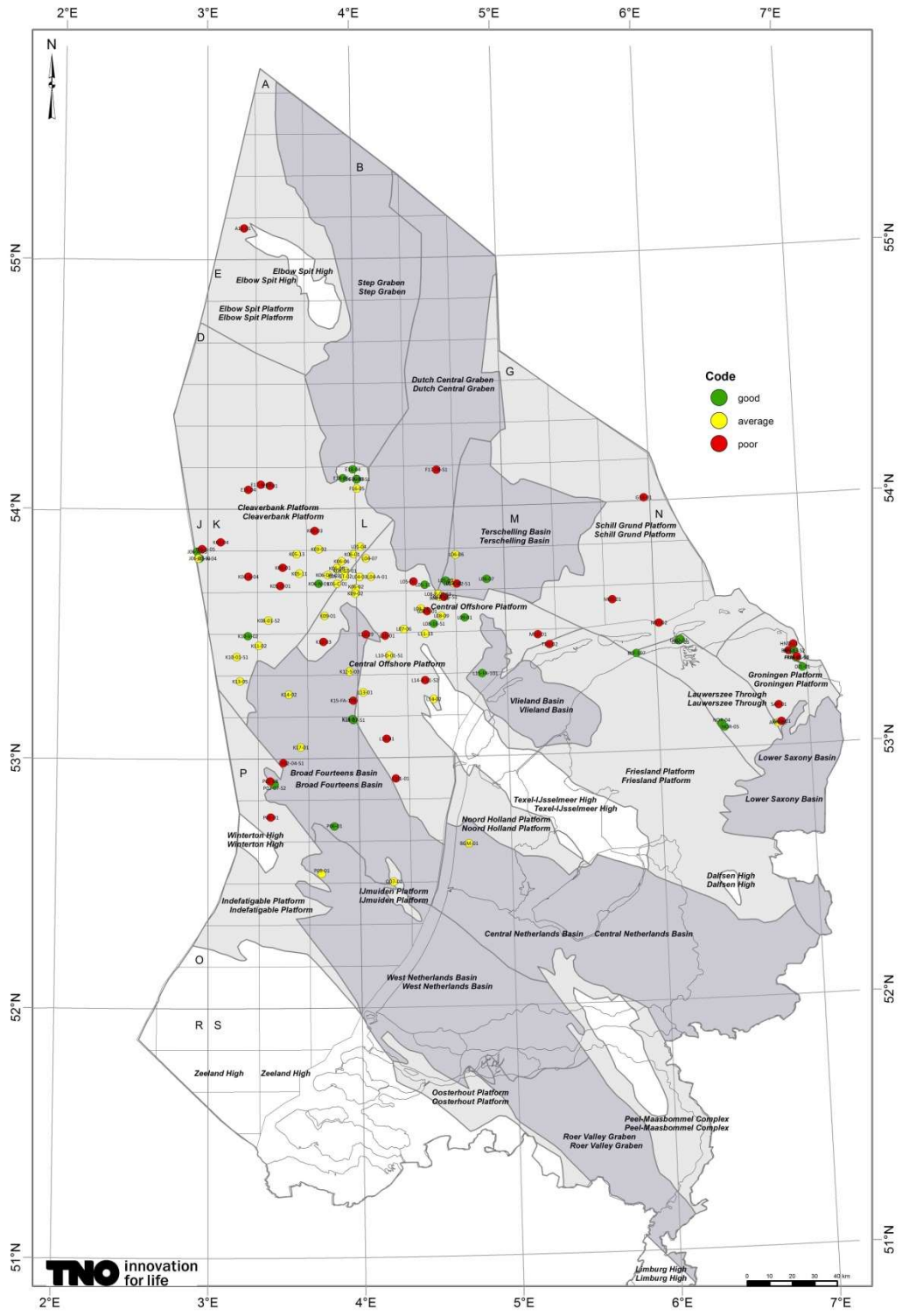

Figure 2-1 Map of the onshore and offshore fields with locations of all wells included in the database. The colour of well locations represents the quality control codes.

MINERALOG data is analysed by a Fourier Transform Infrared spectrometer (FTIR) on powdered samples to identify mineral phases. Mineral identification is possible because minerals have characteristic absorption bands of infrared radiation. For quantification the Fourier spectra are compared to standard mineral spectra.

The present database consists of two sources:
1. Petrographic database compiled during a TNO internship study (Stahl, 2011)
2. Newly compiled data in the present study

Both databases were incorporated after a examination of the data. All of the data was quality controlled (Figure 2-1). In the initial step data with approximate concentrations and with closed sums of below 99% and above 100% was classified as failed but retained in the raw database.

The quality control was based on the number of wells that passed the initial QC step (the higher the number, the higher the QC grade). The existence of point counting data was given the highest ranking, followed by XRD and Mineralog quality and quantity. The datasets were also screened for the existence of sedimentological attributes (identification of depositional environment), core analysis data (porosity, permeability), thin-section and/or SEM images, petrographic report and whether a paragenetic sequence of events was developed (Figure 2-2). The number of analyses was also crucial for the QC because a small number of analyses (< 5) per well is less representative.

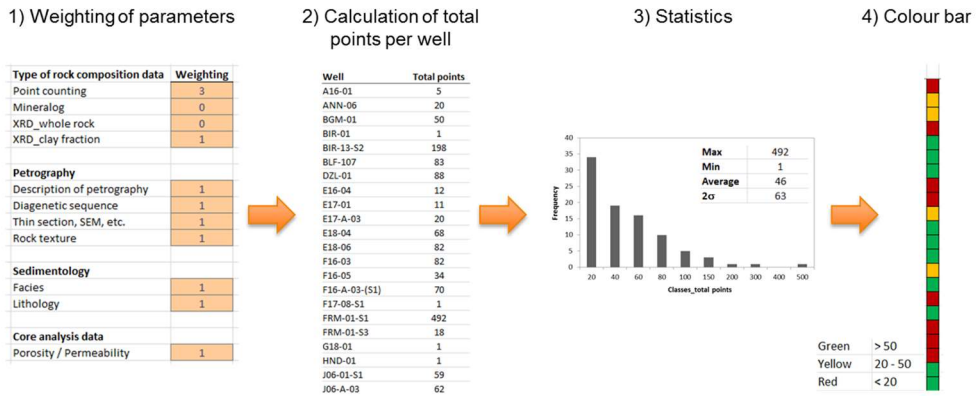

Figure 2-2 Overview of QC procedure for the quality control coding for the QC map.

Additionally, the data was scanned for inconsistencies. Particularly large qualities of minerals that unlikely occur in such abundance in siliciclastics were investigated by referring to original data tables and reports. This helped to eliminate further errors in the database. Generally this concerned transfer errors from report to excel to the database. Occasionally analytical errors were spotted, for example XRD data from well L05-C-02-S1 resulted in high abundances of barite (up to 33%) and halite, which is uncommon. The report clarified that the samples were heavily contaminated with drilling mud that contained barite. For this well barite and halite were excluded and the minerals not affected by drilling mud were scaled to 100%.

2.2 Limitations of the dataset

As evident from the well map (Figure 2-1) the geographic distribution of the wells is not uniform. Wells are scarce in the western Netherlands onshore, Northern and eastern offshore and the P/Q blocks. There are two reasons for this discrepancy. Firstly, prospective reservoirs are not uniformly distributed. The second reason is that for this report we were allowed to only incorporate wells from the public database, available publications and in-kind contribution from TOTAL. An unknown quantity of petrographic data has been gathered in the Netherlands that was not made available for this study.

Core samples for routine core analyses (porosity/permeability) are taken equidistantly (every 30 cm). Only a selection of the core plugs is then further processed for petrographic analyses. Important horizons could thus be missed for petrography. For some wells less than 5 samples were reported, which makes the analyses barely representative.

Petrographic description and point-counting is performed by an analyst and is subjective to their judgement. Minerals may be mistaken for other minerals by a junior analyst as well as the detection of intergranular vs. intragranular pore-space. Point-counting in different laboratories and by different analysts may therefore produce controversial results. The quality of sample preparation and the type of thin-section staining (e.g. carbonate or feldspar staining) of the samples has an impact on the quality of petrographic analysis. Also pervasive cementation that obscures grain boundaries and complete dissolution of early cements provides a source of error that impacts on the detection of intergranular vs. intragranular pore-space and thus calculated intergranular volumes (IGV).

For the XRD and Mineralog data, artefacts such as drilling mud contamination cannot be discriminated. Low quality XRD evaluation does not distinguish between dolomite and ankerite. Pyrite and hematite have the same dominant peaks in the spectra and therefore cannot be easily differentiated, particularly at low quantities.

2.3 Data organisation

The database attributes were combined into categories. Cements and detrital components were combined according to hierarchical categories from Mijnlieff et al. (1999). The 1st level separates the petrographic attributes into detrital and authigenic components (example Figure 2-3). The next level is the sublevel dividing the detrital and authigenic components into main mineral and rock components (such as quartz, carbonate, clay, rock fragments), with further sublevels becoming more detailed.

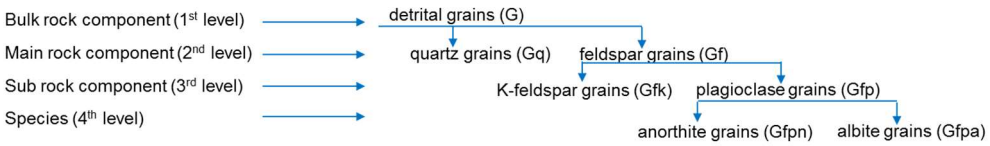

Figure 2-3 Hierarchy of petrographic components on example of feldspars.

The reason for this subdivision stems from the fact that petrographic descriptions and are not uniform. Depending on the laboratory and analyst the descriptions are more or less detailed and can be directly associated with one of the levels. To maximise the amount of comparable data this study focussed on levels 2 and 3. Samples that failed the QC were not included in further data processing. Detrital clay laminae, pseudomatrix and ductile rock fragments were categorised as matrix laminae, since each of these consist of, detrital, ductile, clay-rich components, which can significantly reduce porosity during mechanical compaction.

For further work the data was separated into subsets and normalised to 100%. Point count, XRD and Mineralog data are included if the sum of the minerals (± porosity for the point count data) is between 99% and 101%. For the Mineralog data the sum is always exactly 100%. For the point count data, the porosity is either included or excluded in the sum by the analyst.

The following subsets were used and will be referred to throughout the report:

1. Whole-rock
2. Authigenics
3. Clay-minerals
4. Carbonate-minerals

The **Whole-rock** subset sums up both detrital and authigenic components. This subset is from point count data only.
Subset a: porosity is included; mineralogy and porosity added up to 100%
Subset b: porosity is excluded; mineralogy adds up to 100%

The **Authigenics** subset contains data from point-count analyses only. The Authigenics dataset de-emphasises the impact of the detrital mineralogy, as opposed to the whole rock dataset. The reason for not including XRD and Mineralog data is because a differentiation between detrital and authigenic components is not possible for these techniques. Porosity was excluded to be able to make a comparison with petrographic data that did not include visible porosity.

Thee subset **clay-minerals** contains clays only (scaled to 100%) but without differentiating detrital and authigenic fraction. It serves to compare the clay mineral relationships. For this subset point count, XRD and Mineralog data was utilised. Although chlorite is technically not a clay mineral, it was included in this subset.

Similarly, **carbonate minerals** from point count, XRD and Mineralog were combined and normalised to 100% in order to trace relationships between these cements.

Grain-size classes were also translated into codes (Mijnlieff et al. (1999), table 2) and combined into subclasses, resulting in 12 grain-size classes. The laminated samples contain at least 2 different grain-size classes. They were therefore treated as a separate class (Table 2-1).

Table 2-1 Grain size classes

Grain size code	Grain-size class
L	laminated
TgM	clay
TgJ/TJ2	fine silt
TgJ4	coarse silt
TgS1l	v. fine sand lower
TgS1u	v. fine sand upper
TgS2l	fine sand lower
TgS2u	fine sand upper
TgS3l	medium sand lower
TgS3u	medium sand upper
TgS4l	coarse sand lower
TgS4u	coarse sand upper

The depositional environments that were derived from petrographical and sedimentological reports were combined into eight separate subenvironments (Figure 2-4), being Aeolian bedforms (dunes), Aeolian (dry/wet interdunes), Aeolian sandsheet (homogenised), Desert waterbodies (ponds and playas), Sabkha, Alluvial (distal) mudflat/sandflat, Fluvial (proximal alluvial- unconfined & overbank), and Fluvial (proximal alluvial- channelized). The depositional environment is generally determined from a combination of depositional facies that are interpreted by sedimentological features in cores. Note that it is often difficult to depict facies on a core scale as opposed to an outcrop scale.

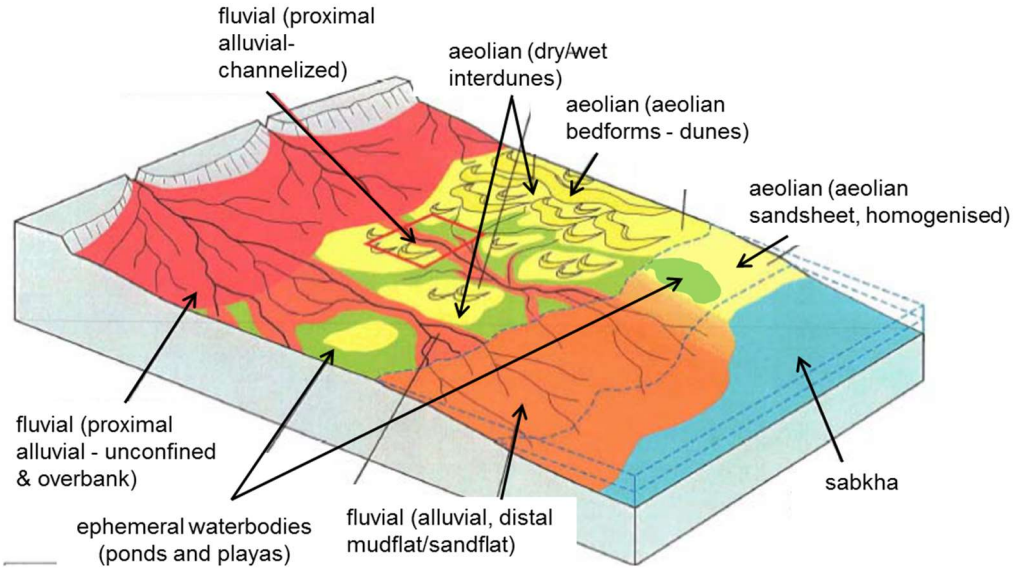

Figure 2-4 A schematic model of the depositional environment, modified after Lafont (2000)

Aeolian bedforms (dunes) are proximal, mostly dry aeolian deposits. The category comprises the reported sun-environments: aeolian dunes, aeolian dune core, aeolian dune cross-sets, aeolian dune slipface, dry aeolian sands (dry dunes), and minor dune fields, aeolian dune base and aeolian dune bottomsets.

Aeolian (dry/wet interdunes) are proximal aeolian deposits that can be dry, intermittently wet, or semi-permanently ponded. Interdunes are the topographic troughs situated between static or mobile dunes, that are not to be confused with larger topographic lows on the landscape in general. This category encloses the reported attributes: dry interdunes, wet interdunes, damp interdunes, and fluvial interdunes.

Aeolian sandsheet (homogenised) comprises distal aeolian deposits. It is an aeolian-dominated environment, topographically relatively flat where larger, complex bedforms do not develop. The facies can be variable, since the deposits are affected by mixed aeolian, runoff, evaporitic and pedogenic processes. This sub-environment comprises the reported categories: aeolian sandflat, damp aeolian sandflat, damp aeolian sands (damp sand sheets), damp sandflat, damp/dry aeolian sandflat, dry aeolian sandflat, dry aeolian sandflat with minor aeolian dunes, dry/damp sandflat, dry sandflat, extradunal wet sandsheets, homogenised aeolian sandflat, homogenised sandflat, fluvial channel/aeolian sandflat, fluvially modified aeolian dunes and desert plain.

The **Desert waterbodies (ponds and playas)** sub-environment comprises the reported categories: the desert lake, desert lake shales, playa and playa shales, sheetfloods alternating with desert lake, and pond. The sediments were deposited in standing-water bodies which were either ephemeral or flooded on a semi-permanent basis.

A **Sabkha** is a somewhat flat, intermittently wet, low-energy domain where evaporitic and aeolian processes (and subordinately runoff) control a variety of facies associations changing vertically and laterally quite rapidly through the stratigraphic column. This category comprises the reported attributes: argillaceous sabkha sandstones, sabkha mudrock, and sabkha mudstones and sandstones.

The **Proximal alluvial - unconfined & overbank** category belongs to a proximal fluvial environment comprising the reported categories: crevasse splay, dewatered sheetflood, floodplain, fluvial sheetflood, homogenised sheetflood, sheetflood with extensive dewatering, structured sheetflood, wet sandflat/fluvial channel, and well-drained floodplain deposits.

The **proximal alluvial – channelized** subenvironment comprises (proximal) fluvial channels, where some degree of aeolian reworking is possible. It includes the reported categories: wadi channel deposits, stream deposits, minor fluvial channel sandstones, medial-proximal fluvial channels, high-energy/proximal fluvial sands (wadi fan belt), fluvial fans, fluvial sands, fluvial channel/damp sandflat, braided fluvial channel, braided plain deposits, distal stream channel fill.

Alluvial (distal) mudflat/sandflat denote a low-gradient environment that is distal from the main channelised runoff pathways. The regime is generally of low-energy with most aggradation related to runoff deposition. The deposits can be affected by secondarily modification by pedogenic, aeolian and/or (bio)chemical processes with evaporitic deposition and secondary modification, that is a frequent occurrence in case of semiarid or arid climate. This category encompasses the reported attributes: sheetfloods, desiccating desert margin with sheetfloods, distal

sheetfloods, fluvial/aeolian sheetfloods/sandflats, fluvial playa with flooding, massive sheetfloods, sheetfloods alternating with damp sandflats, wet sandflats, wet sandflat/mudflat and low-energy/distal fluvial sands (sheetflood delta fringe).

3 Basin Analysis

3.1 Introduction

Basin modelling was performed in the context of this study to collect additional information on spatial and temporal parameters. For single well locations it provides information on the burial history, including the temperature and pressure history of the studied location based on calibrated 1D models. In a larger context it gives information on the regional evolution of a study area, e.g. including source rock maturity and hydrocarbon charge timing and history as well as basin geometry and potential fluid flow direction from 3D models.

3.2 Methods

Basin modelling or petroleum systems modelling was introduced in the 1980s as a tool for hydrocarbon exploration. It uses the present day geological model of the subsurface as mapped from 2D and 3D seismic, converted to depth and tied to stratigraphic well markers if available. The uncertainty related to the input model directly influences the level of detail the model can provide. The modelling requires an initial state (present-day geological model) and needs to comply with several general assumptions and boundary conditions. The main general boundary conditions and assumptions within basin modelling are:

- The model is laterally constrained: no horizontal compression or extension of the basin fill is taken into account.
- Vertical movement only (no lateral deformation of the sediments is included in the model, except for salt movement)
- Salt movement has no direct relation to changes in stress
- Compaction of the basin fill is vertical
- Compaction is mechanical according to a vertical effective stress based rock property model
- Density of pore water is constant
- Conductive heat flow

The basin models used for this study were constructed at TNO between 2008 and 2014 in the context of the mapping of the deep subsurface of the Netherlands Continental Shelf project (NCP-2, Verweij et al. 2009, 2010, Abdul-Fattah et al. 2010, 2012, the onshore focused later projects funded through the Dutch Geological Survey (4DMOD project, Nelskamp & Verweij, 2012) as well as a cooperation with the German Geological Survey (BGR, GPDN project, Heim et al. 2013). They are based on the most recent DGM-diep v3.0 models at the time of their construction without faults and assumed open fluid flow boundaries. In addition to these general limiting assumptions and conditions, default set-ups of the modelling package influence simulation results. Such default set-ups include default relations between standard lithologies and properties through compaction approaches, porosity-permeability relations, thermal models, kinetic models; mixing rules lithology. Check the respective reports and publications for more information on the individual models.

3.3 Results

For the interpretation of the burial history of the area 1D model extractions were made from the 3D models for all wells in the focus area and several key wells in different structural settings throughout the whole of the Netherlands. The temperature evolution for the Rotliegend strata as well as maturity evolution of the Carboniferous source rock intervals are highlighted on the burial history curves. In the following the differences in burial history and temperature evolution in the different structural elements are described. For a detailed explanation of the definition of the structural elements please refer to Kombrink et al. (2012).

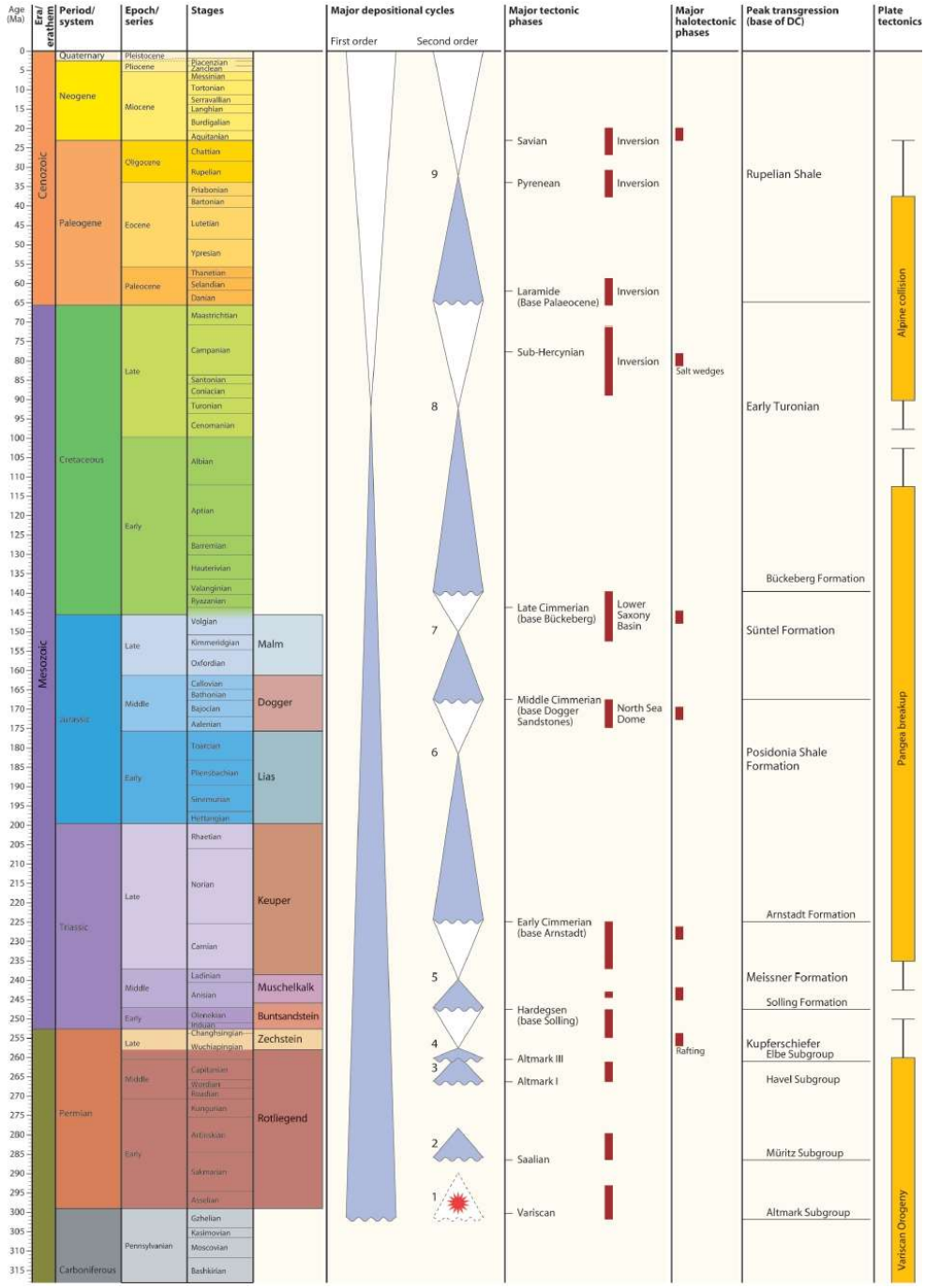

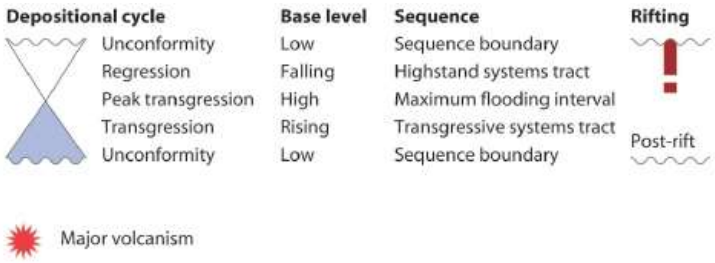

Figure 3-1 Paleozoic to Cenozoic timescale and tectonic phases for the Central European Basin system (from Doornenbal & Stevenson, 2010)

Figure 3.1 shows the main tectonic phases that influenced the geologic evolution in the Netherlands. The descriptions of the burial history follow these phases.

3.3.1 Friesland Platform, Groningen Platform and Lauwerzee Trough

The three structural regions are located in the north of the onshore area of the Netherlands (Figure 2-1). They are all classified as platforms, the main difference being the thickness of the Triassic sediments and the subsidence during the Paleogene and Neogene. They all experienced rapid subsidence in the Late Permian to Early Triassic and significant erosion during the Middle to Late Jurassic (Figure 3-2). Deepest burial and highest temperatures on the Friesland Platform as well as in the Lauwerzee Trough are present day, on the Groningen Platform burial and temperature before the erosion in the Jurassic was in the same range as today.

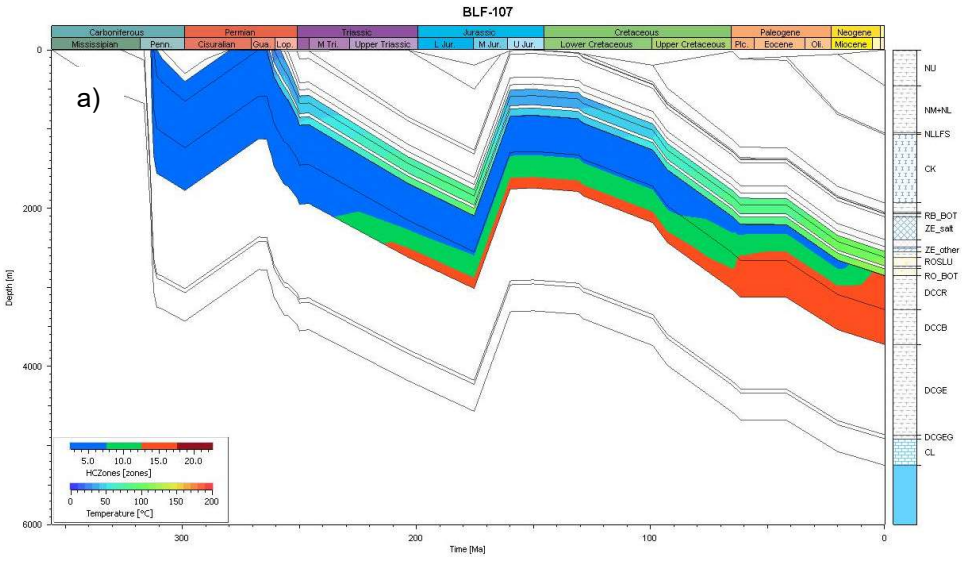

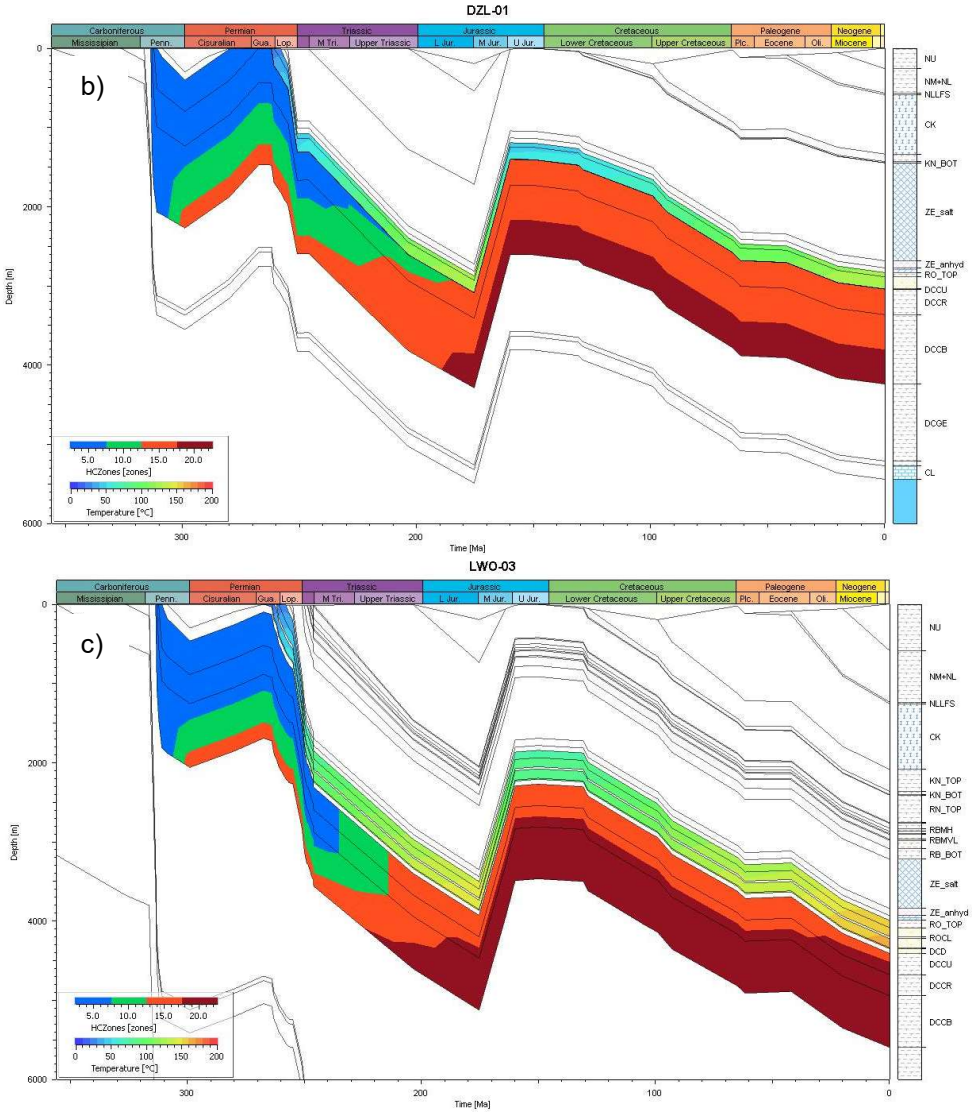

Figure 3-2 Burial histories, temperature and maturity evolution for three example wells of the best fit model of the Friesland Platform (a, BLF-107), the Groningen Platform (b, DZL-01) and the Lauwerzee Trough (c, LWO-03). The maturity calculation of the Carboniferous source rock intervals is based on the model of Burnham (TIII, Burnham, 1989) where blue equals immature for oil and gas generation, green equals oil mature, red equals gas mature and dark red equals overmature for gas generation.

3.3.2 Central Offshore Platform

The northernmost part of the Central Offshore Platform (Figure 2-1) is included in the focus area and discussed there in more detail (Chapter 5).

The Central Offshore Platform has, like most of the Netherlands, experienced rapid subsidence during the Late Permian to Early Triassic (Figure 3-3). Erosion during the Middle to Late Jurassic was most intense in the south on the Texel-Ijsselmeer High, but affected the whole area. Deepest burial as well as highest temperatures are at present-day. More information on the basin model can be found in Verweij et al. (2010).

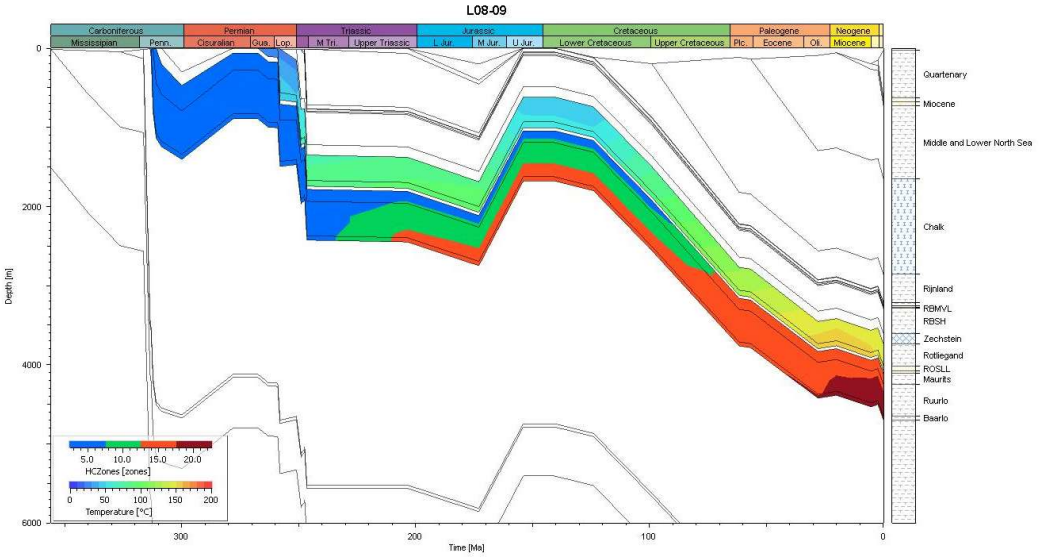

Figure 3-3 Burial history, temperature and maturity evolution for an example wells of the best fit model of the Central Offshore Platform (L08-09) The maturity calculation of the Carboniferous source rock intervals is based on the model of Burnham (TIII, Burnham, 1989) where blue equals immature for oil and gas generation, green equals oil mature, red equals gas mature and dark red equals overmature for gas generation.

3.3.3 Cleaverbank Platform

The southern part of the Cleaverbank Platform (Figure 2-1) is included in the focus area and discussed in more detail in chapter 5. In general the Cleaverbank Platform is characterized by rapid subsidence during Late Permian to Early Triassic and uplift and erosion during the Middle to Late Jurassic (Figure 3-4). In the south of the platform (Blocks J and K) the Jurassic erosion was strongest and removed all sediments up to the Zechstein. Deepest burial and highest temperatures are encountered at present-day. A detailed description of the basin model can be found in Abdul Fattah et al. (2010).

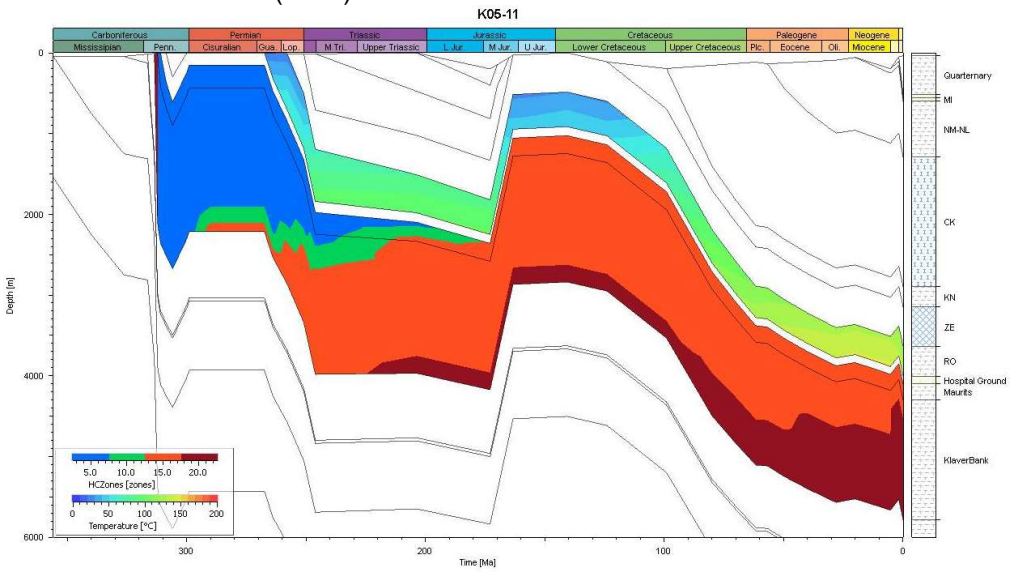

Figure 3-4 Burial history, temperature and maturity evolution for an example wells of the best fit model of the Cleaverbank Platform (K06-11) The maturity calculation of the

Carboniferous source rock intervals is based on the model of Burnham (TIII, Burnham, 1989) where blue equals immature for oil and gas generation, green equals oil mature, red equals gas mature and dark red equals overmature for gas generation.

3.3.4 *Terschelling Basin*

The southwestern part of the Terschelling Basin (Figure 2-1) is included in the focus area and will be described in chapter 5 in detail.

This area is also characterized by rapid subsidence during the Late Permian to Early Triassic, followed by relatively thick Middle to Late Triassic sediments (Figure 3-5). The Middle to Late Jurassic erosion phase removed the Jurassic sediments. Relatively rapid subsidence resumed, interrupted with some minor erosion during the Late Cretaceous inversion. Deepest burial and highest temperatures are at present-day. A detailed description of the basin model can be found in Verweij et al. (2009).

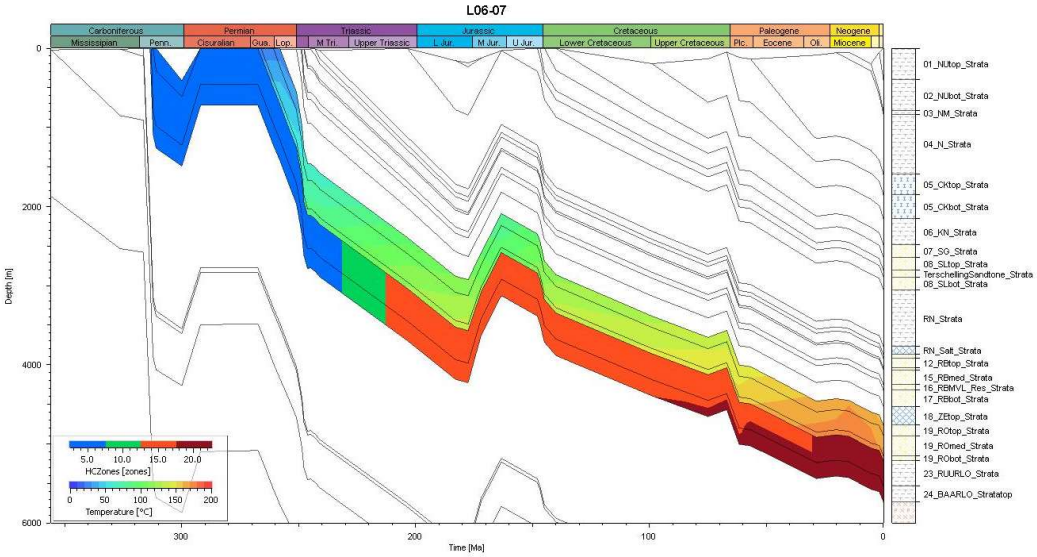

Figure 3-5 Burial history, temperature and maturity evolution for an example wells of the best fit model of the Terschelling Basin (L06-07) The maturity calculation of the Carboniferous source rock intervals is based on the model of Burnham (TIII, Burnham, 1989) where blue equals immature for oil and gas generation, green equals oil mature, red equals gas mature and dark red equals overmature for gas generation.

3.3.5 *Broad Fourteens Basin*

The detailed description of the Broad Fourteens Basin and the offshore part of the West Netherlands Basin models is described in Abdul Fattah et al. (2012). The wells from the Broad Fourteens Basin (Figure 2-1) included in this study are from the basin margins or relative shallow areas from within the basin. The example burial history presented here is of well P06-01 from the basin center. In the basin center the Middle-Late Jurassic erosion had much less effect, compared to the surrounding platforms. Deepest burial as well as highest temperature in this basin center setting is either at present-day or before the Late Cretaceous basin inversion (Figure 3-6).

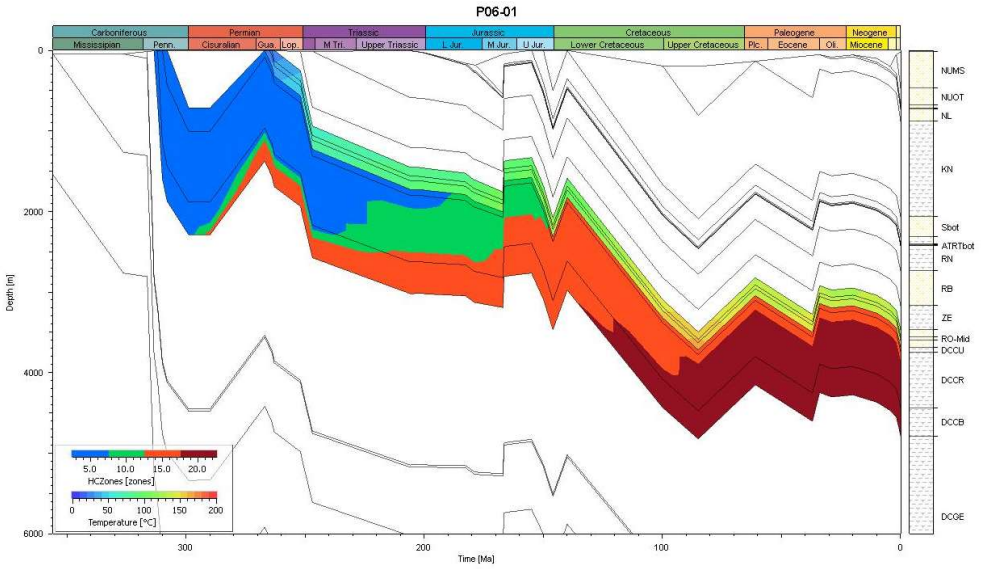

Figure 3-6 Burial history, temperature and maturity evolution for an example wells of the best fit model of the Broad Fourteens Basin (P06-01) The maturity calculation of the Carboniferous source rock intervals is based on the model of Burnham (TIII, Burnham, 1989) where blue equals immature for oil and gas generation, green equals oil mature, red equals gas mature and dark red equals overmature for gas generation.

3.3.6 Past burial maps

The regional evolution of the burial depth before the Middle to Late Jurassic erosion as well as the burial depth immediately after exhumation was extracted from the 3D models in the form of two burial depth maps at these times.

Please note that these are the result of models and are therefore subject to uncertainty, especially with respect to burial before the erosion.

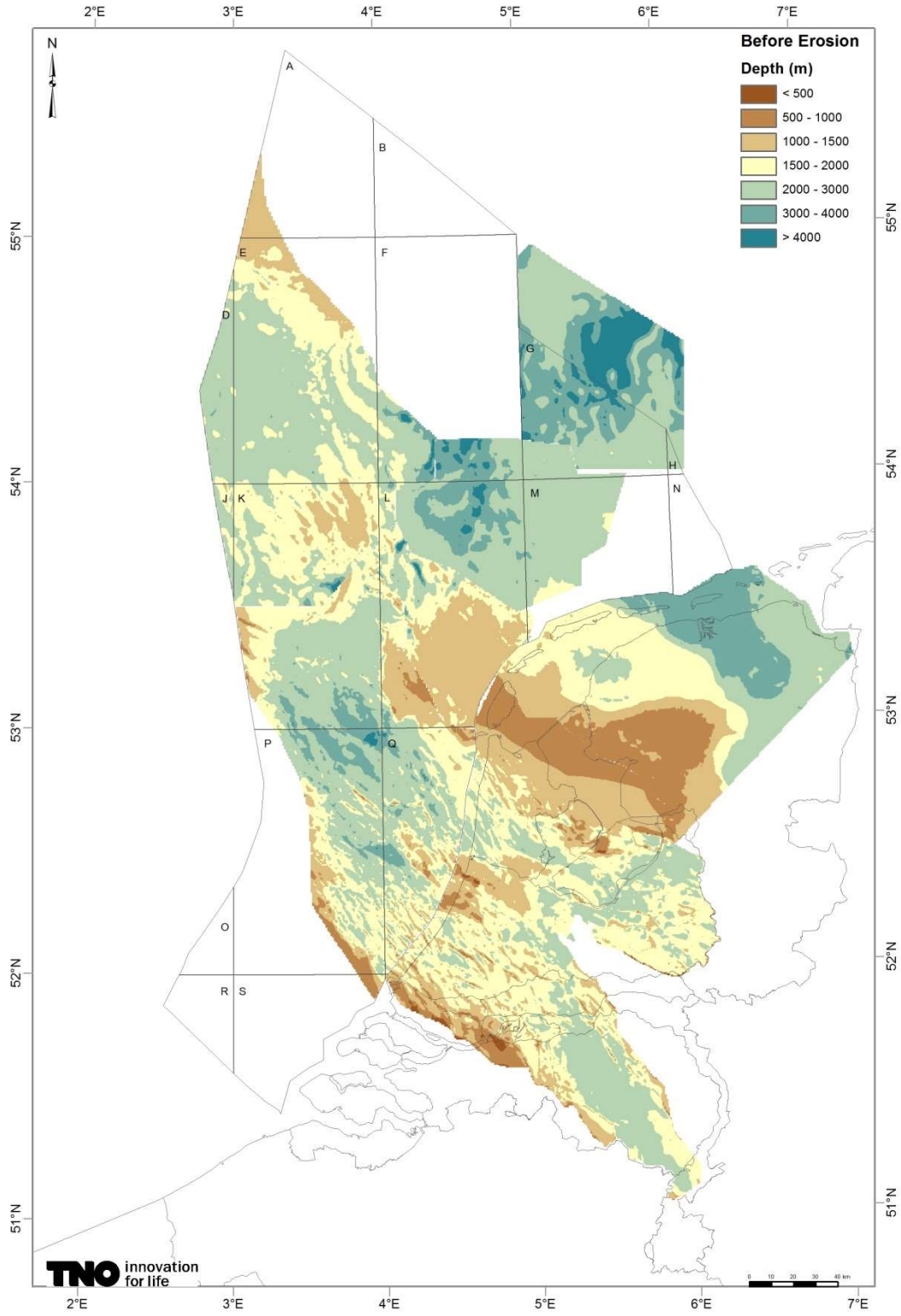

Figure 3-7 Assembled burial maps from all available 3D models for the time of maximum burial before erosion phase in the Jurassic (Middle to Late Cimmerian erosion phase, Figure 3-1) . The colour scale was adjusted to show a clear distinction in the relevant depth ranges.

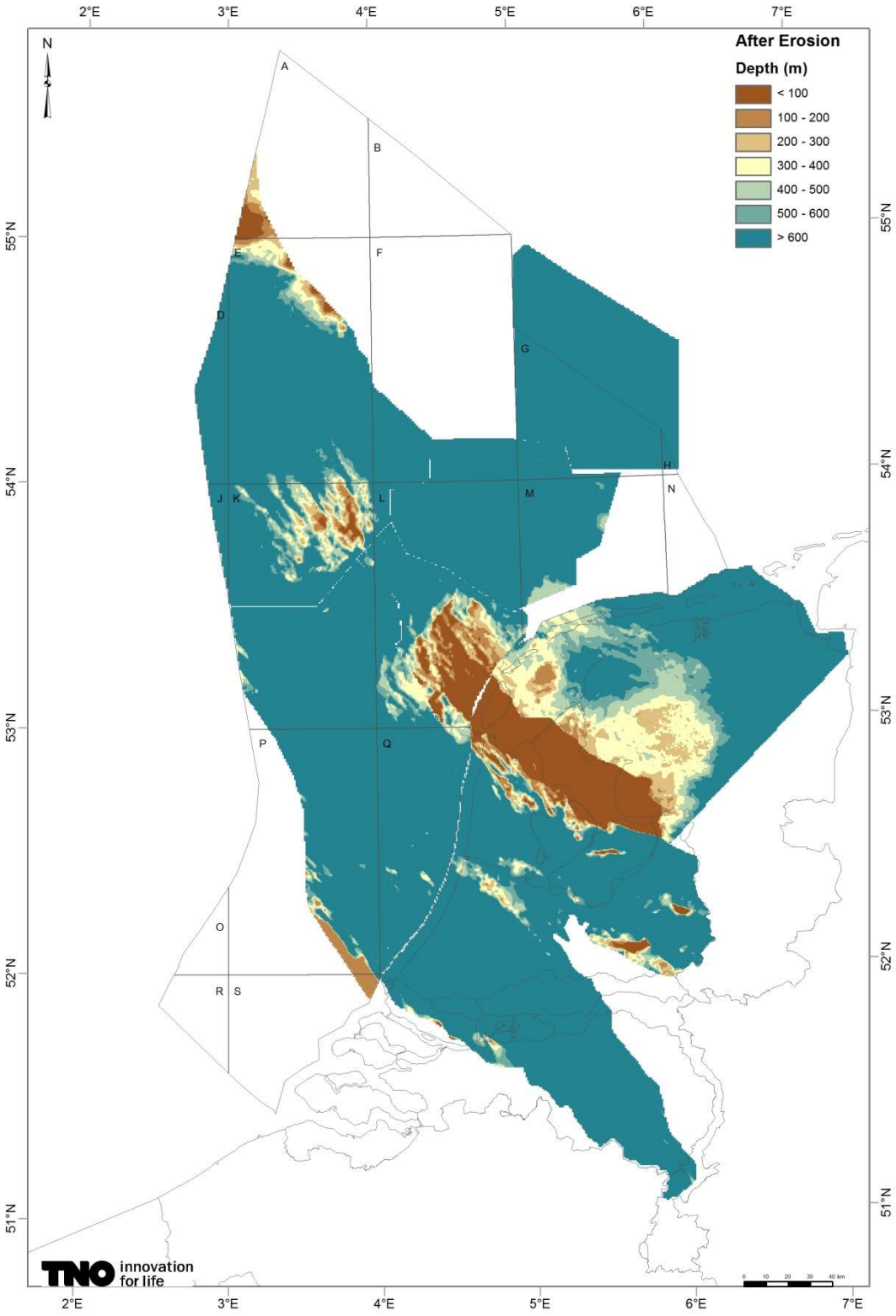

Figure 3-8 Assembled burial maps from all available 3D models for the time of minimum burial just after the exhumation caused by the erosion phase in the Jurassic (Middle to Late Cimmerian erosion phase, Figure 3-1) . The colour scale was adjusted to show a clear distinction in the relevant depth ranges.

4 Reservoir Quality Relation to Cements

4.1 Introduction

A variety of factors drive reservoir quality (related to porosity and permeability) in siliciclastic sediments being, among other, burial depth (compaction), sedimentary environment and composition (grain size, grain texture) and diagenesis (cementation). Theories that were developed during regional diagenetic case studies and were summarised to cover larger areas (see Chapter 1). In this chapter we assess the factors driving reservoir quality in the Rotliegend of the Netherlands with focus on cements. The methodologies include cross-plotting, GIS mapping and statistical analysis. The statistical analysis consists of descriptive parameter statistics, parameters correlations by matrix plots based on Euclidean distance, factor analysis and K-means clustering. It is important to note that we are looking only at wells available in the database, which does not cover all areas in the Netherlands equally (see Figure 2-1).

To assess the effect of different cements on porosity and permeability we compared core analysis data with cement categories by using the subsets Authigenics and Whole-Rock (see Chapter 2.3). Conventional core analyses were available for only about 50% of the dataset. The core analyses (He-porosity and horizontal air permeability) were performed at ambient conditions. Although reservoir pressure can be accounted for by adding a correction factor it may still deviate from the actual value. For two wells core-analyses were performed at quasi-reservoir conditions on a few samples by conducting porosity measurements under high pressure (4400 psi). The correlation between porosity and permeability at ambient and at reservoir pressure was very good (R^2 = 0.99 and 0.96, respectively). Both measurements have a small offset to the 1:1 line with lower porosity and permeability measured at ambient pressures (Figure 4-1). The comparison indicates that although the core measurements under ambient pressure are somewhat lower they can still be utilised for the understanding of reservoir quality.

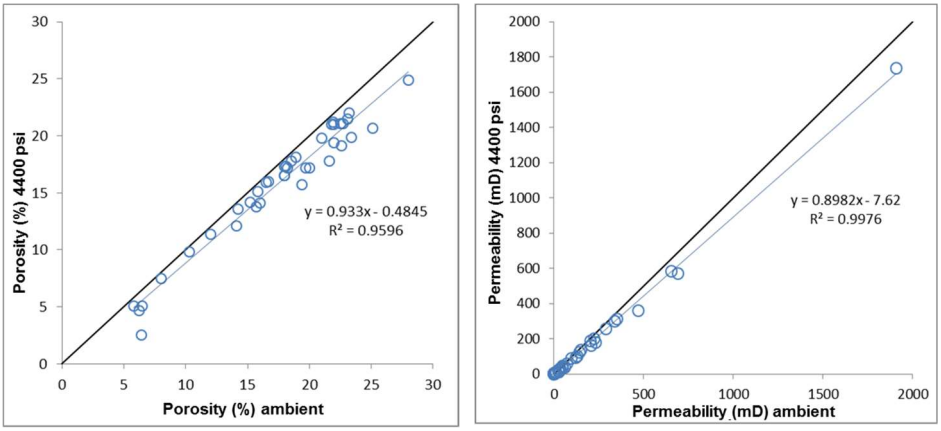

Figure 4-1 He-porosity (left) and air permeability (right) measurements on core plugs under ambient pressure and 4400 psi. Black lines are 1:1 reference lines, blue lines are correlation lines.

4.2 Statistical analyses

4.2.1 Methodology

The statistical analyses were performed on the whole rock subset b (point count porosity excluded). Since the correlation of cements to reservoir quality require the inclusion of values for helium porosity and permeability, only those samples could be used in the analysis for which these values were available. A total number of 623 samples was available.

The maximum burial depth is included in the correlation analysis. In the cluster analysis, the maximum burial depth is excluded. The permeability values in mD were converted to log (k).

Statistical analyses were performed with the statistical software program SPSS Statistics version 20. The results from any statistical analysis need to be interpreted with care since anything with statistical significance does not necessarily imply significance from the geological point of view. Expert judgement is always required to evaluate the outcome. For the principle component and clustering analyses standardized values were used. Variables were standardized by the following equation:

Standardized value = (original value – mean) / standard deviation

Standardization is necessary to correct for different scales of the different variables. For permeability, the log (k) was standardized.

4.2.1.1 Descriptive statistics and correlation matrix

Descriptive statistics were obtained for each of the variables in the dataset and a correlation matrix was produced. Such a matrix calculates the degree of correlation between two variables and is expressed by the Pearson correlation value R. A positive correlation implies that if one variable is high, the other is high too. And if one is low, the other is also low. A negative correlation implies that if one variable is high, the other is low. The value for R above which a correlation (or below for negative correlations) is significant is ambiguous. In any case, the expert judgement is required to validate the correlation. High R values (above 0.8 or below -0.8) are generally significant. Yet a low correlation does not necessarily mean it is insignificant or absent. Correlation plot diagrams will be used to support the correlation matrix.

4.2.1.2 Principle Component Analysis

A PCA is a statistical method to evaluate which of the (correlated) variables (parameters) can explain the largest part of the original variance between the samples. Variables with high inter-correlations might represent one underlying variable, which is called a principle component. The Z score defines the correlation coefficient between the variable and the component, where the squared factor loading (like Pearson's R) represents the percent of variance in that variable explained by the component. The number of principle components is equal to, or lower than the total number of variables. The first principle component explains the largest part of the variance, the second the second largest part and so on. The amount of variance that the component explains is defined by the eigenvalue. A

component with an eigenvalue >1 explains more of the variance between the samples than the separate variables of that component add. A lower eigenvalue does not give additional information on the variance. It can be argued whether the PCS should be performed on the absolute values or standardized values. Both were tested and the results were not significantly different. We only show the results using the absolute values. Results are also very similar for analysis with and without Helium porosity and permeability. The results are shown including these two parameters.

4.2.1.3 Cluster analysis

Cluster analysis enables the identification of groups of samples with relatively similar petrographical characteristics. The results were used to assess diagenetic processes and geographical trends.
The results from different methods for clustering were compared. The difference between the methods is in random versus pre-defined initial cluster centres, a pre-defined number of clusters or not and the measurement of the distance between the variables. The method which gave most useful results was the K-means clustering In this approach the number of clusters needs to be defined a priori. Initial cluster means are random and samples are assigned to the clusters to which they are nearest to. The cluster means are re-calculated based on the assigned samples. Subsequently, the samples are re-assigned to the clusters based on their new cluster means, and the cluster means are re-calculated again. This process is iterated until the cluster means are stable or the maximum number of iterations is reached. The distance between selected variables of the different samples is a measure of how far apart the variables are. The k-means method uses the simple Euclidean algorithm for calculating the distance between two samples:

$$d_{x,y} = \sqrt{\sum_{j=1}^{J} (x_j - y_j)^2}$$

Where x and y represent two values from the two different samples for the same variable, and j = 1 ….. J represent all the variables included in the analysis.
Standardized values of the variables were used for the clustering, to prevent that the variable with the highest values, which probably will also have the largest (absolute) spread, will dominate the clustering procedure. Clustering was performed for a varying number of clusters. The results were compared and the optimal number of clusters was selected.

4.2.2 Results

4.2.2.1 Descriptive statistics

The descriptive statistics for the parameters are given in Appendix A-C. All minerals, except quartz, and (He) porosity range from 0 to a maximum value. The minimum quartz content is close to 0. The largest ranges are present for quartz, rock fragments, matrix (clay, laminae and other), and anhydrite, although only quartz has a high mean value implying that for the other parameters the high values are exceptions. The positive skewness values for all parameters except for quartz, imply that the distribution is asymmetric, with longer, or fatter tails on the right side of the mean value.

The very high values for the kurtosis (the tailedness) demonstrate that a large part of the variance is the result of rare, extreme deviations from the mean value. A kurtosis of 3 represents a normal distribution. The (He) porosity and log permeability are close to normal distributions, with skewness values close to 0 and low kurtosis values. Other parameters with near normal distributions are authigenic quartz and kaolinite.

4.2.2.2 Correlation matrix

The correlation matrix is subdivided into 4 tables because of its size (see Appendix). Only very few parameters how high correlation. These include:

1) The negative correlation between detrital quartz and matrix clay;
2) The positive correlation between visible porosity and helium porosity;
3) The positive correlation between permeability and visible/helium porosity.

These correlations were confirmed by plots (Figure 4-2).
Intermediate negative correlations, which were also confirmed by plots, between:

1) Helium porosity and ankerite;
2) Helium porosity and matrix clay.

Other intermediate correlations, such as the positive correlation between maximum burial depth and detrital feldspar was shown by the plot to be insignificant (Figure 4-2). Whereas a plot of permeability versus maximum burial depth demonstrates a significant negative correlation, although the R value is very low (Figure 4-2). This demonstrates that the results from the correlation matrix should always be evaluated with support from correlation plots.

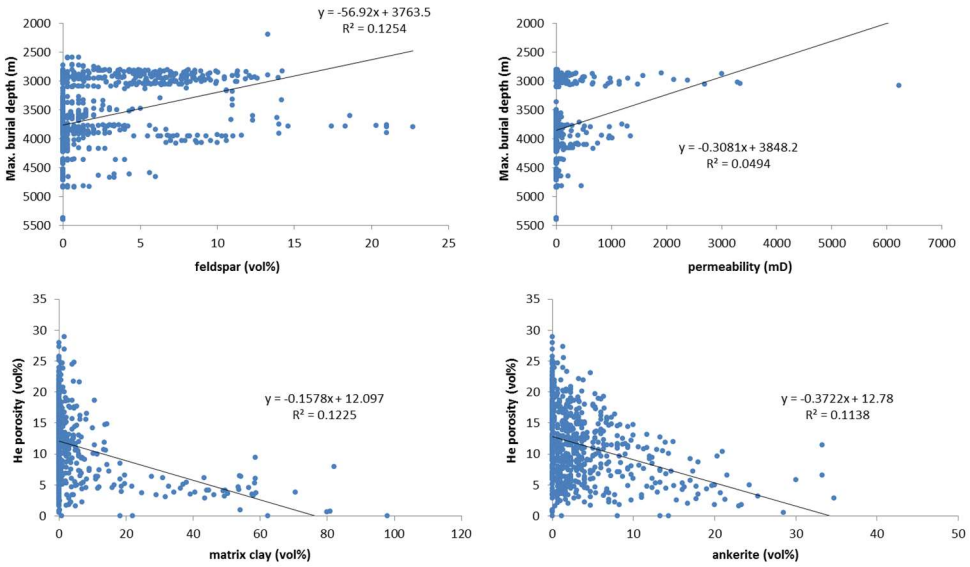

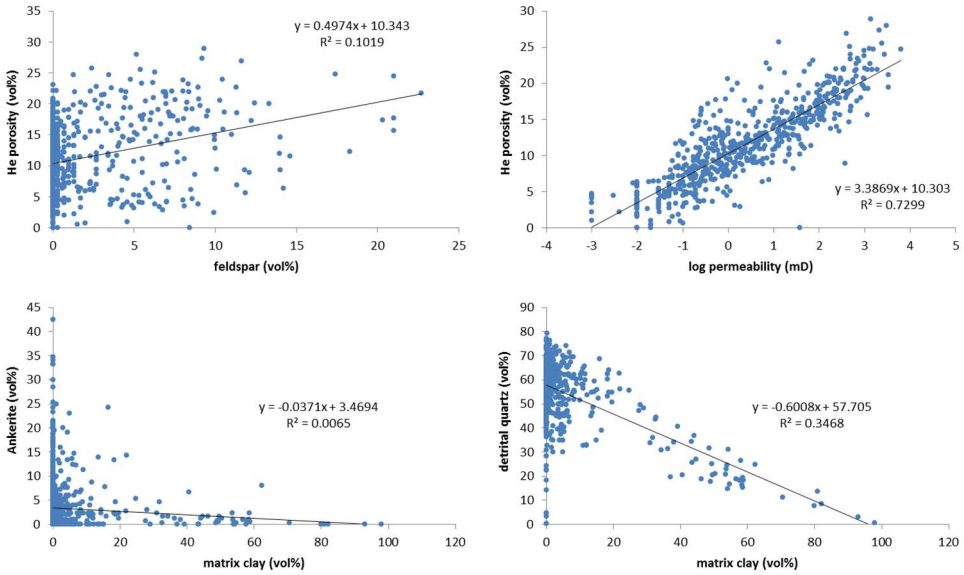

Figure 4-2. Graphs showing (some) correlation between mineral concentrations and/or parameters.

4.2.2.3 *Principle Component Analysis (PCA)*

The results for the PCA analysis are shown in Table 4-1. Additional information on eigenvalues and percentage of variance explained for each component can be found in the Appendix. It shows that there are 12 components (factors) with an eigenvalue above 1, which was set as boundary condition. In total the 12 components with eigenvalues > 1 explain 65% of the total variance. Another way to identify the number of significant factors (and not to overestimate this number by using all components with eigenvalues > 1) can be determined from the scree plot (Appendix D). Where the plot makes an angle due to a drop in marginal gain in variance explained, the additional components do not have significant contribution. In Appendix D, such an angle is not clear, implying that all parameters have a significant contribution to the variance between the samples.

Several components seem to show relevant geological, depositional or diagenetic processes, whereas some are based on analyst bias (e.g. component 3) or insignificant variables (e.g. component 6). The relevant components are discussed:

- The first component has very high scores for (He) porosity and permeability, moderate score for feldspar and moderately negative for ankerite. Hence, the largest part of the variance between the samples can be explained primarily by porosity and permeability, which have moderately positive correlation with feldspar and moderately negative with ankerite. The correlations between porosity and ankerite was also shown in the correlation matrix and supporting plot (Figure 4-2). High feldspar can be due to the originally high detrital feldspar deposition. If feldspar is not converted to clays and provided there is no strong ankerite cementation, the porosity and permeability are retained.

- The second component is characterized by the high positive correlation between matrix clay, mica and pyrite, which correlate moderately negative with detrital quartz. It basically represents clay(-rich) rocks.
- Component four is based on a strong positive correlation between barite and siderite, and moderately strong with authigenic quartz. All three variables represent cement types and the correlation probably implies a specific fluid composition influx. Hypothesis: Feldspar contains high amounts of barium, which then precipitates as barite. Authigenic quartz is a by-product of the conversion of feldspar to kaolinite.

Table 4-1. Z-scores of the rotated principle component matrix, values higher than 0.4 or lower than 0.4 are highlighted.

Rotated Component Matrix

	Component											
	1	2	3	4	5	6	7	8	9	10	11	12
Zscore: d-quartz	.012	-.555	-.432	.088	.317	-.001	.050	-.284	-.248	.104	-.141	-.115
Zscore: d-feldspar	.543	.102	.112	-.256	-.530	.019	.099	.068	-.002	-.032	.029	.031
Zscore: d-mica	-.104	.793	-.057	-.032	.019	-.036	.087	.031	.188	.119	-.071	.102
Zscore: rock fragments	-.019	-.202	.626	-.140	.006	.058	.268	.291	-.110	-.171	.197	.273
Zscore: d-clay	-.066	-.059	.337	-.139	-.098	-.033	-.327	-.237	.248	.294	-.015	.026
Zscore: d-heavy minerals	-.089	.030	-.050	-.068	.017	-.062	-.025	-.001	-.027	.765	-.142	.084
Zscore: d-other	-.090	.091	.011	.065	.258	-.029	.045	.249	.678	-.003	-.191	-.158
Zscore: matrix-clay	-.196	.838	.046	-.056	-.147	.047	-.060	.011	-.055	.039	-.049	-.025
Zscore: matrix-laminae	-.070	-.002	-.043	-.029	-.077	.008	-.005	-.137	.840	-.042	.127	.087
Zscore: matrix-other	.001	-.017	.018	.070	.010	.023	.119	.047	-.032	.556	.332	-.023
Zscore(a_calcite)	-.038	.013	.150	.104	.043	.025	.623	-.091	.005	.007	.067	-.073
Zscore(a_dolomite)	-.228	-.049	-.222	-.187	-.021	-.052	.639	.108	.029	.082	-.134	.050
Zscore(a_ankerite)	-.456	-.143	-.182	-.204	.145	-.095	-.257	.098	-.035	-.151	.427	.056
Zscore(a_siderite)	-.022	-.101	-.098	.740	.017	-.069	.111	-.012	-.010	.052	-.014	-.059
Zscore: carbonate indeterminate	.007	.042	.829	-.060	.007	-.031	-.059	-.054	-.032	.027	-.078	-.101
Zscore: illite/smectite	.026	-.054	-.004	-.056	.012	-.094	.085	-.837	-.042	-.110	-.048	.077
Zscore(a_kaolinite)	.009	-.106	.120	.143	.522	-.056	-.338	.125	.155	.067	-.326	-.269
Zscore(a_chlorite)	-.006	.002	.035	.075	.044	-.001	-.018	.030	.022	.050	.717	-.086
Zscore: clay indeterminate	.272	-.056	-.287	-.301	-.370	.206	.034	.297	-.061	.104	-.054	-.165
Zscore(a_quartz)	-.033	-.169	.040	.436	.266	.029	-.410	.219	-.119	-.052	.151	.010
Zscore(a_anhydrite)	-.176	-.112	.057	.157	-.686	.080	-.140	-.012	-.033	.002	-.206	-.138
Zscore(a_barite)	.090	.026	-.042	.702	-.039	-.019	-.084	.042	.033	-.058	.032	.075
Zscore(a_Fe_OX)	-.260	.035	.056	.036	.041	-.168	.051	.477	-.051	-.267	.008	.286
Zscore(a_pyrite)	.014	.606	-.057	-.015	.202	.020	.020	-.020	-.096	-.105	.053	-.091
Zscore(a_halite)	.063	-.003	.001	.039	.037	.056	-.054	-.005	.002	.081	-.092	.843
Zscore(a_opaques)	-.008	.093	-.078	-.059	.049	.842	-.017	.003	-.048	.001	-.034	-.020
Zscore: other auth.	.064	-.063	.063	-.028	-.153	.803	.017	.037	.035	-.044	.026	.072
Zscore: Visible porosity	.860	-.063	-.023	.081	.025	-.009	-.124	-.004	-.047	-.079	.102	-.063
Zscore(He_porosity)	.902	-.152	.009	-.046	.027	.011	-.139	-.138	-.065	-.001	-.085	.050
Zscore: log perm	.889	-.146	-.076	.065	.087	.043	-.019	.002	-.064	-.054	-.044	.089

- Component five illustrates a negative correlation between feldspar and anhydrite with kaolinite. It implies the conversion of feldspar to kaolinite, which is not as advanced in samples with anhydrite cementation.

- Component seven shows the correlation between calcite and dolomite, which negatively correlate with authigenic quartz. Potentially the cementation by calcium-rich cements prevent the precipitation of authigenic quartz.

4.2.2.4 Cluster analysis

The K-means clustering resulted in two main clusters (with 193 and 350 samples) with rather average compositions and 10 smaller clusters representing only few samples with significantly deviating compositions. The average composition of the two main clusters and the total averages are shown in Table 4-2. The difference between the two main clusters can be explained by the first principle component from the PCA (see Table 4-1): high porosity-permeability with relatively high feldspar and low ankerite content and low porosity-permeability with relatively low feldspar and high ankerite (Table 4-2). The high porosity-permeability cluster in addition shows low average matrix content (detrital clay matrix, laminae and other matrix) and carbonate and anhydrite cement, and relatively high indeterminate authigenic clay. The low porosity-permeability cluster also shows low matrix content, but higher than the high porosity-permeability cluster. Note that these are average values, the 'high porosity-permeability' cluster also contains samples with e.g. low porosity and permeability. These samples were assigned to this cluster based on the other characteristics, such as high feldspar and low ankerite.

The other clusters represent:

- Claystones with low porosity and permeability, low quartz and high matrix content.
- High calcite cluster with low porosity-permeability, but this is due to high dolomite or matrix clay.
- High kaolinite cluster with low porosity-permeability. No other characteristics present to cause low porosity-permeability.
- High anhydrite cluster with low porosity-permeability, however, the high anhydrite often goes together with high matrix clay, kaolinite or indeterminate clay. It is unclear whether anhydrite adds to the low porosity-permeability.
- Siderite and barite go hand in hand with high authigenic quartz content. This cluster has intermediate porosity-permeability on average, but values vary significantly between practically 0 to extremely high.

Further sub-clustering of the high porosity-permeability cluster separately did not give further insight in the characteristics of the samples within this cluster. Further clustering of the low porosity-permeability cluster gave some more insight up to 3 clusters. Above 3 clusters, only small outlier clusters were identified apart from the primary cluster.

Like the principle component analysis, the cluster analysis becomes disturbed by the relatively insignificant categories, like 'other authigenics' or 'opaques' which are the result of difficult characterization or specific components and/or analyst bias. For this reason, manual clustering was performed based on the insights obtained from the PCA, K-means clustering and the correlation plots.

Table 4-2. Total average composition and average composition of the two main clusters from the K-means clustering.

	Average all samples	cluster 'high poro-perm'	cluster 'low poro-perm'
d-quartz	57.1	57.3	59.5
d-feldspar	1.9	**4.3**	**0.5**
d-mica	0.3	0.2	0.1
rock fragments	7.1	6.6	7.8
d-clay	0.3	0.3	0.3
d-heavy minerals	0.1	0.0	0.1
d-other	0.1	0.0	0.1
matrix-clay	3.2	**0.7**	**1.8**
matrix-laminae	0.8	**0.1**	**0.7**
matrix-other	0.1	**0.0**	**0.1**
calcite	0.0	0.0	0.0
dolomite	3.3	**2.1**	**3.8**
ankerite	3.8	**1.8**	**5.4**
siderite	1.0	**0.6**	**1.2**
carbonate indeterminate	0.8	**0.7**	**1.0**
illite/smectite	2.1	2.0	2.4
kaolinite	4.6	4.5	4.6
chlorite	0.0	0.0	0.0
clay indeterminate	1.3	**2.5**	**0.6**
quartz	3.5	**3.3**	**3.7**
anhydrite	0.9	0.6	0.6
barite	0.1	0.1	0.1
Fe_OX	1.4	0.4	2.0
pyrite	0.1	0.1	0.0
halite	0.0	0.0	0.0
opaques	0.1	0.1	0.1
other auth.	0.0	0.1	0.0
Visible porosity	6.0	**11.6**	**3.4**
porosity	11.6	**17.6**	**9.1**
permeability	115.2	74.2	3.5
average log perm	0.4	**74.1**	**0.5**
Number of samples	619	193	350

The manual clustering was performed in the following way:
First all samples with high siderite (>5 vol%) and/or barite (>2 vol%) were selected from the database. Siderite and/or barite came up in the PCA as well as the cluster analysis, without significant effect on porosity and permeability. Then, all samples with extremely low quartz and high matrix (clay + laminae + other) were selected to separate the claystones. Of the remaining samples, all samples with permeability > 70 mD were selected. Of the remaining samples with permeability < 70 mD, clusters were made based on specific characteristics:

- High dolomite/carbonate
- High matrix (clay + laminae + other)
- High anhydrite

- High kaolinite
- High ankerite
- High secondary clays
- High authigenic quartz
- Claystones

In the clustering of the low permeability samples, samples in one cluster were not excluded from the other clusters since a priority between the characteristics was not made. Hence, some samples are represented by more than one cluster.

Table 4-3 shows average compositions of the total number of samples and of the different clusters. In the bottom row the number of samples per cluster is given. Numbers highlighted in green are significantly higher than average, numbers in blue are significantly lower. Looking in more detail at the variation among the samples within each of the clusters it becomes clear that a large part of these significant deviations from the average do not always have significance for the entire population of the cluster. A distinction can be made between the samples from the wells in the north of the Netherlands and well BGM-01, and the wells in the E-, F-, K- L- and P-blocks. The first set of samples, from now on referred to as **subset a**, contains a lot of feldspar and on average less kaolinite and authigenic quartz than the second set of samples which will be referred to as **subset b**, and on average less ankerite. This corresponds with principle component 1, and partially with component 5 (see Table 4-1) except for the relation with anhydrite which is not present in these sets.

Cluster 1, which is based on high permeability shows in addition high average porosity and feldspar content, and low matrix and ankerite content. Separating this cluster into the two sets of samples (as described above) shows that the only correspondence between the two sets is the low matrix clay and laminae content (Table 4-4). The maximum feldspar content in the E-, F-, K- L- and P-blocks is 3.3 vol%, whereas in the North of Groningen and in well BGM-01 the content increases to 22.7 vol%. Separating these in two sub-clusters 1a and 1b respectively shows that 1b with low feldspar content also shows higher ankerite contents than 1a samples, and occasionally high kaolinite, authigenic quartz or anhydrite content. Cluster 1a actually corresponds with principle component 1 (see Table 4-1), whereas 1b does not.
Cluster 2 is based on high barite and/or siderite. In addition, samples show high average kaolinite and authigenic quartz and low feldspar content. The average porosity and permeability values are intermediate, between the samples porosity varies between 2.2 and 24.7 % and permeability between 0.01 and 1570 mD. This cluster corresponds with principle component 4 with positive correlation between barite, siderite and authigenic quartz. Except for 1 sample, all samples are from the subset b.
Cluster 3 is based on low permeability and high dolomite or indeterminate carbonate. No other significant characteristics show in this cluster. It corresponds to principle component 7. Like cluster 1, this cluster can be separated into two subsets. High feldspar in subset a, corresponding with low kaolinite and authigenic quartz. Subset b with low feldspar does not necessarily correspond to high kaolinite and authigenic quartz.
Cluster 4 has low permeability and high anhydrite. High feldspar in subset a and low feldspar in subset b, but without correlations with kaolinite, ankerite and authigenic

quartz. For both subsets these are all below average. Hence, porosity and permeability seem to be strongly reduced by anhydrite cementation. Anhydrite precipitation might be linked to influx of sulphate-rich waters.
Cluster 5: Low permeability and high kaolinite. For subset b this is in line with principle component 5 including low feldspar and anhydrite content. For subset a, the high kaolinite goes hand in hand with high feldspar and anhydrite.
Cluster 6: Samples with low permeability and high matrix content. There is no principle component in line with this cluster. Subset a with high feldspar shows low ankerite content, subset b high ankerite. Kaolinite and authigenic quartz are average for both subsets.
Cluster 7: Low permeability and high ankerite. For subset a the authigenic quartz content is low, for subset b it is higher than average.
Cluster 8: Low permeability and high authigenic clay (illite/smectite and clay indeterminate). There is no principle component in line with this cluster. For subset b the kaolinite content is higher in addition to low feldspar.
Cluster 9: Low permeability and high authigenic quartz. For subset b the kaolinite and ankerite contents are higher and anhydrite content is low, in addition to low feldspar. This is consistent with the reverse of principle component 1 and with component 5.
Cluster 10: Very low quartz content and very high matrix clay/laminae. These samples have extremely low permeability, high mica content and basically represent claystones.
Cluster 11: all low permeability leftovers that did not fit in any of the previous low permeability clusters. This cluster has a relatively high average detrital quartz content.

Maps with the sample distribution were made for each cluster. They can be found in the Appendix.

To summarize, a clear distinction can be made between the samples from the wells in the North of Groningen and in well BGM-01 (subset a) and the samples in the E-, F-, K- L- and P-blocks (subset b). In the first group feldspar contents are high. In addition, *on average*, kaolinite, authigenic quartz and ankerite contents are low and anhydrite contents are high compared to subset b, but the quantities fluctuate a lot. The principle components 1 and 5 are more related to this grouping than to the clustering.
Samples of both subsets are represented in all of the clusters, except for the barite-siderite cluster. The samples in the barite-siderite cluster are only present in subset b and they are absent in the North of Groningen and Friesland. Anhydrite cluster is present in subset a, and in the K-block samples from subset b. It is not represented in the E-, F- and L-blocks.

High porosity and permeability can primarily be linked to a low detrital clay and matrix clay/laminae content. The correlation with high feldspar and low ankerite content (principle component 1) only accounts for subset a. Much more samples from subset a are represented in this cluster than from subset b although subset b is much larger, but high feldspar and low ankerite samples from this subset are also represented in the low porosity and permeability clusters. The negative correlation between feldspar and ankerite, kaolinite and authigenic quartz is very clear in the high porosity and permeability cluster, but it is exactly the opposite for subsets a

and b. This correlation and the distinction between the subsets is less clear in the low permeability clusters.

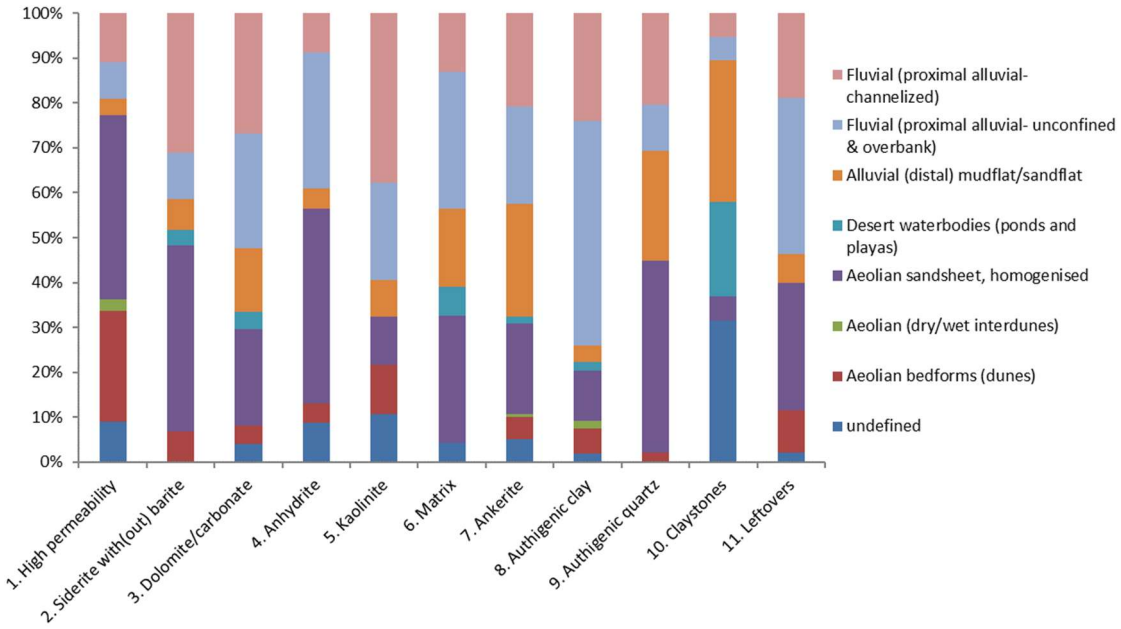

Figure 4-3. Relative distribution of facies for each cluster.

In Figure 4-3 the relative distribution of facies per cluster is shown. The high permeability cluster has a large share in Aeolian deposits. The siderite/barite and anhydrite clusters also have a relatively large share in Aeolian deposits, but less than the permeable samples. The other, low permeability clusters have higher shares in primarily fluvial deposits.

Table 4-3. Average compositions of the manual clusters. Green: significantly higher than average. Blue: significantly lower than average.

	total	Cluster 1	Cluster 2	Cluster 3	Cluster 4	Cluster 5	Cluster 6	Cluster 7	Cluster 8	Cluster 9	Cluster 10	Cluster 11
		High permeability	Siderite ± barite and authigenic quartz	low permeability and high dolomite	Low permeability and high anhydrite	Low permeability and high kaolinite	Low permeability and high matrix content	Low permeability and high ankerite	Low permeability and high authigenic clay	Low permeability and high authigenic quartz	Very low permeability claystones	Low permeability leftovers
d-quartz	56.97	57.98	58.92	55.27	55.60	55.53	53.66	56.54	60.24	56.44	19.23	63.29
d-feldspar	1.91	3.01	0.27	1.48	3.27	0.97	0.92	0.70	2.27	0.46	2.71	1.13
d-mica	0.36	0.12	0.12	0.42	0.09	0.47	1.51	0.19	0.25	0.06	2.86	0.19
rock fragments	7.04	6.71	4.92	8.99	6.19	5.27	5.72	7.03	5.83	6.68	1.27	7.69
d-clay	0.26	0.04	0.00	0.32	0.17	0.22	1.11	0.37	0.15	0.11	0.11	0.34
d-heavy minerals	0.06	0.02	0.02	0.06	0.05	0.07	0.12	0.08	0.06	0.06	0.05	0.08
d-other	0.13	0.06	0.21	0.19	0.04	0.66	0.43	0.11	0.00	0.12	0.18	0.03
matrix-clay	3.39	0.43	0.24	2.82	1.33	1.08	13.49	1.59	1.07	0.74	52.81	1.35
matrix-laminae	0.73	0.10	0.25	0.34	0.07	0.93	2.60	0.85	1.11	0.24	7.62	0.51
matrix-other	0.08	0.02	0.10	0.00	0.12	0.00	0.63	0.03	0.01	0.12	0.00	0.03
calcite	0.01	0.00	0.00	0.03	0.00	0.00	0.02	0.00	0.01	0.00	0.00	0.00
dolomite	3.26	2.23	0.87	7.98	1.94	1.85	3.38	2.72	2.88	1.38	2.85	2.15
ankerite	3.80	1.36	1.89	3.07	1.58	3.10	3.62	11.44	2.24	4.57	0.87	2.04
siderite	0.58	0.31	6.68	0.74	1.15	1.03	0.36	0.86	0.32	1.63	0.00	1.39
carbonate indeterminate	0.85	0.13	0.34	2.92	0.61	0.39	1.45	0.08	0.70	0.77	0.00	0.32
illite/smectite	2.07	2.04	1.08	1.90	1.84	1.28	0.98	1.63	3.36	0.55	0.14	2.25
kaolinite	4.61	4.01	3.69	3.84	2.65	13.82	3.42	4.62	3.42	5.39	3.11	4.97
chlorite	0.01	0.01	0.00	0.00	0.00	0.00	0.00	0.02	0.00	0.03	0.00	0.01
clay indeterminate	1.26	2.15	0.28	1.08	2.51	0.02	0.11	0.67	3.60	0.62	0.79	0.33
quartz	3.46	2.91	3.99	2.61	2.75	4.80	2.34	3.98	1.67	10.77	0.42	3.15
anhydrite	0.93	0.69	1.81	0.64	14.79	1.25	0.69	0.19	0.39	0.73	0.74	0.43
barite	0.14	0.07	1.52	0.04	0.06	0.23	0.06	0.09	0.01	0.53	0.00	0.11
Fe_OX	1.43	0.33	1.51	1.79	0.53	1.82	0.47	2.01	0.20	1.62	3.00	1.86
pyrite	0.07	0.06	0.06	0.07	0.00	0.02	0.28	0.04	0.09	0.04	0.21	0.05
halite	0.03	0.16	0.00	0.00	0.00	0.00	0.00	0.00	0.00	0.00	0.00	0.02
opaques	0.13	0.19	0.02	0.06	0.07	0.05	0.20	0.07	0.09	0.11	0.50	0.14
other auth.	0.04	0.13	0.00	0.01	0.15	0.00	0.00	0.02	0.03	0.03	0.00	0.02
Visible porosity	5.96	12.79	7.27	3.30	2.45	5.10	2.38	4.03	4.74	6.09	0.51	6.07
porosity	11.59	19.39	11.57	8.93	8.30	10.47	7.81	8.58	12.29	9.80	4.01	12.04
average log perm	2.41	331.39	5.71	0.55	0.37	0.91	0.16	0.41	1.06	1.52	0.03	2.06
Number of samples	622	110	29	149	23	38	46	139	54	49	20	95

Table 4-4. Average compositions for the total number of samples, cluster 1 and cluster 1a and 1b.

	total	Cluster 1	1a	1b
d-quartz	56.97	57.98	56.15	60.83
d-feldspar	1.91	5.01	8.07	0.24
d-mica	0.36	0.12	0.16	0.06
rock fragments	7.04	6.71	7.50	5.47
d-clay	0.26	0.04	0.00	0.10
d-heavy minerals	0.06	0.02	0.03	0.01
d-other	0.13	0.06	0.00	0.14
matrix-clay	3.39	0.43	0.69	0.03
matrix-laminae	0.75	0.10	0.00	0.26
matrix-other	0.08	0.02	0.00	0.06
calcite	0.01	0.00	0.00	0.00
dolomite	3.26	2.23	2.63	1.60
ankerite	3.80	1.36	0.56	2.61
siderite	0.98	0.31	0.28	0.37
carbonate indeterminate	0.85	0.13	0.12	0.15
illite/smectite	2.07	2.04	2.16	1.86
kaolinite	4.61	4.01	2.38	6.55
chlorite	0.01	0.01	0.00	0.01
clay indeterminate	1.26	2.15	3.39	0.22
quartz	3.46	2.91	1.34	5.35
anhydrite	0.93	0.69	0.54	0.93
barite	0.14	0.07	0.00	0.17
Fe_OX	1.43	0.33	0.21	0.53
pyrite	0.07	0.06	0.05	0.08
halite	0.03	0.16	0.24	0.02
opaques	0.13	0.19	0.17	0.23
other auth.	0.04	0.13	0.20	0.01
Visible porosity	5.96	12.79	13.27	12.05
porosity	11.59	19.39	20.20	18.13
average log perm	2.41	331.39	404.15	243.24
Number of samples	**622**	110	67	43

4.2.3 *Discussion*

In general, it can be said that the data is not easy to interpret. The correlation matrix shows only a few significant correlations. Plots show correlations which were not identified using the matrix and vice versa. Trends were found but many exceptions were observed.

The cluster analysis resulted in average compositions for low and for high porosity and permeability samples. The low porosity and permeability cluster has lower average feldspar content and higher average matrix and carbonate content compared to the high porosity and permeability cluster. The low porosity and permeability cluster contains primarily samples with low feldspar content, whereas the high porosity and permeability cluster also contains many samples with low

feldspar content although the average is high. This demonstrates a correlation between porosity/permeability and feldspar content which was not recognized in the correlation matrix and the plots; high feldspar content is often related to high porosity and permeability, whereas low feldspar content is not related to either high or low porosity and permeability. For carbonates, anhydrite and matrix content a similar mechanism applies: a high content generally leads to low porosity and permeability whereas a low content does not necessarily lead to high porosity. These correlations were not identified in the correlation matrix, and for feldspar this was also not well visible in the plots.
Principle component 1 (see Table 4-1) is related to these trends with high porosity and permeability related to high feldspar and low ankerite. The other way around, low feldspar and high ankerite would imply low porosity and permeability. Obviously the correlation of feldspar with ankerite is stronger than with other carbonates. All the other significant principle components relate low porosity and permeability to either high matrix or carbonate content. In addition, they demonstrate additional correlations, such as a positive correlation between siderite and barite, and between dolomite and calcite and a negative correlation between anhydrite and kaolinite. Each of these correlations could imply certain diagenetic processes.
Note that the trends are averages. When looking in more detail at the sample level, exceptions to the trends can be observed. For example several samples from the BLF well have intermediate feldspar, low carbonate and matrix content, very high porosity but very low permeability. The low permeability is probably due to high detrital clay content and potentially to pore filling kaolinite. Although kaolinite in general does not seem to have a strong impact on reduction of porosity and permeability.

Feldspar conversion to kaolinite and authigenic quartz is a well-known diagenetic process which seems to be much more advanced in the western part of the Netherlands than in the North-east. Yet, this conversion does not seem to be the main reason for the permeability reduction. Cementation by carbonates or anhydrite or the presence of detrital clay or matrix has much more effect on reservoir quality.

4.3 Porosity and permeability relation to authigenic minerals

To determine the effect of cementation on the reservoir quality single cements were plotted against porosity and permeability. The plots show an envelope trend, depicted by a dashed line in the plots. The maximum porosity in a well sorted, uncemented sandstone is possibly 30% (maximum 40%) at depth. For example total carbonate the cementation decreases the porosity volume from 30% to zero with 30% volume of carbonate cement. The values above the envelope indicate a large number of grain-replacing cements. The cement contents here do not differentiate between the pore-filling and grain-replacive cements because the petrographic data was only partially subdivided into these categories. This may be one of the reasons for not seeing a better correlation between the cements and the reservoir quality. Furthermore, the area under the envelope is influenced by other porosity and permeability determining factors, such as grain-sorting, grain-size, cement habitus/texture, other cements and especially detrital clay content.

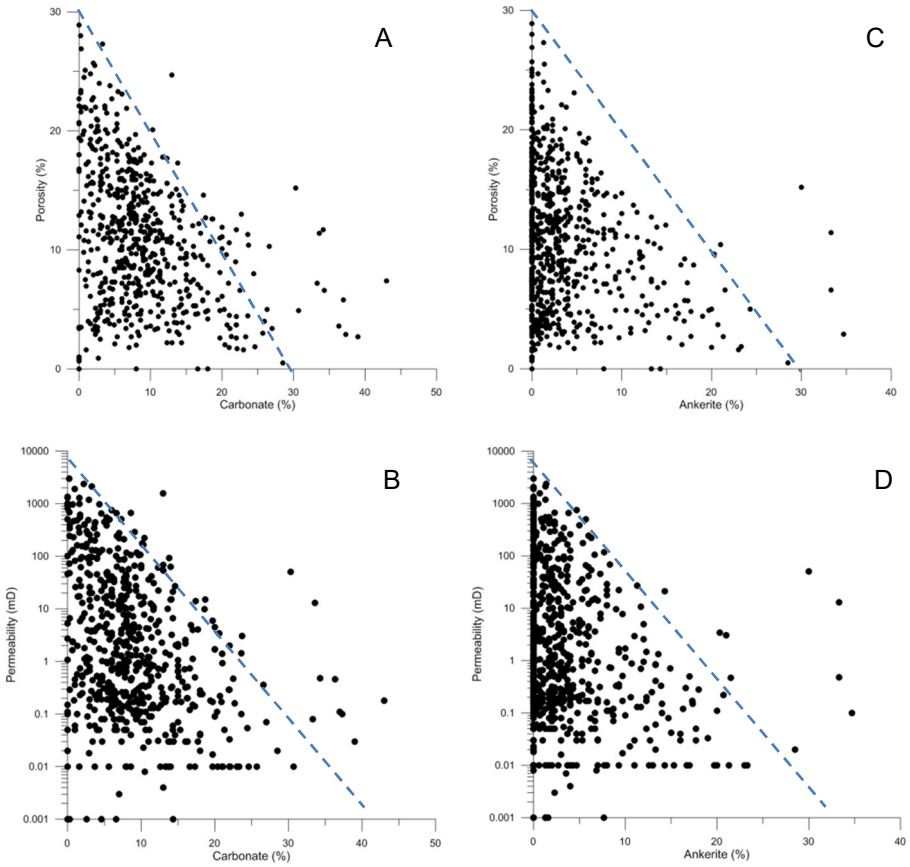

Figure 4-4 Effect of carbonate cements on reservoir quality (Whole-Rock subset). A and B: All authigenic carbonates vs porosity and permeability. C and D ankerite cement vs porosity and permeability, respectively. Dashed lines depict envelope trends.

None of the signally plotted authigenic minerals, being illite, kaolinite, chlorite, quartz, pyrite, anhydrite, barite, calcite, dolomite, siderite, ankerite and Fe-oxides, clearly showed a porosity or permeability enhancing effect. However, when taken together, the authigenic clay minerals had a general trend towards higher porosities with increasing authigenic clay content (Figure 4-5A). Authigenic clay minerals replace feldspar and rock fragments. The dissolution of feldspar does not always lead to re-precipitation of all the dissolved components and particularly clay minerals precipitate in small crystal aggregates that contain a large amount of microporosity. On the contrary, permeability is either not affected (e.g. by kaolinite) or is reduced by clays such as illite. For the given dataset precipitation of illite indeed does not impact on the porosity but reduces permeability (Figure 4-5B). Decreasing permeability by illite is commonly observed in siliciclastic sediments and calls for more detailed investigations of illite genesis.

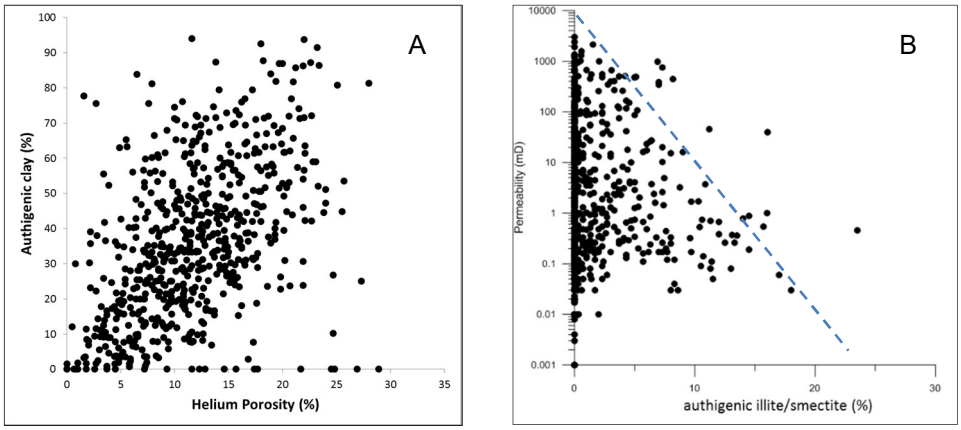

Figure 4-5 A: He-porosity vs. total authigenic clay (Authigenics subset). B: Permeability vs. authigenic illite/smectite (Whole-Rock subset). Dashed lines depict envelope trends.

A further group of minerals that has a negative effect on reservoir quality are carbonate cements (Figure 4-4). Porosity and permeability generally diminished with increase of total carbonate cement. The main carbonate mineral that reduces reservoir quality is ankerite (Figure 4-4C, D), as also recognised in the statistical analysis (Chapter 4.2.2).

Anhydrite also tends to reduce porosity locally (Figure 4-6). The statistical analyses also identified a cluster (cluster 4) with low permeability and high anhydrite (Table 4-3). Several cements, such as authigenic quartz, do not correlate with porosity or permeability for the studied dataset.

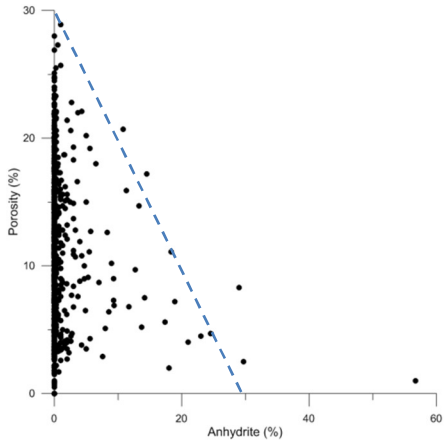

Figure 4-6 Anhydrite content of whole rock vs. He-porosity (Whole-Rock subset). Dashed lines depict envelope trends.

The observed correlations with porosity and permeability are not or less significant when looking at the correlation coefficients ($R^2 < 0.5$). We nevertheless classify a trend as an effect on reservoir quality. This is because other factors, such as grain size and compaction, play an equally important role in steering the reservoir quality and can only be partially taken out of the equation.

4.4 Grain size control

One of the main parameters that controls reservoir quality is the (detrital) grain size. Clay- and silt-sized siliciclastics, tied to their poorly sorted nature, have lower porosities and permeabilities compared to the sand sized sediments (Figure 4-7, Figure 4-8). Within the sand-sized sediments the total range of porosity and permeability does not vary much, nevertheless, on the whole, an increase in the average composition of porosity and permeability is evident. From fine-sand upper to coarse sand-size the differences are insignificant. The grain-size effect is more apparent for porosity than for permeability.

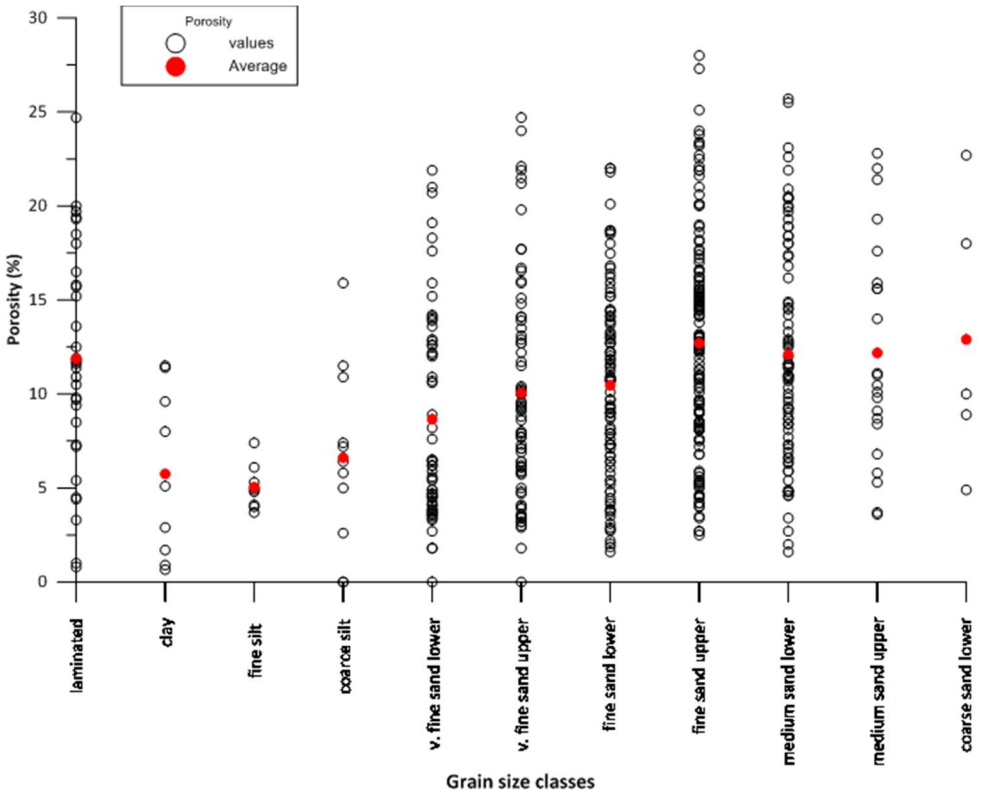

Figure 4-7 Grain size plotted against He-porosity. Red circles represent averages of He-porosity for each grain size class.

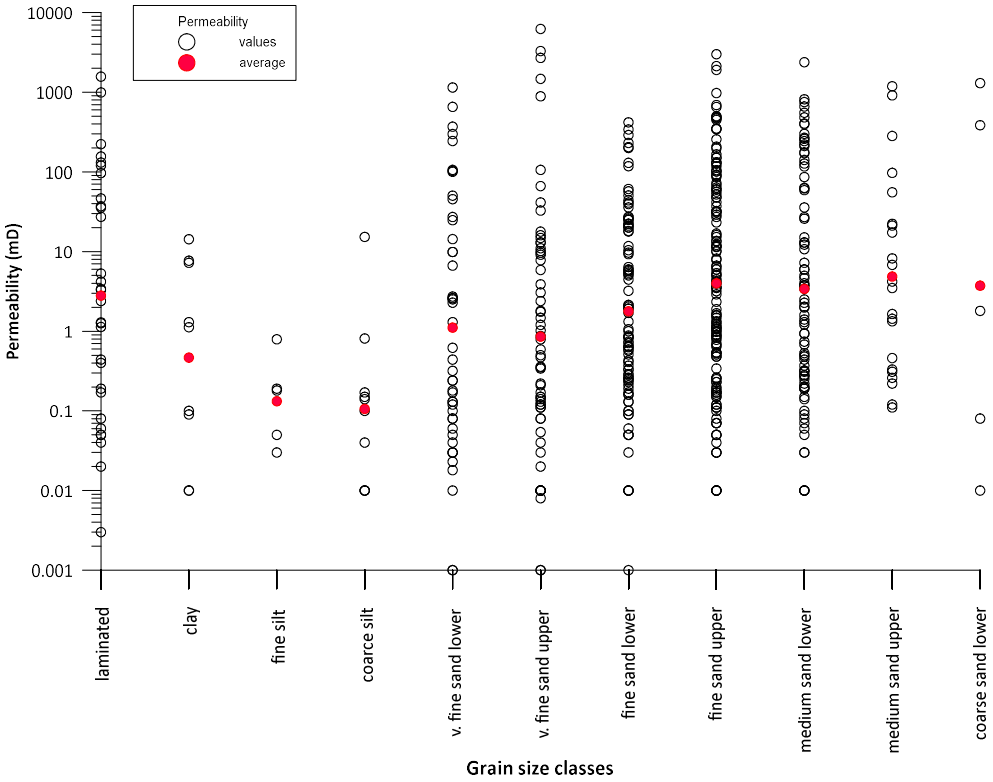

Figure 4-8 Grain size plotted against horizontal permeability. Red circles represent averages of air permeability for each grain size class.

To investigate whether the grain-size effect may have obscured the relationship between reservoir quality and different cement types we compared the cement content and reservoir quality for different grain sizes. The example on carbonate cement indicates that by removing the smaller grain sizes a somewhat better correlation is achieved between carbonate and He-porosity (Figure 4-9A, B). However, on the whole the trend remains similar. For other minerals, for example anhydrite the relation to porosity is entirely independent of grain size (Figure 4-9 C, D). In summary, although grain size has an impact on reservoir quality it does not obscure the relationship to of the reservoir quality to authigenic minerals in this study.

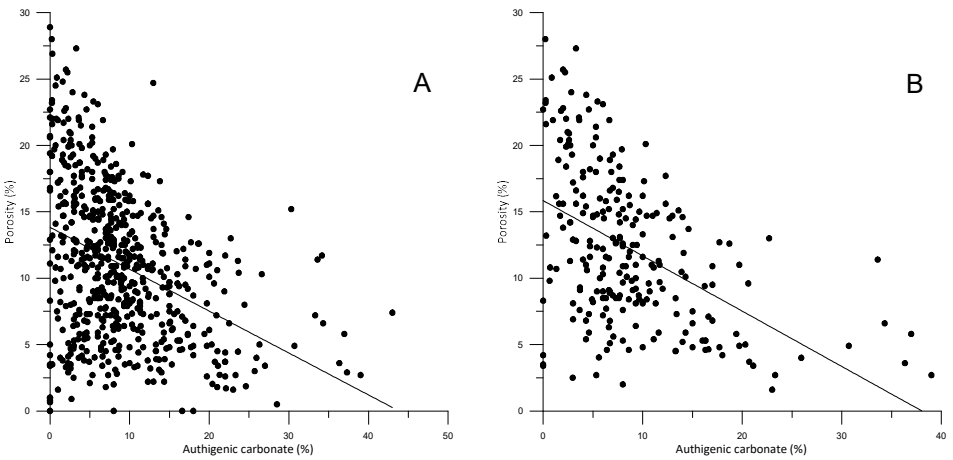

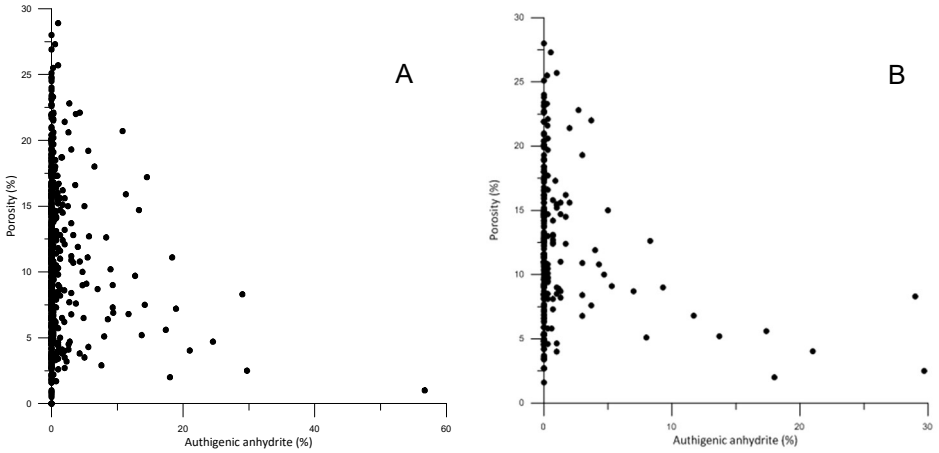

Figure 4-9 He-porosity relation to total authigenic carbonate and anhydrite cement (Whole-Rock subset) for A: carbonate for all grain sizes; B: carbonate for grain size fine sand upper to coarse sand; C: anhydrite for all grain sizes; D: anhydrite for grain size fine sand upper to coarse sand.

4.5 Cement relation to burial

Compaction of siliciclastic sediments generally increases with burial depth. The present day depth of the reservoir is not representative due to the historical inversion and uplift. Here we compare the maximum burial depth, taken from basin modelling to reservoir quality and different cements. As already determined by statistical analyses, both porosity and permeability decline with maximum burial depth. Although the relationship between permeability and maximum burial depth is less certain (Figure 4-10). In sandstones, the main compaction occurs within the first 2 km of burial (e.g. Ajdukiewicz & Lander, 2010). The difference in the burial depth in this study is between 2.2 and 5.4 km, which may be a reason for the poor correlation.

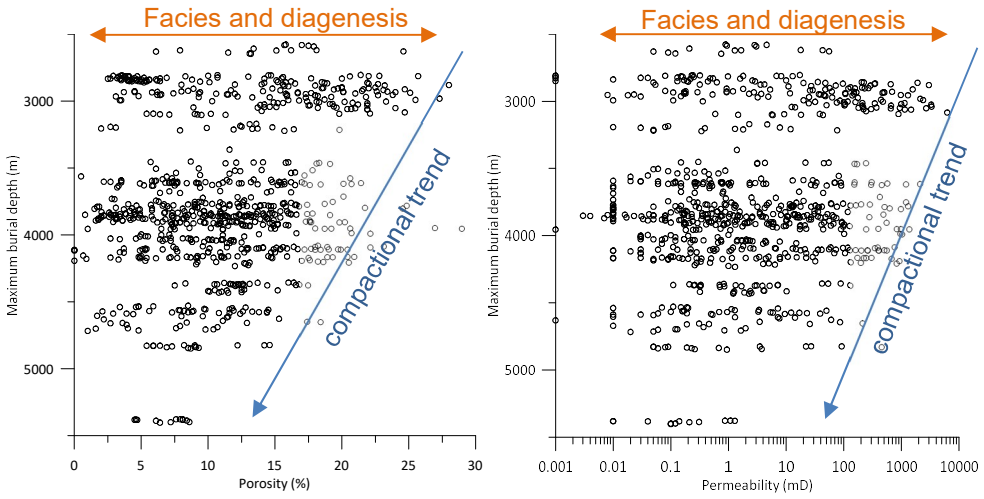

Figure 4-10 Maximum burial depth compared to He-porosity (left) and horizontal air permeability (right).

The compactional burial trend is depicted by the blue arrows in Figure 4-10. The range of porosity and permeability is further driven by the facies (grain-size, grain-sorting, ductile grain content) and the diagenesis (cementation). The porosity and permeability reducing trend with maximum burial depth has been studied in more detail by Kempen et al. (2016) on larger datasets. The authors identified the overall compactional effect on the reservoir quality but also referred to the underlining cementational porosity loss.

The impact of compaction has often been measured by the size of the intergranular volume (IGV). The IGV represents the sum of primary porosity (intergranular porosity), the cemented intergranular space and the clay matrix. The lower the IGV, the larger is the effect of mechanical compaction. The reduction of IGV is not only driven by burial depth but also by the amount of ductile detrital components (e.g. clay grains, mica, pseudomatrix). To be able to calculate IGV the petrographic point-count analyses needs to differentiate between different types of pores and cements (e.g. pore-filling and grain-replacive). IGV can be further masked by totally dissolved cemented grains with the same cement also filling the pore-spaces. The analyst also has to be able to recognise all these differences, which is not commonly the case. We did not calculate the IGV in this study, mainly because this level of detail was not provided for at least half of the samples.

To a certain degree, cementation is also related to burial depth. However, we do not observe a trend with burial depth for total cement or any of the single cements (see examples Figure 4-11,Figure 4-12). There are several reasons for the lack of correlation. Firstly, cementation can occur mainly or only during early burial. Secondly, many minerals are not temperature (i.e. depth) dependent and finally, other aspects play a more important role. A common hypothesis in respect to burial depth was postulated for illite, which precipitates at expense of kaolinite with depth (Gaupp & Okkerman, 2011). Although this may be the case locally, the kaolinite(+ dickite)/illite(+ smectite) ratio does not decrease (or increase) with burial depth across the studied wells. In the previous chapter (4.2) we observed a decline of detrital feldspar with burial depth, which is likely due to the greater dissolution of feldspar at higher pressures and temperatures. Although illite can also replace feldspar, kaolinite is a much more common substitute (see chapter 1.3). It is possible that the conditions (e.g. pH, salinity, K+ activity) after feldspar dissolution favoured kaolinite precipitation and this is one of the reasons we observe a steady kaolinite content in deeper buried samples. Counterintuitively, illite content shows a decrease with burial depth. This can be observed in the whole-rock dataset but not in the authigenics dataset. The relationship may thus not be indicative.

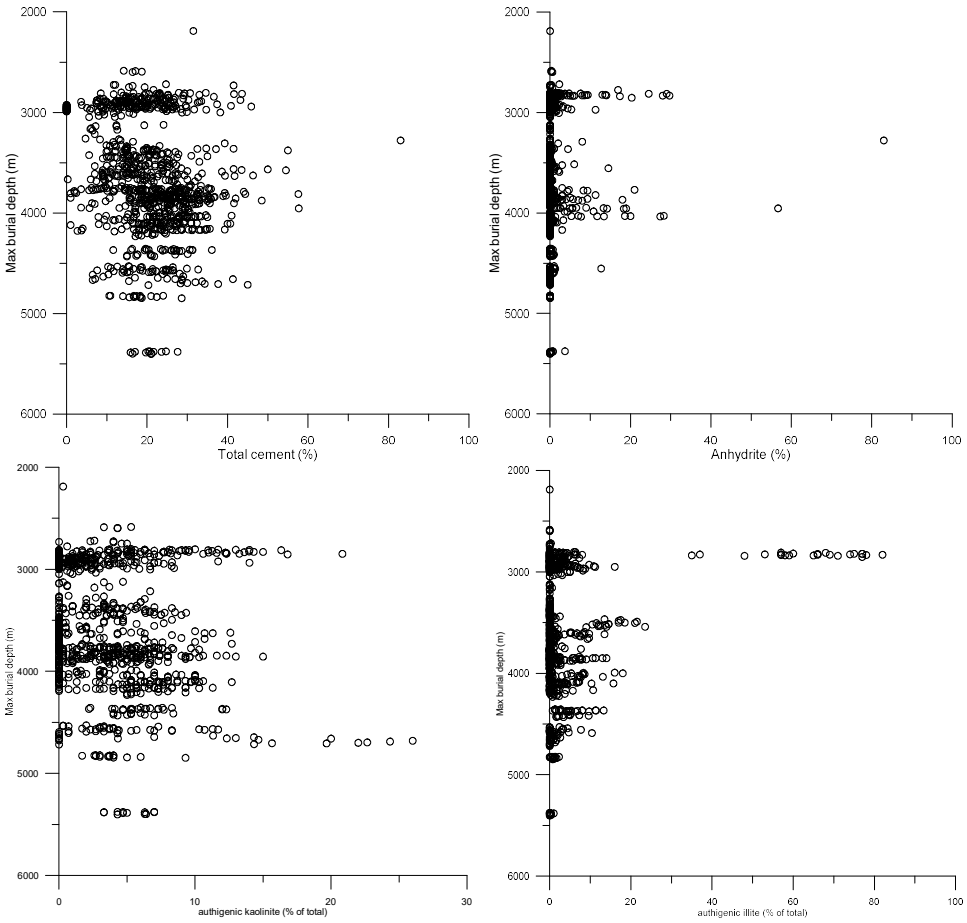

Figure 4-11 Maximum burial depth in relation to authigenic minerals (whole-rock subset).

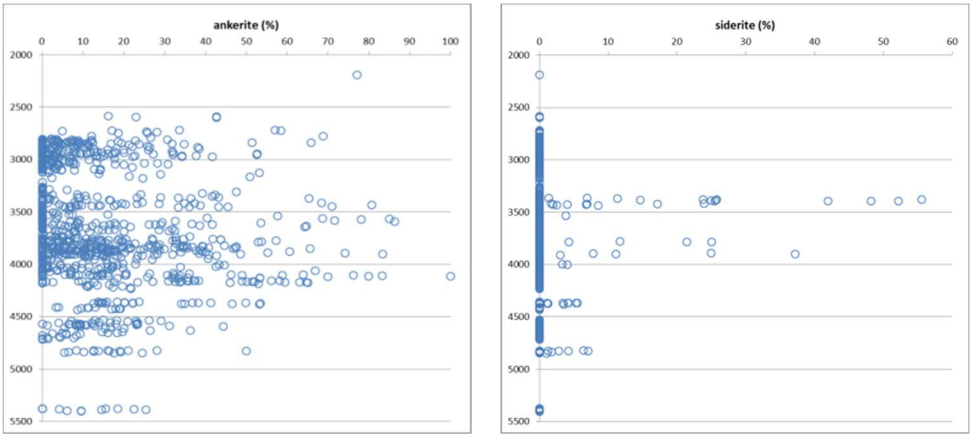

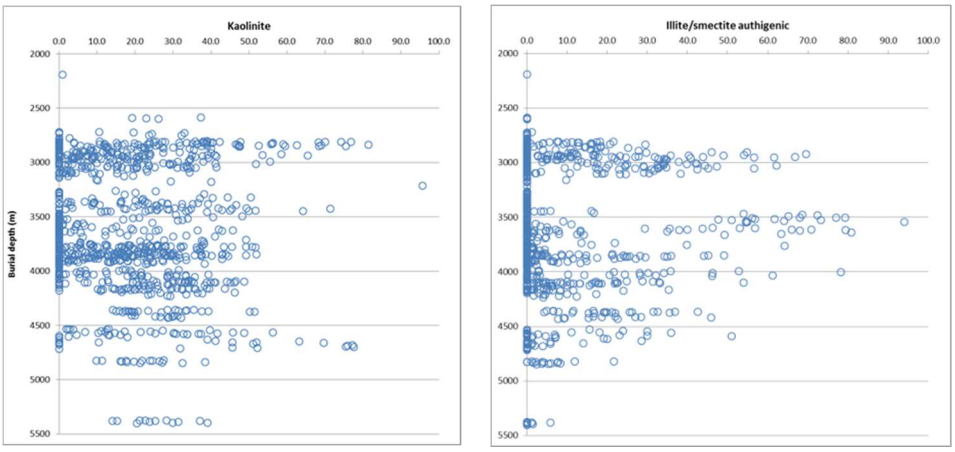

Figure 4-12 Maximum burial depth in relation to authigenic minerals (Authigenics subset)

Although cementation does not increase or decrease in with maximum (or present) burial depth there is a relationship to structural elements for the authigenic clay distribution. In basin lows (e.g. Broad Fourteens Basin, Terschelling Basin) illite a tendency to be the dominant clay mineral, whereas in structural highs (e.g. Groningen Platform) kaolinite is more prominent (Figure 4-13). The reason for a higher illite contents in deeper set areas is the kinetically driven illite growth with deep burial. The duration of deep burial is thus more important the present or maximum burial depth.

This relationship is leading but is not applicable to all offshore and onshore wells in the Netherlands. For example, three wells in the Lauwerszee Through have high illite abundances, whereas well L06-06, situated in the Terschelling Basin contains mostly kaolinite (Figure 4-13). Duration of deep burial may be leading but other aspects, such as depositional environment and proximity to other formations and sub-active faults, also play a significant role in the formation of illite and will be discussed later.

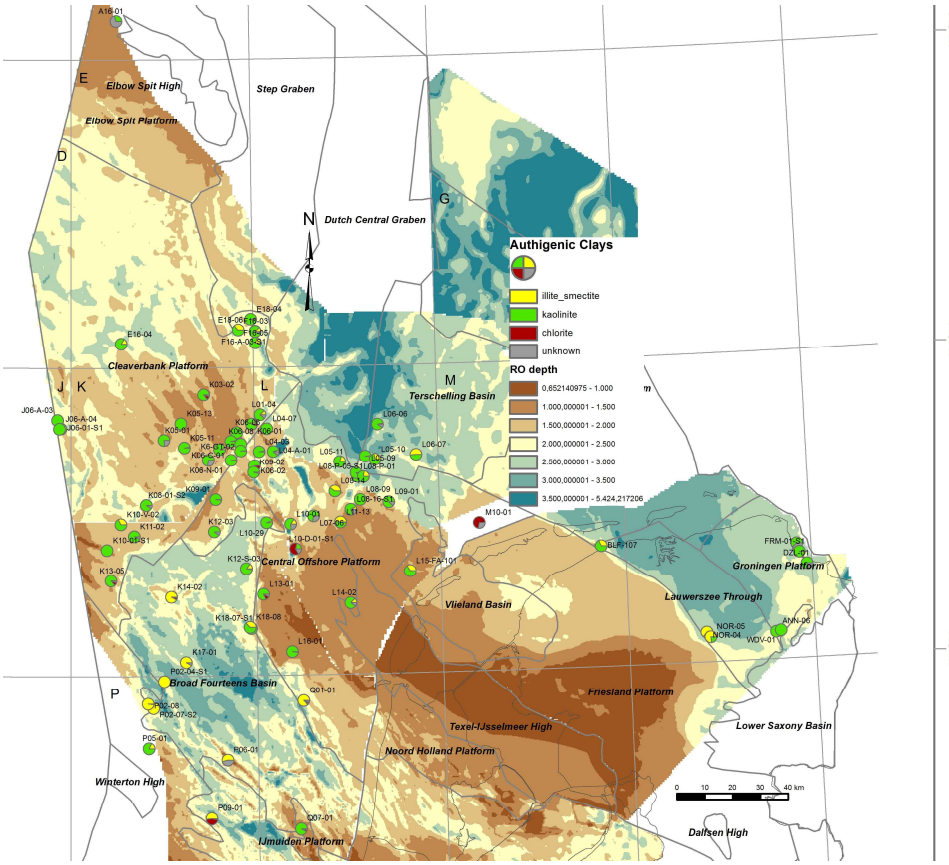

Figure 4-13 Authigenic clay distribution (from the Clay-minerals subset) plotted on maximum depth of the Top Rotliegend before the Middle-Late Jurassic uplift phase according to 3D basin modelling and the top Rotliegend depth map.

4.6 Environmental control on cementation

The depositional environment has an influence on the both detrital minerals and on the distribution of eodiagenetic and shallow-burial cements (Gaupp et al., 1993). Although it does not have a direct influence on mesodiagenetic processes, early cements can be dissolved and re-precipitated in-situ (e.g. eodiagenetic gypsum to mesodiagentic anhydrite).

Reservoir quality is considered to be better in specific depositional environments. Aeolian sediments are generally better sorted and contain lower amounts of detrital clay, which tends to have a positive impact on porosity and permeability. In the Rotliegend of the Netherlands higher porosities and permeabilities are observed in aeolian sandstones and lower porosities and permeabilities in fluvial and Sabkha sediments (Figure 4-14). Fluvial sediments are more clay rich and less well sorted, whereas the playa and Sabkha siliciclastics can be very clay rich and contain depositional carbonates and sulphates. Nevertheless, good reservoir quality can occur in fluvial and playa deposits. Similarly, aoelian sediments can have locally poor reservoir quality.

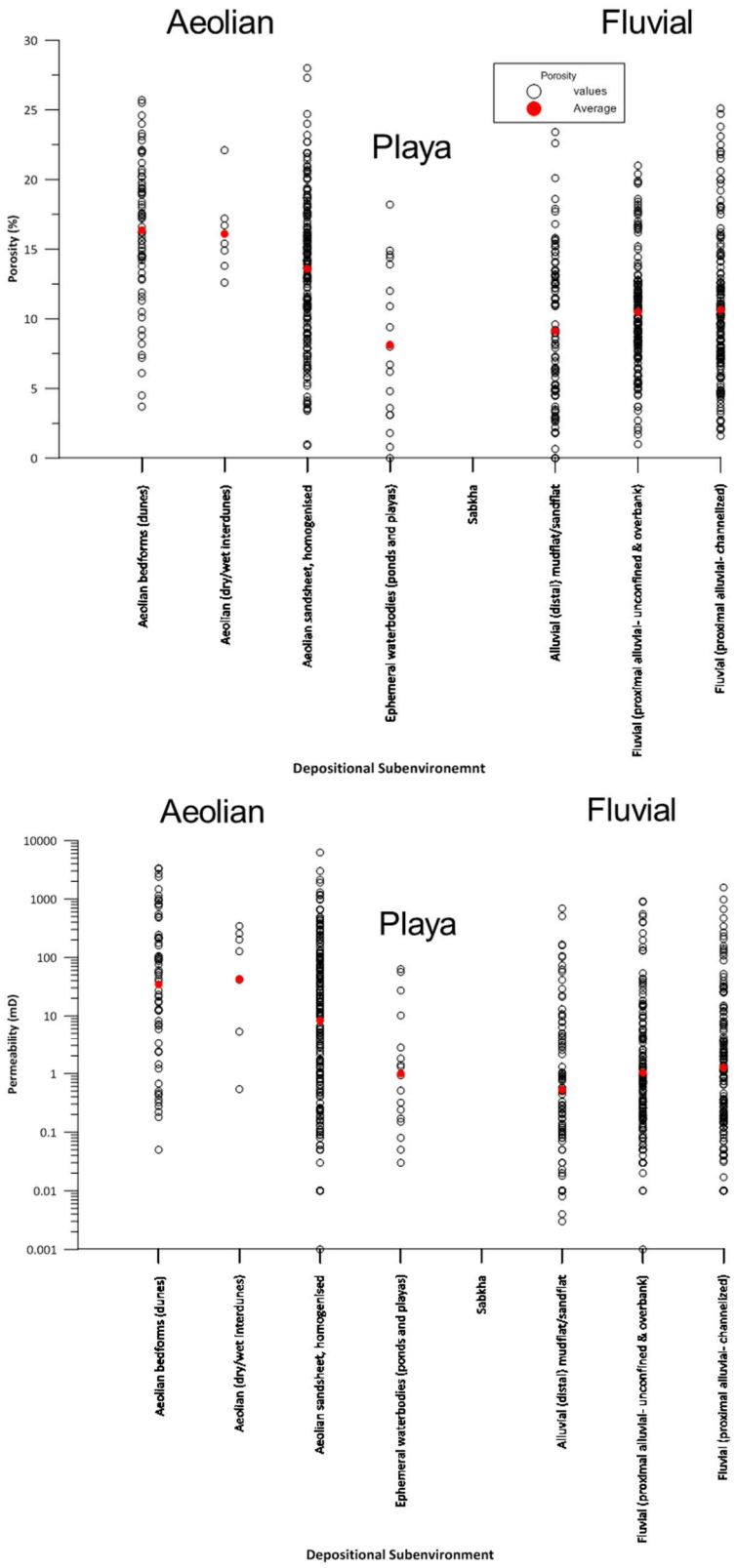

Figure 4-14 Depositional subenvironments vs. (top) He-porosity and (bottom) horizontal air permeability

From the basin centre to the basin margin the presence of carbonates increases whereby sulphate and halite cementation decline (Drong, 1979; Platt, 1994). Due to the stronger evaporation of fluids from basin margin to basin calcretes and dolocretes form in wet evaporative areas further away from the sabhka (Figure 4-15). Dolocretes are thus common in distal fluvial deposits, whereas calcretes in proximal (Morad 1998). Calcretes and dolocretes may also develop in fluvial channel deposits by the dissolution and re-precipitation of carbonate intraclasts derived from erosion of floodplain calcretes (Morad, 1998). Differential rates evaporation can, however, reverse the precipitation sequence of evaporites.

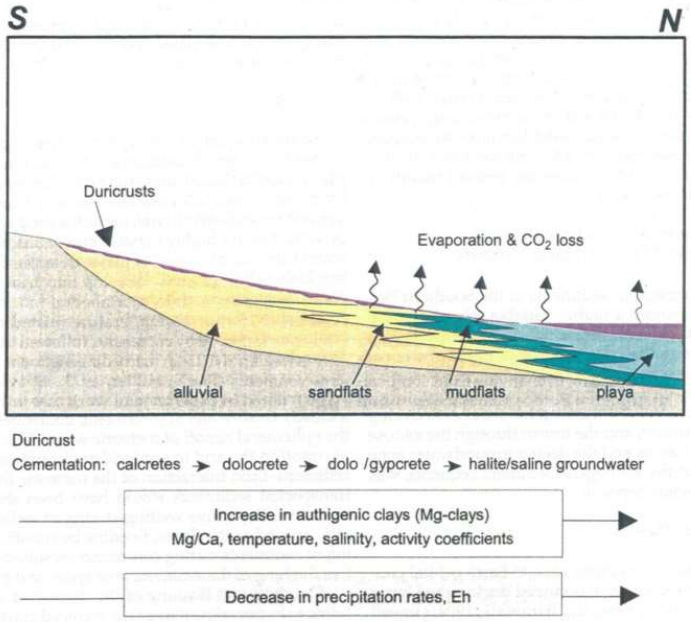

Figure 4-15 Conceptual model of groundwater evolution and mineral precipitation (from Gaupp & Okkermann, 2011)

Early sulphate is generally common in the lake marginal sandstones and in the mudflats. Halite and Gypsum occur mostly in the lacustrine and near basin centre environment (Gaupp et al., 1993). Gypsum can be easily dissolved my meteoric water and reprecipitated in the phreatic zone beneath ephemeral pools. Anhydrite commonly forms due to the dehydration of gypsum and conversion into anhydrite during burial (Glennie et al., 1978; Dixon et al., 1989), which can remain in-situ. Alternatively, in the Rotliegend of the Netherlands detrital gypsum/anhydrite grains were observed that were windblown from nearby Sabkha deposits into an aeolian setting (Henares et al., 2014).

Early chlorite cements precipitate in shoreline sandstones and aeolian sandstones that interfinger with Sabkha/lacustrine environments (Gaupp et al. 1993, Ziegler, 2006). Illite grain coats are common in proximal/distal alluvial fans and ephemeral fluvial environments (Wilson, 1992; Gaupp et al., 1993) and build nucleation and recrystallization cites for authigenic illite formation during burial (Ziegler, 2006).

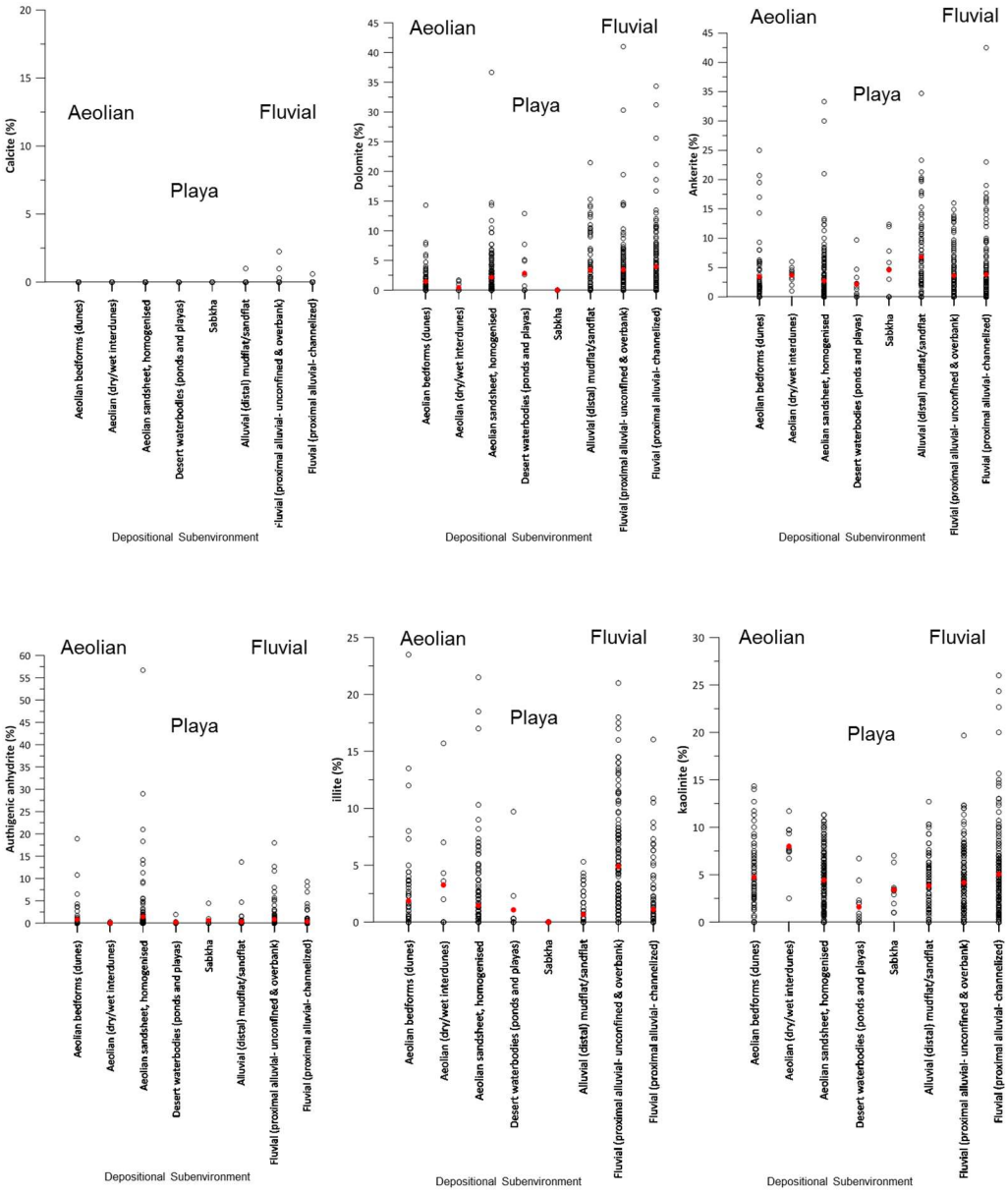

Figure 4-16 Authigenic minerals per subenvironment. Red circles are average values for each subenvironment.

For the current dataset, all cements occur in almost all environments with some cements accumulating in distinct settings. For carbonate cementation we observe a higher potential in fluvial settings (Figure 4-16). Calcite occurs in fluvial settings only. Being a rare cement in this study, calcite distribution may not be representative. Early calcite cement is easily dissolved and redistributed to other carbonate cements (such as dolomite and ankerite) during burial (Saigal and Bjørlykke, 1987; Bjørlykke et al., 1989). Dolomite is common across all fluvial realms (Figure 4-16) but contrary to the conceptual model from Gaupp & Okkermann (2011) is not restricted to proximal environments. Dolomite would have

formed initially as an early diagenetic dolocrete. Ankerite and siderite do not have preference for a specific environment, which suggests that these cements are mostly of late diagenetic origin.

Anhydrite is most common in aeolian homogenized sheetsands that were deposited close to the lake margin (Figure 4-16). In this case early diagenetic gypsum cement (gypscrete) would have formed along the lake margin, where fluids were pushed from lake to lake margin during burial. Further burial converted gypsum to anhydrite. Environmental control is not the only factor for sulphate cementation. Distal alluvial and overbank setting do not show much anhydrite accumulation and on the contrary, anhydrite is common in proximal settings (fluvial and aeolian). Evidently, other (late diegenetic) factors were also responsible for sulphate cementation.

Authigenic illite is most abundant in proximal alluvial (unconfined and overbank) environment. This is in agreement with early illite/smectite grain coat formation and subsequent recrystallization and growth of authigenic illite with burial. Interestingly, illite is also abundant in some aeolian deposits, which may indicate a different source and/or timing of illite formation. In summary authigenic illite is driven by both (early) depositional and (late) diagenetic processes.

Quartz and kaolinite do not seem to be influenced by the depositional environment. This may be related to their mesodiagenetic origin or distribution of detrital grain types (e.g. feldspar vs quartz). Chlorite, gypsum and halite are too low in content to be representative.

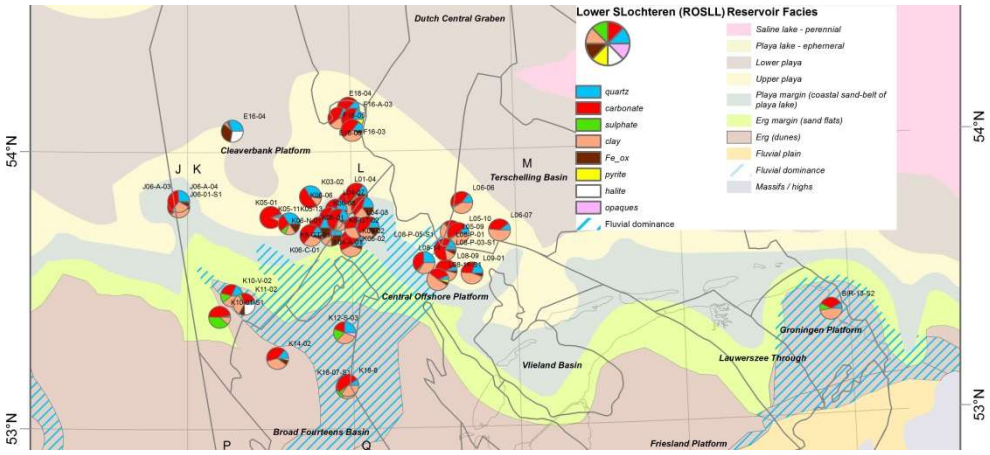

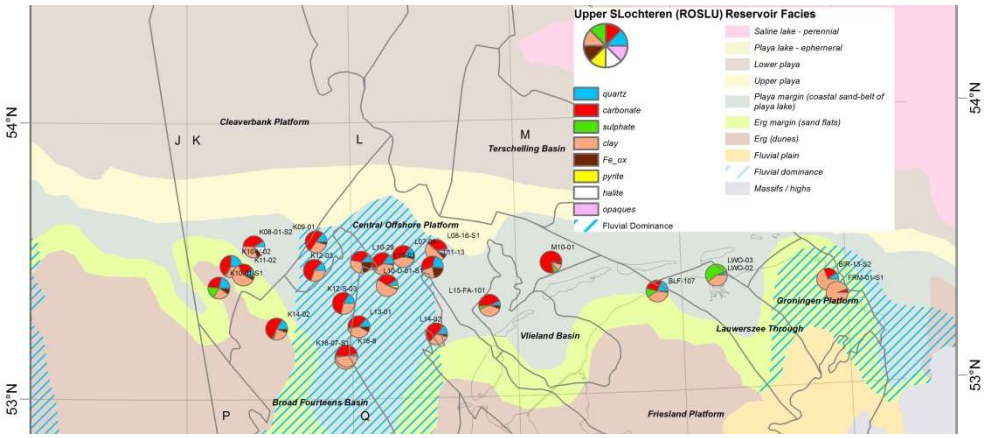

Figure 4-17 Facies map (from Doornenbal & Stevenson, 2010) of ROSLU (top) and ROSSL (bottom) with authigenic minerals per well (Authigenics-subset).

To examine whether environmental distribution can be identified spatially the cements for Lower and Upper Slochteren Members were plotted on facies maps from the SPBA atlas (Doornenbal & Stevenson 2010). Single cements as well as cement ratios were visualised against the depositional facies (example Figure 4-17) but distinct relationships could not be traced. The main reason for this detachment is that the facies maps are generalised for each member. In reality, the members interchange with time and thus different environments intercalate within a member (example Figure 1-2). Further, as previously shown, late diagenetic cements are also present and thus overprint some of the early cementation that would have been environmentally driven. Lastly, the sample size is reduced due to the subdivision into single members. A differentiation between the different members was not always made, thus these samples are not included in the map overview.

4.7 Stratigraphic cement distribution

Differences in cements with stratigraphic unit were observed in a previous diagenetic study of the Dutch Rotliegend by Stahl (2011). Regarding the clay mineralogy, the Lower Slochteren Member was observed to contain almost exclusively illite and the Upper Slochteren Member contained mainly kaolinite and some chlorite. This was attributed to deeper burial and illitization of kaolinites.

In this study we see that authigenic illite, kaolinite and chlorite are present in all members, with the illite/kaolinite ratio being higher in the Lower than in the Upper Slochteren. The average authigenic illite and kaolinite as part of whole rock are similar in all members, which is inconsistent with the previous study. We attribute this difference to a larger and better quality controlled database and to the fact that XRD data was used in the Stahl (2011) study, which does not differentiate between authigenic and detrital clay. The slightly higher illite/kaolinite ratio is not related to burial depth (see chapter 4.5). It may be related to the proximity of the Lower Slochteren to the Carboniferous or the dominance of fluvial deposition in the Lower Slochteren in the studied dataset.

Anhydrite contents are highest in the Silverpit Formation and decrease in the Upper Slochteren and again in the Lower Slochteren. The higher anhydrite content in the

Silverpit Formation is related to the depositional environment being close to the Silverpit saline lake. The decrease of anhydrite concentation stratigraphically could either be related to the distance to and thus the influence of the Silverpit or to the Zechstein evaporites.

The anhydrite and barite contents were plotted against the shortest vertical distance to the contact with the Silverpit Formation, because the Silverpit Formation can occur above or below the Slochteren Formation. The same was done for the distance to the contact with the overlying Zechstein. Anhydrite increases with proximity to both Silverpit and Zechstein (Figure 4-18), meaning that both had fluid interaction with the Slochteren Formation. In the wells where the two higher anhydrite data points that are somewhat further away from the Silverpit Formation occur in wells that are overlain by the evaporite containing Silverpit Evaporite Member and the Upper Silverpit Claystone member. Barite does not relate to Zechstein but possibly proximity to Silverpit Formation also impacted on barite formation (Figure 4-18).

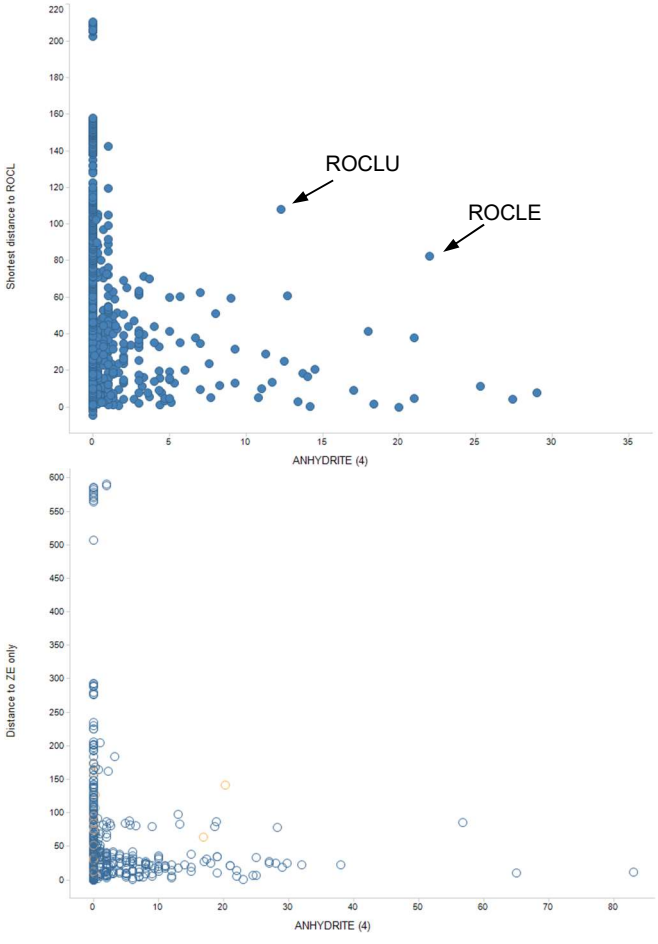

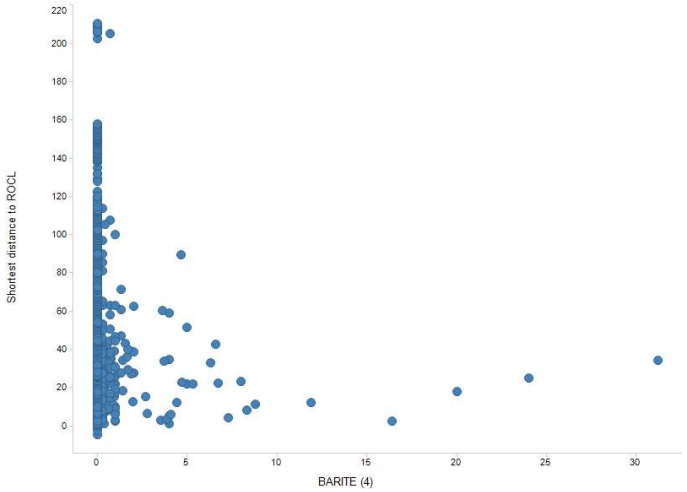

Figure 4-18 Anhydrite and barite contents plotted against shortest distance to the Silverpit or Zechstein.

Certain carbonate cements may form due to the interaction with the Silverpit fluids. This is evident for ankerite and partially for dolomite (Figure 4-19). Dolomite, on the other hand, is not as clearly associated with the Silverpit fluids, as high contents are also found further away from the Silverpit Formation.

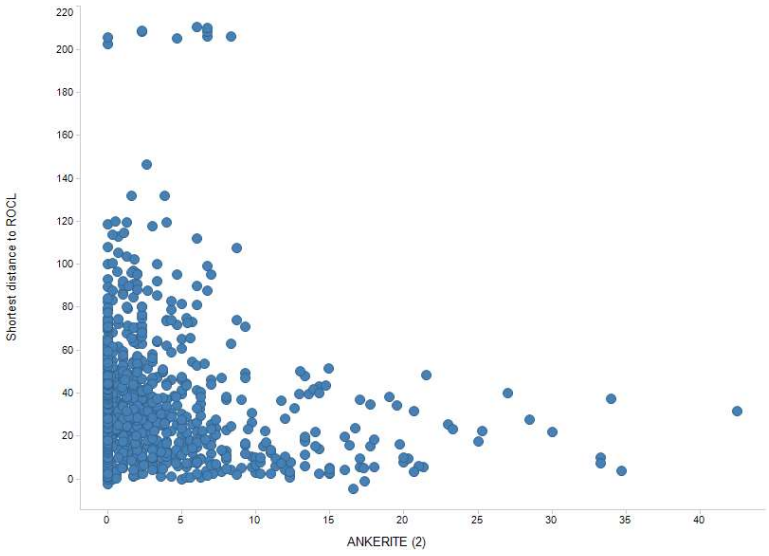

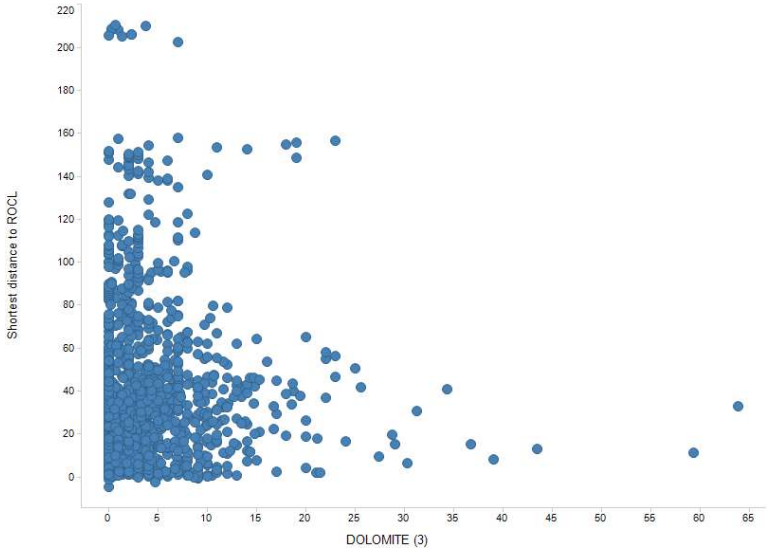

Figure 4-19 Ankerite and dolomite contents plotted against the shortest distance to the Silverpit Formation.

Late diagenesis was suggested to be partially related to the underlying Carboniferous strata because fluid migration from the coal-bearing Carboniferous had an effect not only on the petroleum generation in reservoir rocks but also on the late cement diagenesis in the Rotliegend sandstones (Gaupp & Okkerman, 2011). To test whether this can be observed spatially, we plotted different cements and cement ratios (e.g. authigenic clays and carbonates) on the Carboniferous subcrop map (example Figure 4-20). The Carboniferous strata is differentiated into Stephanian and Westphalian A, B, C and D. The Stephanian does not contain source rocks. Coal deposition mainly occurred in the poorly drained fluvial and floodplain deposits with most coal deposited per total rock volume during the Westphalian B to C (Maurits Member, DCCU). Westphalian A contains less coal than B and C but has a high total coal volume due to the larger rock volume (Figure 4-20). Westphalian D is almost barren coal deposits.

Age	Rock volume (10^3 km^3)	Coal % (av. est.)	Coal volume (km^3)
Westphalian D	3	0.1	3
Westphalian C	7	1.6	114
Westphalian B	23	2.1	477
Westphalian A	82	1.0	820
Namurian	116	0.1	116
Total	**231**		**1530**

Figure 4-20 Coal percentage and coal volume of the different stages of the Upper Carboniferous (from van Buggenum & den Hartog Jager, 2007)

A relationship to the Carboniferous subcrop could not be identified for any of the minerals on a map view (example Appendix E). A closer look at the proximity to the Carboniferous strata and cement generation revealed that certain cements were influenced by the Carboniferous. Some carbonate cements increase with proximity

to Carboniferous. Particularly ankerite shows an increase in abundance towards the Carboniferous (Figure 4-22). Siderite tends to also increase towards the Carboniferous. Dolomite does not show a clear tendency. Anhydrite does not have a relation to the Carboniferous. Barite tends to increase towards the Carboniferous boarder, however the data is relatively sparse to be conclusive (Figure 4-22). Kaolinite, although not exclusively, increases with proximity to the Carboniferous (Figure 4-22), whereas authigenic illite does not have a relationship. Authigenic quartz abundances are higher with proximity to Carboniferous but the relationship is not decisive.

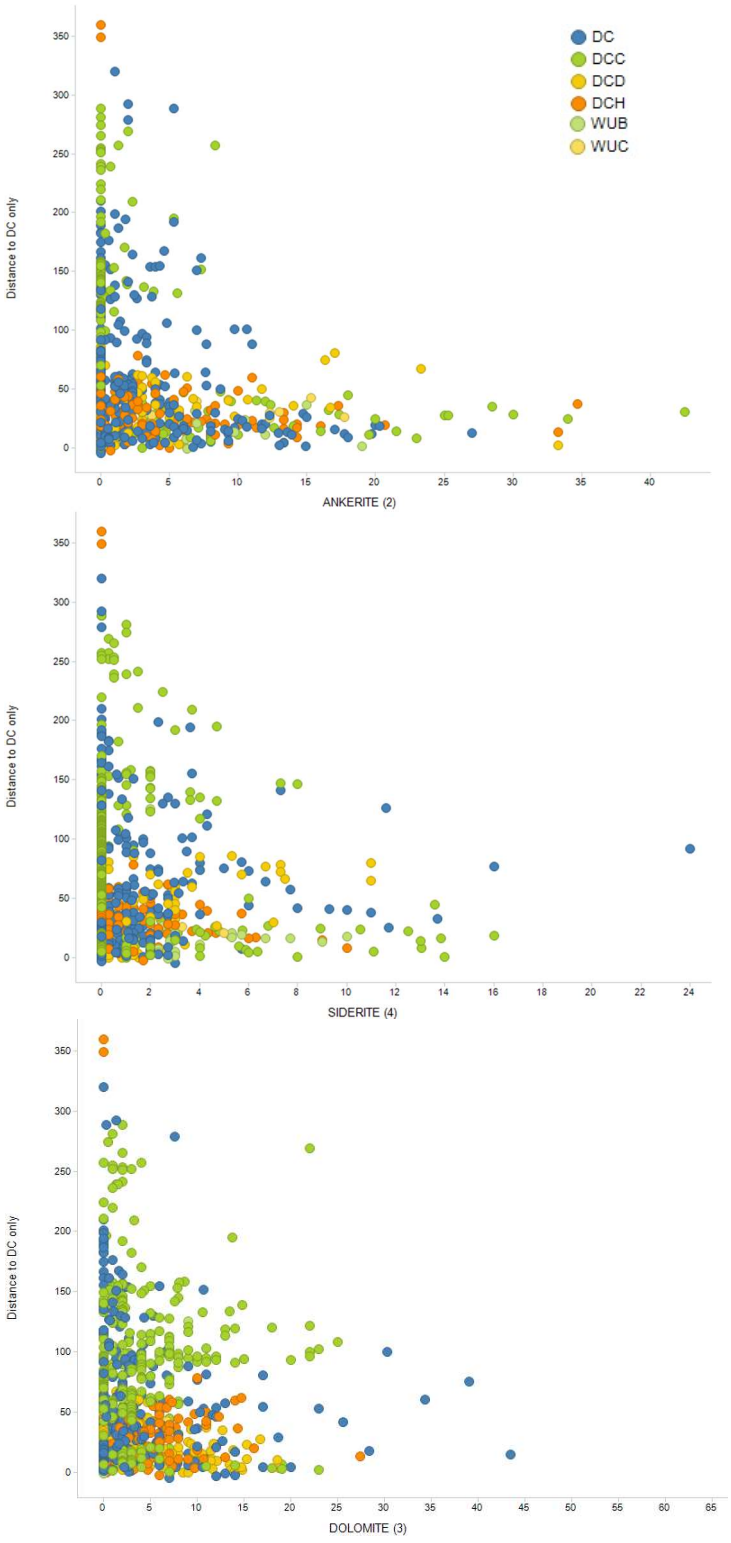

Figure 4-21 Carbonate mineral contents plotted against the distance to the Carboniferous subcrop. The subcrop types are colour-coded.

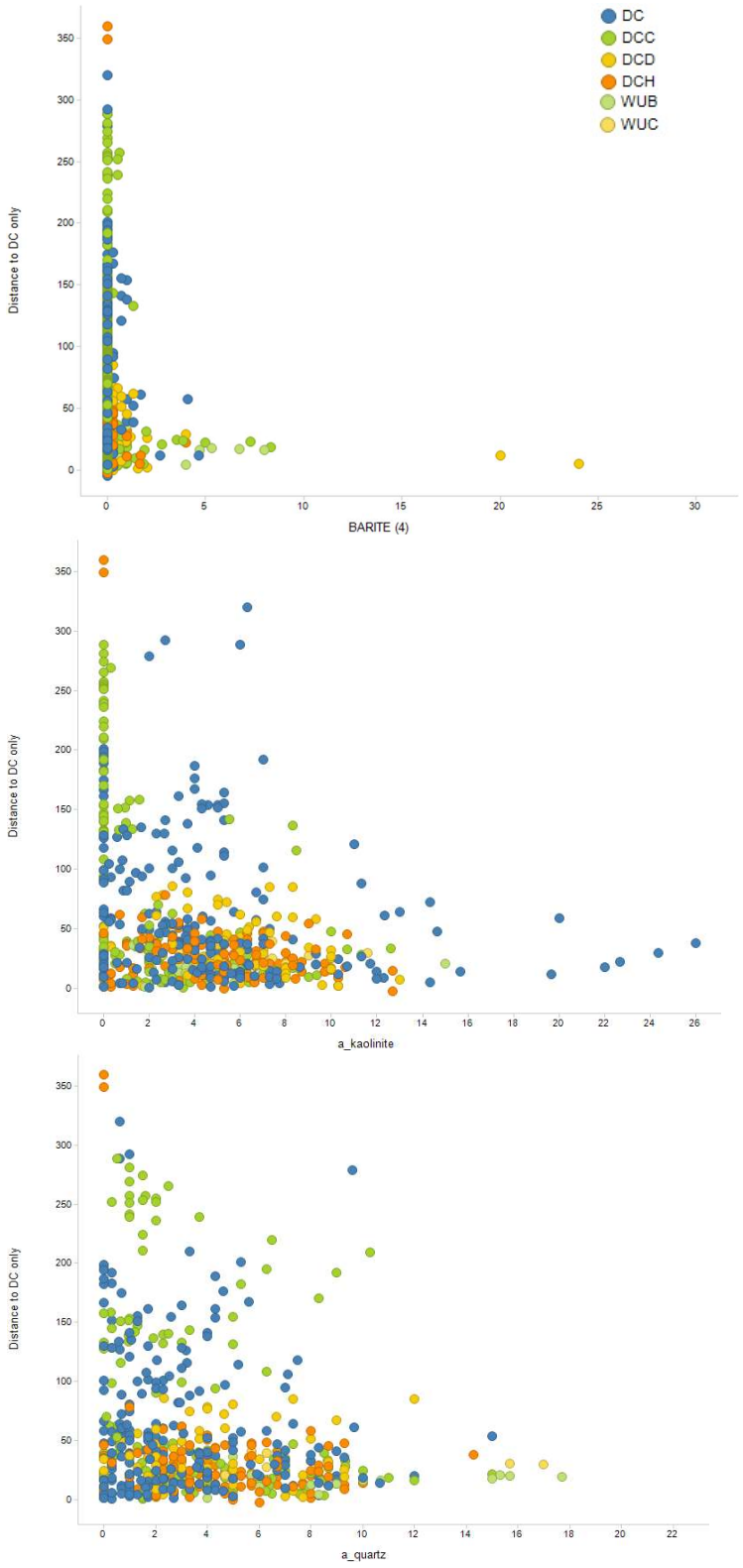

Figure 4-22 Authigenic barite, kaolinite and quartz contents plotted against the distance to the Carboniferous subcrop. The subcrop types are colour-coded.

The connection to the type of subcrop was more difficult to assess because for most wells the Carboniferous stratigraphy was not further defined into formations and members.

Magmatic activity can also mobilize fluids that can affect late diagenetic cementation. Authigenic minerals were plotted on a map containing locations of known intrusive and extrusive events (Figure 4-23). Visually, a relationship to authigenic mineralogy could not be drawn.

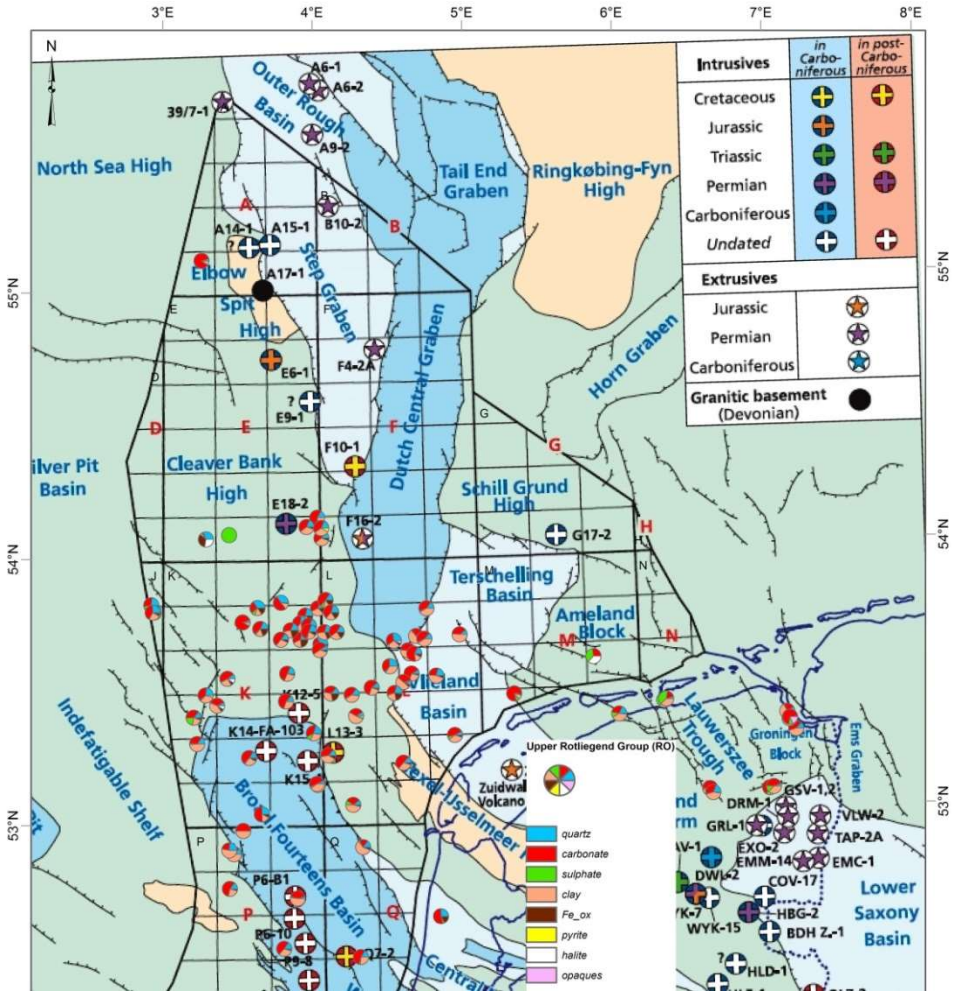

Figure 4-23 Authigenic mineralogy (Authigenics subset) plotted on the map of the intrusive and extrusive events (map from Van Bergen and Sissingh, 2007).

4.8 Summary and concluding remarks

High porosity and permeability is favoured in sandstones with high feldspar and low detrital clay and matrix content. Lower detrital clay contents are generally found in aeolian, rather than fluvial deposits. Therefore, aeolian sediments, (that are also generally better sorted), have a better porosity and permeability.

Low porosity and permeability in sandstones, on the other hand, is related to high detrital clay matrix/laminae. Statistically, high detrital matrix content is the only parameter that, without exception, results in low porosity and permeability. Additionally, porosity and permeability generally diminishes with increase of total carbonate cement (mainly ankerite). Anhydrite also tends to reduce porosity locally. The statistical analyses showed that high porosity and permeability was also connected to low ankerite content, and to a lesser extent low dolomite, siderite and anhydrite content. Authigenic illite does not have an impact on the porosity but clearly reduces permeability.

The low porosity and permeability cluster also showed low average feldspar content. Samples in the north of the Netherlands and in well BGM-01 generally have high feldspar contents and on average low kaolinite, authigenic quartz and ankerite. Many of these samples have high porosity and permeability, unless extensive cementation by carbonates or anhydrite significantly reduced the reservoir quality. Samples in the E-, F-, K- L- and P-blocks have low feldspar contents and on average high kaolinite, authigenic quartz and ankerite and the largest part of the samples belong to the low porosity and permeability cluster. Feldspar conversion to kaolinite and authigenic quartz is a well-known diagenetic process. Yet, this conversion does not seem to be the main reason for the permeability reduction. Cementation by carbonates or anhydrite or the presence of detrital clay or matrix has much more effect on reservoir quality.

Clay- and silt-sized siliciclastics have lower porosities and permeabilities compared to the sand sized sediments. Although grain size has an impact on reservoir quality it does not obscure the relationship to of the reservoir quality to authigenic minerals in this study. Both porosity and permeability decline roughly with maximum burial depth, which is possibly caused by mechanical compaction. The reason for particularly poor reservoir quality in clay-laminae and other ductile grain rich sediments is the larger effect of mechanical compaction on these type of sediments.

We do not observe a significant trend with burial depth for total cement or any of the single cements. The illite/kaolinite ratio does not increase with depth. The reason for a higher illite to kaolinite ratio in deeper set areas may be the a kinetically controlled illite formation during prolonged deep burial.

Some (early) cements form preferentially in specific environments. Dolomite cementation was observed to be higher in fluvial settings and authigenic illite tends to be most abundant in proximal fluvial (alluvial unconfined and overbank) environment. Anhydrite is most common in aeolian homogenized sheetsands. The Silverpit formation contains more sulphate (mainly anhydrite) than the Slochteren Formation. The sediments of the Slochteren Formation also show an increase in anhydrite with progressive proximity to the Silverpit Formation and the Zechstein Group. Silverpit fluids also had an impact on ankerite cementation and partially on

dolomite. Ankerite and siderite cements also have a tendency to increase in abundance towards the Carboniferous. Authigenic kaolinite and quartz increase with increasing proximity to the coal-bearing Carboniferous but the correlation is not conclusive.

Although there are general trends for cementation, a single diagenetic model does not exist for the entire Dutch on- and offshore. A combined paragenetic sequence was proposed by some authors for the Rotliegend in the Netherlands (e.g., Gaupp & Okkerman, 2011). However, there are distinct differences in the timing and type of cements locally because mineral authigenesis and reservoir quality have locally different principal drivers. Some blocks were uplifted and inverted in the post-Permian, whereas others experienced longer and deeper burial, all of which affected the authigenic mineralogy. These structural drivers are superimposed on sedimentological and depositional effects.

The results of this chapter demonstrate that careful analysis and evaluation of a multi-vintage and multi-source petrographic dataset can reveal and support known trends presented in literature and allow new insights. It also became clear that using this dataset petrographic provinces can be distinguished.

A preliminary message from this study is that expanding and detailing the dataset with the data not yet available in the public domain or project domain knowledge and theories can be enhanced and validated.

5 Case Study

5.1 Introduction

The case study is an in-depth assessment of the diagenetic cementation, requiring a closer look at the burial history, the mineralogical evolution and the structural regime. The differences in timing of cement and pore-space evolution affect the evolution of the reservoir quality. This calls for the re-construction of the paragenetic sequence of events for the focus area. Additional parameters included in the case study were 1D basin models for all wells, overpressure calculations, fault modelling, differentiation of gas/water wells and contacts, available gas compositions and clay volume calculation for a few wells. For carbonates and sulphates XRD and Mineralog data was combined with the point-count data because all the minerals were classified as authigenic. Authigenic clay mineral and authigenic quartz data was taken from the point-count data only.

A focus area was chosen for the the case study that contained a sufficient number of wells that have good quality petrographic data (see chaper 2.1). The focus area was identified within in the K and L blocks (Figure 5-1). The area is situated in the Dutch offshore and covers parts of the Cleaverbank Platform, Central Offshore Platform and the Terschelling Basin. It comprises the wells K05-01, K05-11, K05-13, K06-01, K06-02, K06-08, K06-C-01, K06-DN-01, K06-GT-01, K06-GT-02, K06-N-01, L04-03, L04-07, L04-A-01, L05-06, L05-09, L05-10, L05-11, L06-06, L06-07 and L01-04. Although the area also covers parts of the Dutch Central Graben this element could not be studied because it did not contain any good pertrographic data.

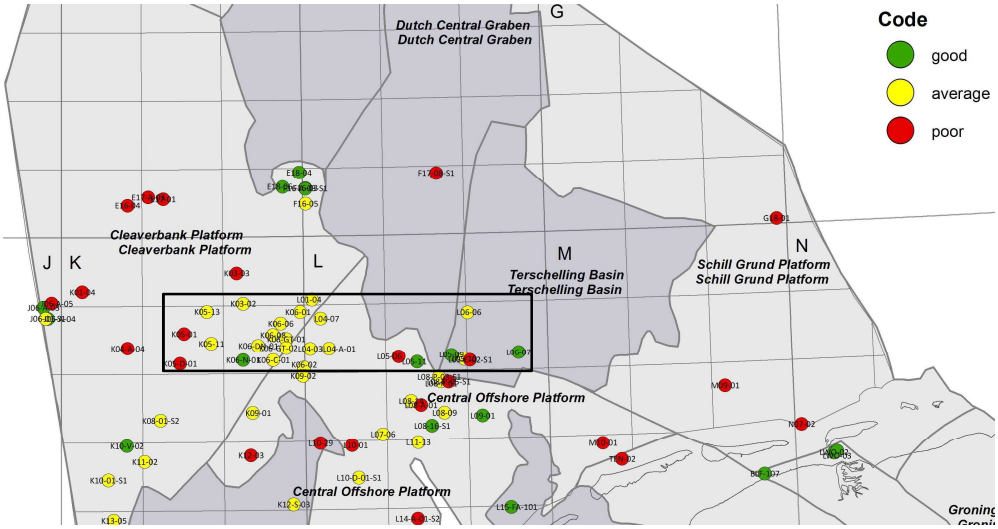

Figure 5-1 Map with well locations with the focus area outlined by the black square.

The Rotliegend in the focus area comprises the Silverpit and the Slochteren Formations. The Lower Slochteren Member is succeeded by the Silverpit Formation and underlain unconformably by the Westphalian Limburg Group. Only the Lower Slochteren Member was analysed in this study.

The differences in the basin history, diagenetic and structural evolution called for a subdivision of the study area into mainly two parts, the western area A and the eastern area B (Figure 5-2). A further distinction was made within the area A with subdivided into A and A2.

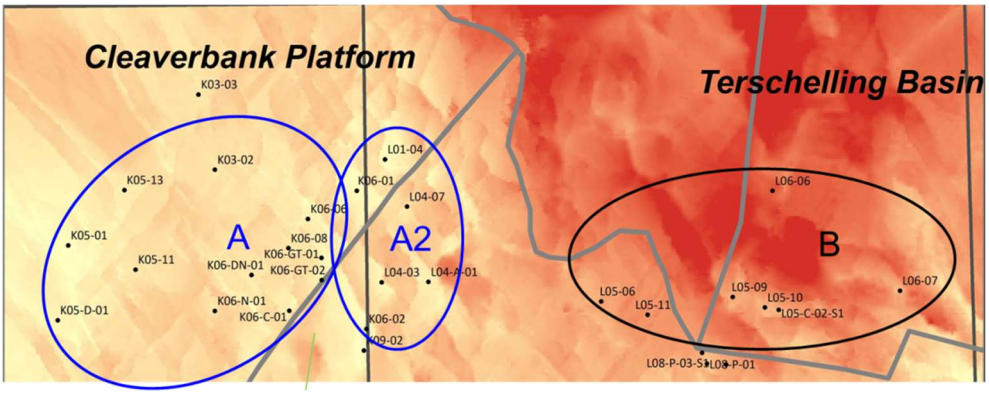

Figure 5-2 Close-up of the focus area with well locations and the subdivision into A, A2, B and B2 zones.

5.2 Burial history and paragenesis

Overall, the entire region experiences a similar evolution of initial burial from the Permian to the Late Jurassic, an uplift/inversion in the Mid Jurassic and a second deeper burial during the Cretaceous to the Neogene. There are, however, distinct differences in the burial depth and thermal evolution. The initial burial was faster and deeper in area B compared to area A (Figure 5-3). During the Jurassic the Rotliegend was uplifted to a shallower depth in area A, with erosion of the overlying deposits up to the Zechstein compared to area B. The subsequent burial up to the present day resulted in the Rotliegend being buried deeper and experiencing higher temperatures in area B, as opposed to A.

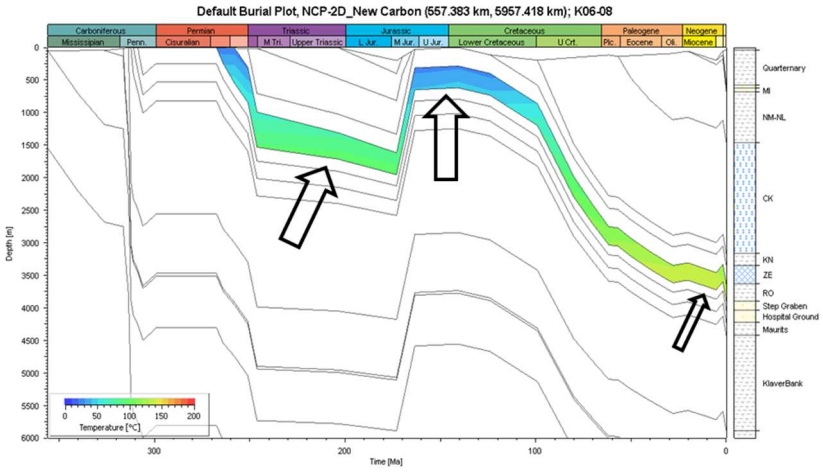

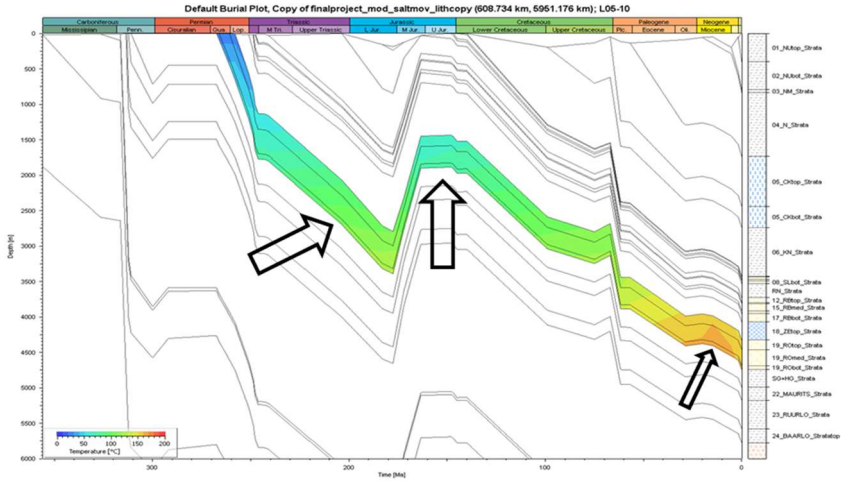

Figure 5-3 Burial and thermal history of the focus area with well K06-08 (top diagram) as examples for area A and well L05-10 (bottom diagram) as example for area B. The Rotliegend is highlighted by the colour coded thermal evolution. The arrows depict major differences in the burial history.

The mineral paragenesis and was assessed from geological well reports. In area A the majority of the wells were analysed in a diagenetic study from Girard et al., 2008 (Total internal report). The study contains a diagenetic sequence of minerals. We adapted the diagenetic sequence for the timing of the illite and siderite emplacement by taking into account the thin-section and SEM image observations from the other wells, not included in the Total study and the few thin-section images that were enclosed in the Total study.

For area B we consulted all available petrographic reports that partially contained interpreted diagenetic sequences, thin-section images and SEM images. Mineral relationships can be inferred by looking at their geometric orientation and habitus. In the examples below (Figure 5-4 A) an SEM image shows detrital quartz grains (Q) with the authigenic cements illite (i), ankerite (fd) and authigenic quartz (q). The grain-rimming (arrowed) illite was the first to form. Pore-filling illite and authigenic quartz succeeded the grain rimming illite and show idiomorphic habitus. Ankerite (fd) grew at a later stage, which is indicated by its growth around the euhedral authigenic quartz and illite.

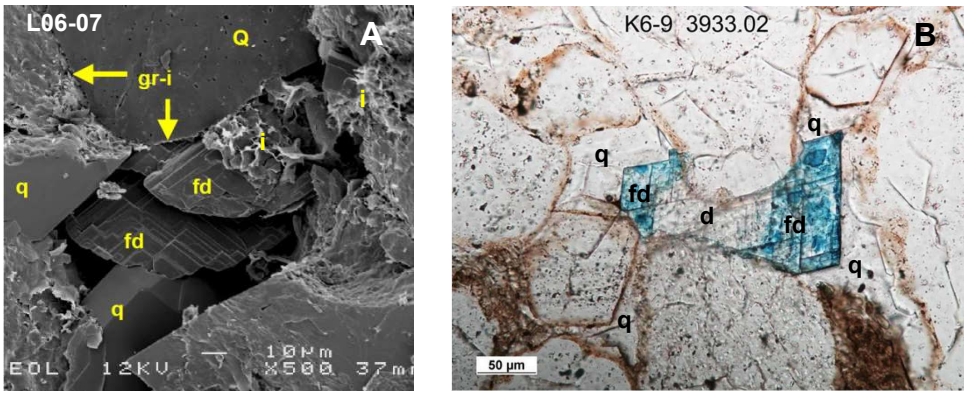

Figure 5-4 A: SEM image from a sample from well L06-07 (modified after Pierau, 2010). B: Thin section image of a sample from well K6-N-01 (modified after Girard et al., 2008).

Abbreviations: i = illite, gr-I = grain rimming illite, fd = ankerite (= ferroan dolomite), q = athigenic quartz, Q = detrital quartz grains.

The mineral paragenesis is somewhat different in area A, with a much earlier formation of carbonate cements. Dolomite formed relatively early (eodiagenetically) and partially overlapped with ankerite formation. Dolomite is often overgrown by ankerite in thin sections (Figure 5-4 B), indicating the emplacement of ankerite post-dolomite. Ankerite grew euhedrally and was later enclosed by quartz cement.

In the paragenetic sequences we differentiated between early, intermediate and late diagenesis. Early diagenesis is restricted to eodiagenesis. Intermediate diagenersis refers to mesodiagenesis before the basin inversion and late diagenesis represents telodiagenesis and the second mesodiagenetic event. Note that the paragentic sequences are an interpretation of what can be observed today. Early cements may have dissolved and later succeeded by renewed cementation. The boarders between the events are not sharp because the minerals are not dated. In well L06-06 from area B the carbonate cements were dated with isotope geothermometry. Oxygen isotopes measured on dolomite cements revealed the lowest crystallisation temperatures of 36 to 40°C. Dolomite was succeeded by ankerite growth precipitated at temperatures of above 91°C. The latest carbonate mineral to form was siderite at above 95 °C. In area A, a low temperature (<10-15°C) was inferred for dolomite crystallisation from oxygen and carbon isotope analyses (Girard et al., 2008). The oxygen isotope geothermometery provides only an indication of temperatures. Due to the poor knowledge of the $\delta^{18}O$ of ambient pore-waters the temperatures represent estimates rather than fact values. A better method to date carbonates (and other minerals) is clumped isotope thermometry and fluid inclusion thermometry.

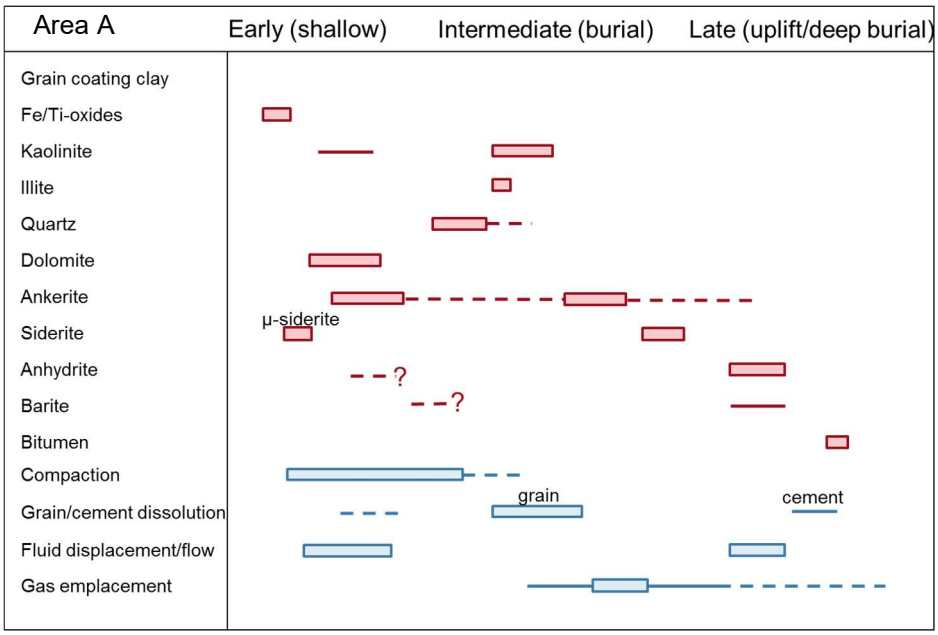

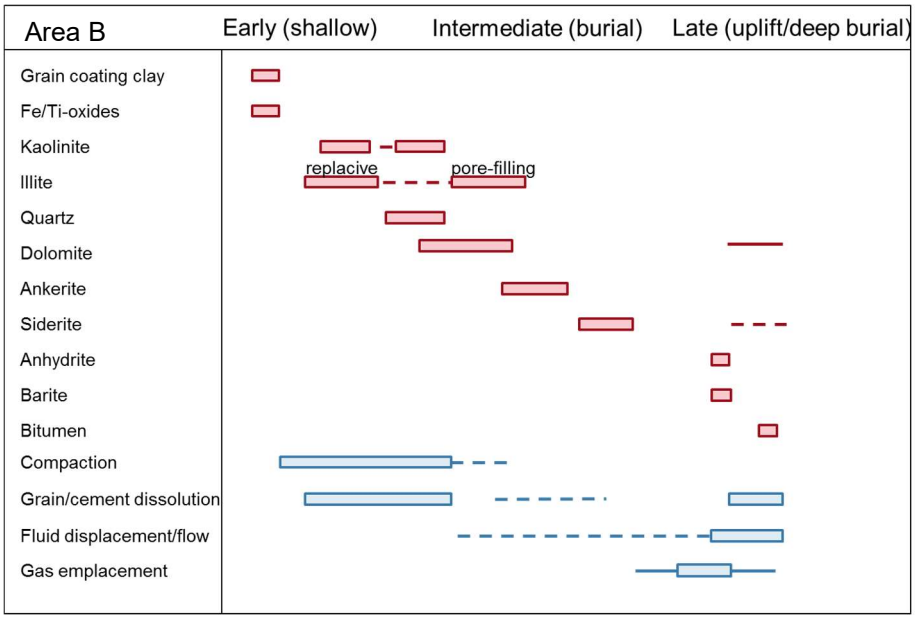

Figure 5-5 Paragenetic sequences of events for area A (top figure) and area B (bottom figure). Mineral growth is indicated by red squares and the other events in blue. Minor events are indicated by lines and major by squares. Dashed lines and question marks depict uncertain timing of emplacement of events.

Although the diagenetic minerals are similar in both areas their emplacement history and extent varies considerably (Figure 5-5). During early diagenesis illite grain coatings are only present in area B. Early to intermediate diagenetic cements in area B consist of clay minerals illite and kaolinite. Particularly grain-rimming and pore-filling illite is prevailing. On the contrary, in area A carbonate minerals dominate the early to intermediate diagenetic stage. Particularly ankerite is pervasive and precipitated in at least two stages of diagenesis. In area B carbonate minerals succeed clay minerals and quartz. Siderite is generally an intermediate to late precipitate. In area A siderite occurs also earlier in the diagenetic sequence. Sulphate cements (anhydrite and barite) precipitated both early and late in area A, whereas in area B they are restricted to late diagenesis only. Both grain and cement dissolution occurred early in area B. In area A grain dissolution took placed during intermediate diagenesis. Post inversion grain (or grain filling-cement) was dissolved in area B, that created secondary porosity not occluded by extensive mineral precipitation (Figure 5-6), while area A experienced minor cement dissolution in the late stage. The diagenetic sequence may be slightly different between areas A and A2 but the distinction could not be made with the available material.

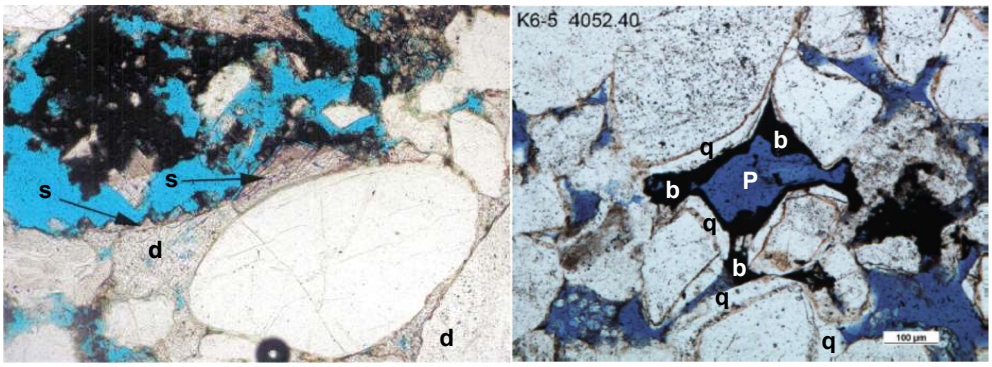

Figure 5-6 Left: Thin-section image from well L05-10 modified after (Adelmann, 2004). Pore space is coloured blue. The image shows the contour of a dissolved detrital grain with minor late siderite (s) precipitation. Dolomite (d) cement precipitated prior to grain dissolution in intergranular pores. Right: Thin-section image from well K6-DN-01 (modified after Girard et al. 2008). Bitumen coating (b) filled the pore-space (P) around detrital grains and authigenic quartz (q) cement.

Fluid displacement was interpreted from the diagenetic mineral dissolution and precipitation. It involves meteoric water ingression, in-situ fluid cycling, acidic hydrocarbon-bearing fluids and alkaline Rotliegend and Zechstein brines. Hydrocarbon expulsion occurred most likely during later diagenesis. Basin modelling shows two main phases of hydrocarbon generation and expulsion from the Westphalian coals in the focus areas, the first during the Late Triassic to Early Jurassic in the more deeply buried areas and the second during the Paleogene to Neogene (Chapter 3, de Jager & Geluk, 2007). An initial pulse of CO_2 and CH_4 is assumed for the Rotliegend around the Mid Jurassic with another smaller phase in the Lower Cretaceous (Gaupp & Okkerman, 2011). Bitumen was observed in both areas to have entered the reservoir after the formation of authigenic minerals (Figure 5-6), most likely during the second mesodiagenesis phase. This could be related to the charge of liquid hydrocarbons from different sources such as the Jurassic Posidonia Shale Formation in the case of area B or from organic rich Zechstein intervals in the case of area A.

We do not observe a significant difference in the gas composition between the wells and the areas (Table 5-1). The main gasses that could influence the cementation are H_2S and CO_2. Where measured, H_2S was absent and CO_2 concentrations varied between 1 and 6 mol-%. There is no relationship between the CO_2 content and mineralogy. Overpressures were derived from published fluid and leak-off pressure data (see Verweij et al. 2012). There is a significant difference in overpressure between area A and B. In area B overpressures are quite high (24 to 38 Mpa). High porosities have previously been connected to high overpressures (e.g. Nguyen et al., 2013). In this study we do not observe higher porosity with overpressure differences. Average porosity is identical in areas A and B. Overpressure has generally no effect on the authigenic mineralogy.

Table 5-1 Available gas composition data and calculated overpressure for the wells in the focus area (*exact depth not provided).

Well	Depth of gas sample	CH4	C2+	CO2	N2	H2S	Depth Pressure measurement	Overpressure
	MD_AH	mol%	mol%	mol%	mol%	mol%	TVDss	Mpa
K05-11	3964 to 3984	87.099	6.3	3.856	2.733		3911.73	4.46
K05-11							3915.58	3.74
K05-11							3939.39	4.30
K05-13							3857.53	4.72
K05-D-01							3683.20	4.47
K05-D-01							3708.20	4.13
K06-01	3640 to 3660	77.22	8.67	3.16	10.95	0	3621.80	6.29
K06-02	3359 to 3422	84.9	8.48	1.49	5.1	0	3333.28	5.60
K06-02							3392.43	5.01
K06-06	3807.5 to 3840.5	84.11	9.04	2.155	4.703	0	3782.93	5.33
K06-06							3785.33	5.67
K06-08	3889 to 3925	85.341	8.2	2.361	4.052		3852.95	4.89
K06-C-01	Slochteren*	87.67	7.39	1.4416	3.5047	0	3731.13	5.59
K06-C-01							3775.59	5.69
K06-DN-01	3830 to 3873	88.163	7.1	1.426	3.314		3837.28	4.94
K06-DN-01							3844.59	5.08
K06-DN-01							3856.93	5.01
K06-GT-01	3910 to 3962	84.65	9.29	1.643	4.434	0	3817.81	5.04
K06-GT-01							3827.60	4.01
K06-GT-02	Lower Slochteren*	86.277	7.8	1.467	4.431	0	3734.67	5.74
K06-GT-02							3757.64	5.68
K06-N-01	3926 to 4000	88.301	6.5	2.879	2.315		3886.51	5.26
K06-N-01							3919.71	4.94
L04-03	Rotliegend*	86.13	5.83	1.859	6.075	0	3673.48	4.61
L04-03							3687.85	4.63
L04-03							3707.54	4.54
L04-07	3830 to 3894	90.51	2.58	4.293	2.553	0	3801.03	6.73
L04-A-01	3784 to 3862	90.43	3.12	2.85	3.51	0	3773.03	7.13
L04-A-01							3796.99	6.90
L05-09	4675 to 4765	91.86	1.42	6.268	0.433	0	4632.52	23.63
L05-09							4673.04	23.73
L05-10	4503.25	91.2	1.69	5.9	0.15		4343.76	26.22
L05-11	4857.8	96	0.71	0.57	2.7			
L06-07	4692.5 to 4716.5	94	1.5	4.1	0.4	0	4365.72	37.90

5.3 Fault modelling

The fault modelling study of the focus areas was performed in Petrel (Schlumberger, 2015). The top Rotliegend surface (base ZE) depth map was taken from TNO's DGM v4.0 (as available on www.nlog.nl). Additionally, TOTAL E&P Netherlands kindly provided their fault model for a large part of area A (and A2). The TOTAL model has a much higher level of detail and contains fault gaps. The TNO model is less detailed and has a continuous surface without fault gaps. The Total model input was combined with the existing TNO model to increase the accuracy. For the remaining area the existing TNO model was used. Note that the data retrieved from the TNO model is less accurate than the TOTAL model output.

For each well the distance from the Lower Rotliegend to the surrounding faults was determined together with the juxtaposed stratigraphy. The juxtapositioning ranged from self-juxtaposition to partial, full or cross reservoir juxtaposition with the Silverpit, Carboniferous and Zechstein formations.

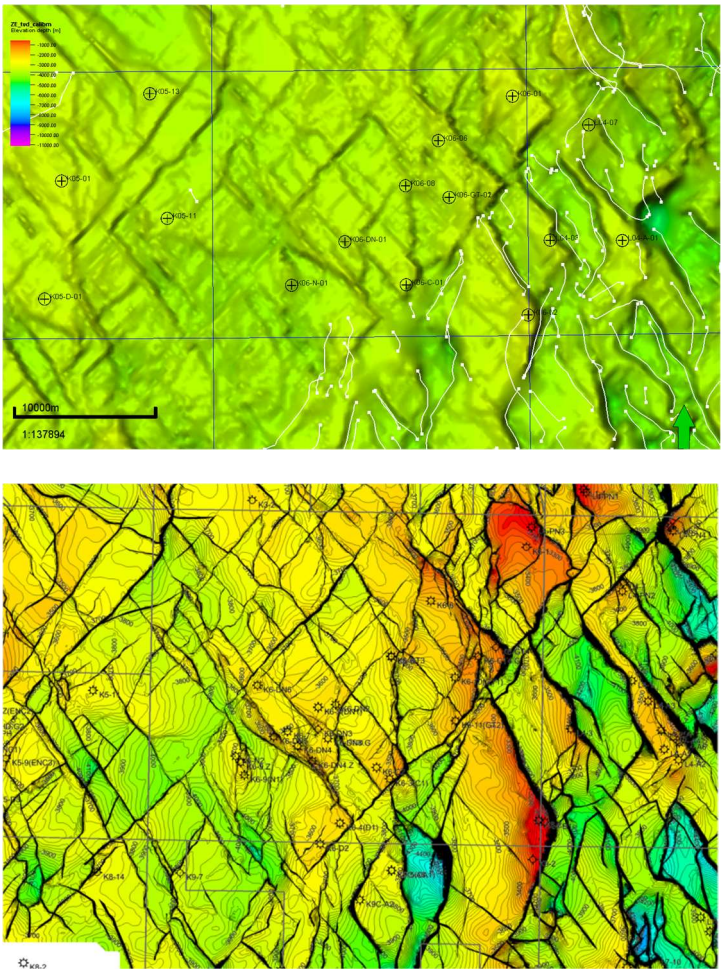

Figure 5-7 Top figure: Part of the focus area A with well locations superposed and fault information on the top RO (base ZE) depth map from TNO's DGM v4.0. Bottom figure: The same area modelled by TOTAL.

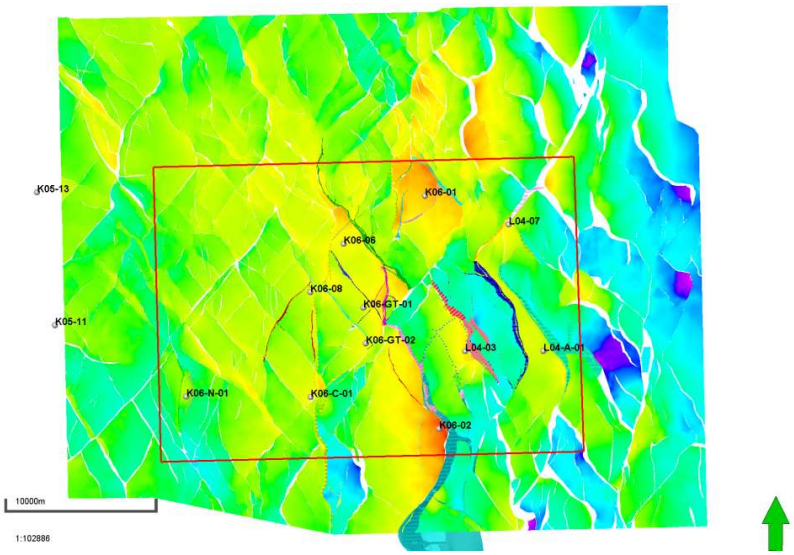

Figure 5-8 Combination of the TNO model with the fault data from TOTAL (indicated by the red square).

5.4 Cementation

5.4.1 Sulphates

Two sulphate cements were identified in the focus area; anhydrite and barite. The sulphate content decreases from area A to B. Anhydrite is the dominant sulphate in the study area (up to 21%). Barite is mostly absent but can amount up to 8%.

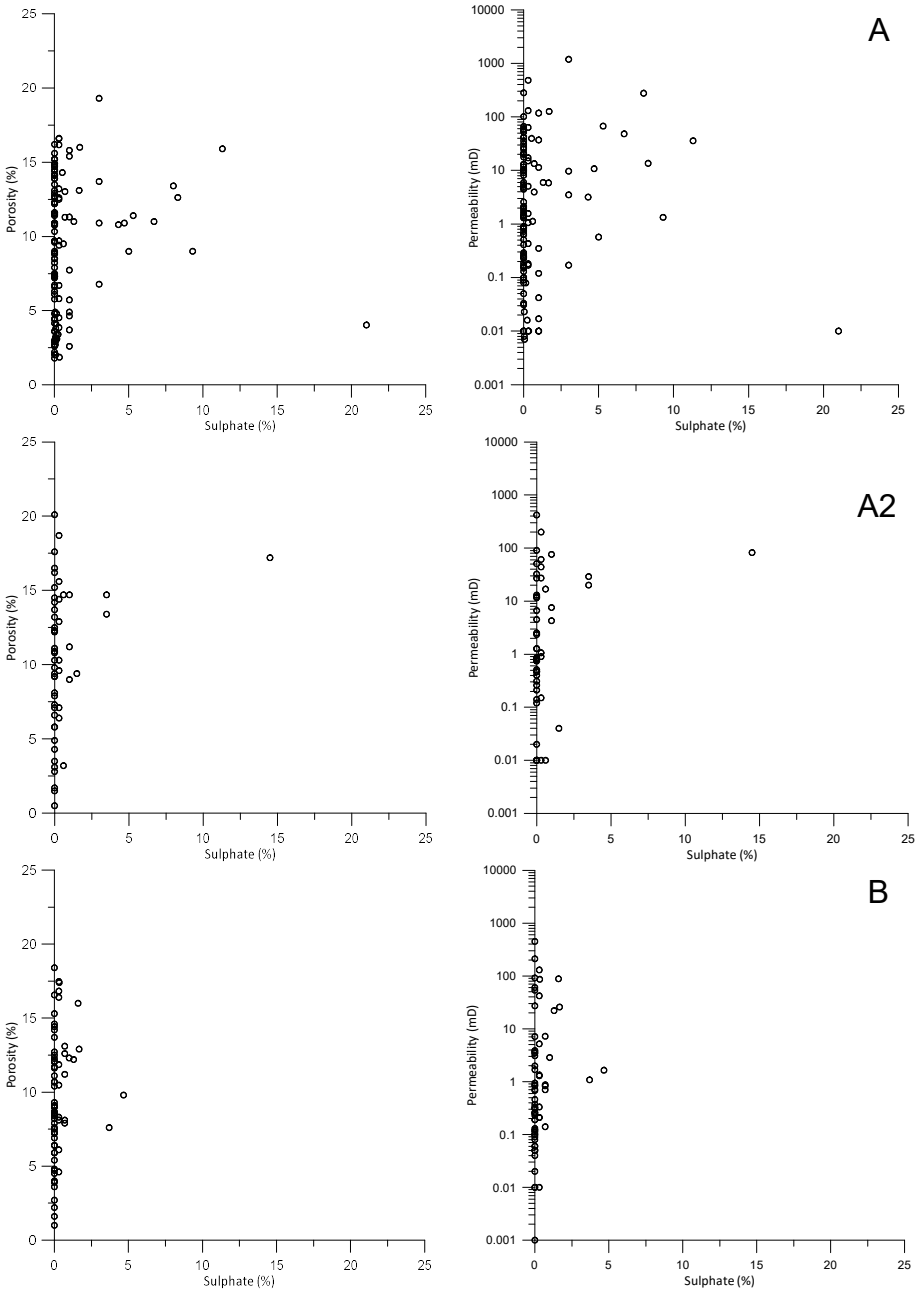

Figure 5-9 Sulphate plotted against He-porosity and horizontal permeability in area A, A2 and B

The reservoir quality is not affected much by sulphate cementation (Figure 5-9). In area A anhydrite has a local impact only (wells K06-06, L01-04, K06-GT-01). Thin

section images show that anhydrite is poikilotopic and fills intergranular porosity pervasively, as well as being present as fracture fill (Figure 5-10).

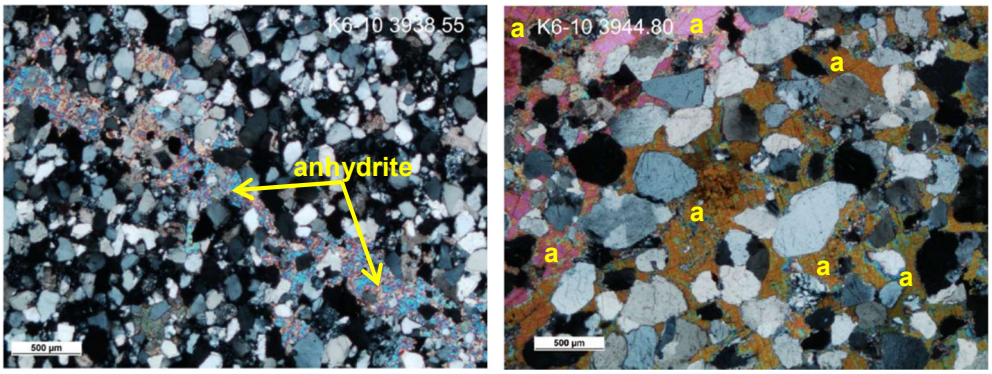

Figure 5-10 Poikilotopic anhydrite cement in area A occuring as intergranular fracture fill (left) and pore-fill (right) cement from well K06-GT-01 (modified after Girard et al., 2008).

Anhydrite tends to increase towards the Silverpit Formation (Figure 5-11), which has also been observed for the entire dataset. A possible explanation for the increase of anhydrite towards Silverpit is the influence of saline fluids from the Silverpit shales. The process could have happened syn-sedimentarily, as the environment was changing to more evaporitic conditions towards the Silverpit formation. Alternatively, the influx of the Silverpit fluids may have occurred during the Zechstein transgression (e.g., Platt, 1994). During early burial compaction of the Rotliegend playa shales could have released hyper saline fluids that then entered the adjacent sandstones, resulting in gypsum (or anhydrite) cementation. In area A, early diagenetic sulphate cementation is assumed but not certain (Figure 5-5). For area B eodiagenetic sulphate cements are unlikely. It is possible that the early cements were dissolved and displaced later in the diagenetic history, thus overprinting any trace of the early cements.

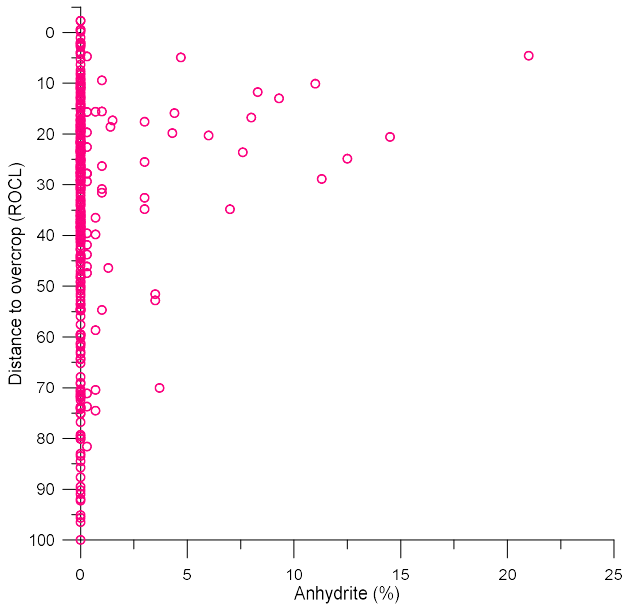

Figure 5-11 Anhydrite content from all wells in the study area plotted against the distance to the overlaying Silverpit Formation.

In both areas a late generation of sulphates is much more apparent. Anhydrite and barite were placed in most reports in the mesodiagenetic stage as one of the last cements to precipitate. The influence of Zechstein fluids that are supersaturated in regard to SO_4^{2-} ions could have influenced their cementation. Sulphur isotopes measured on anhydrites in well K06-06 are of the same composition as Thuringian massive anhydrite deposits and other European Zechstein evaporites (Girard, 2008). The question is how and when did the Zechstein fluids interact with the Lower Slochteren sandstones.

Lateral flow of fluids from Zechstein into the Rotliegend could have occurred at or near uplifted blocks where Zechstein was juxtaposed against the Rotliegend (Gaupp et al., 1993, Platt, 1994). We calculated the distance of the Lower Slochteren to the nearest fault zones. Only one well (L01-04) where Zechstein was set in direct contact to the Lower Rotliegend has elevated anhydrite content (Figure 5-12). A direct evidence for the influence of faults was not found for anhydrite and barite cementation otherwise.

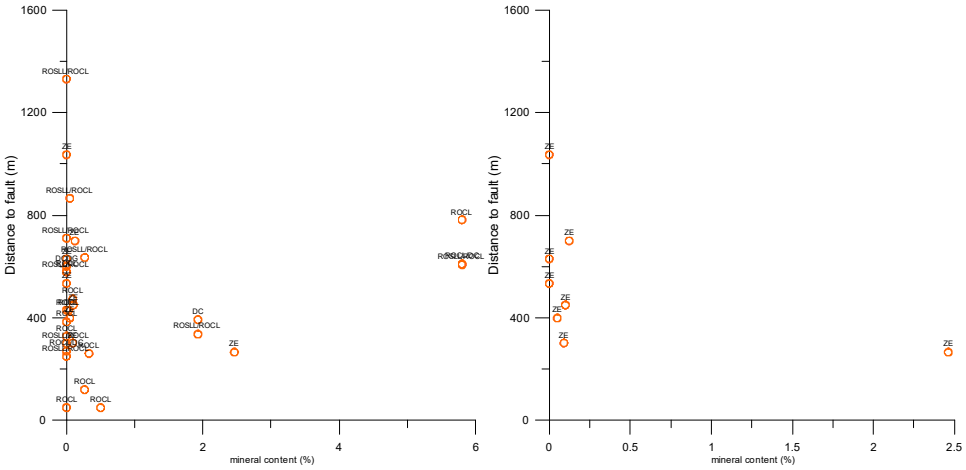

Figure 5-12 Average anhydrite and barite contents per well plotted against the lateral distance to the nearest faults. The juxtaposed formations are labelled per well. The left figure includes all nearest faults and the right figure juxtaposed Zechstein only.

A second possibility is a telodiagenetic formation of sulphates. During the Mid Cretaceous, Zechstein and the Rotliegend deposits were uplifted to the zone where meteoric fluids could have started interacting with the Permian rocks. Infiltration of meteoric waters into the Rotliegend sandstones would have been close to the structural highs. Due to the high solubility of gypsum and anhydrite (Purvis, 1992) meteoric waters could have dissolved evaporitic deposits and carried the sulphate-rich fluids by diffusion and density driven flow towards the Rotleigend sandstones.

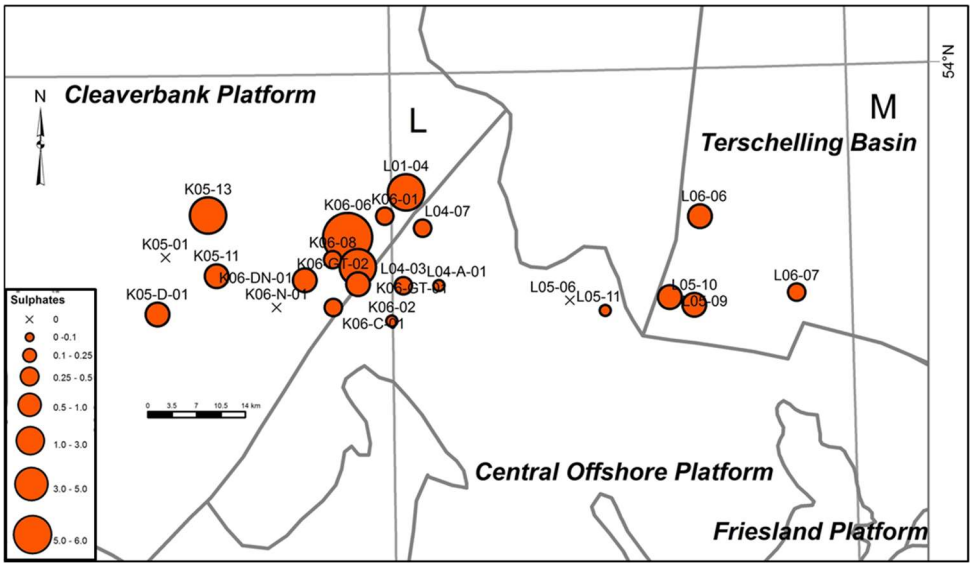

Figure 5-13 Average authigenic sulphate (anhydrite and barite) values for each well in the focus area.

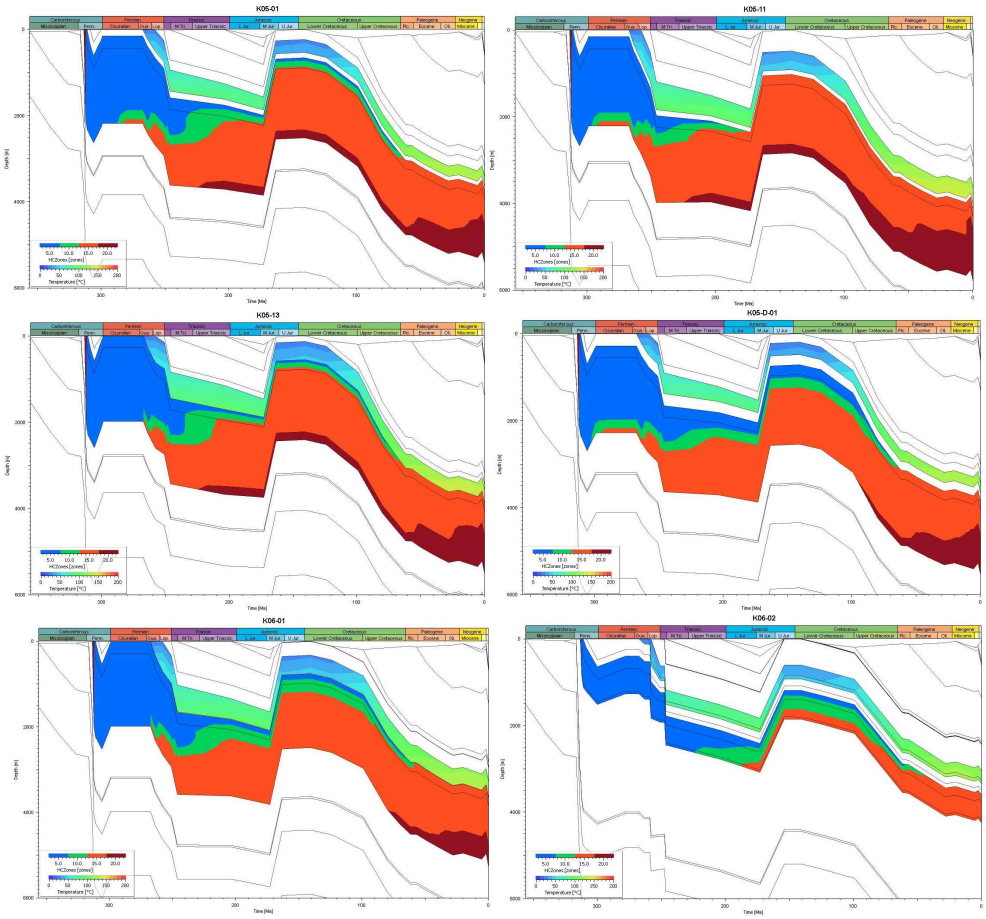

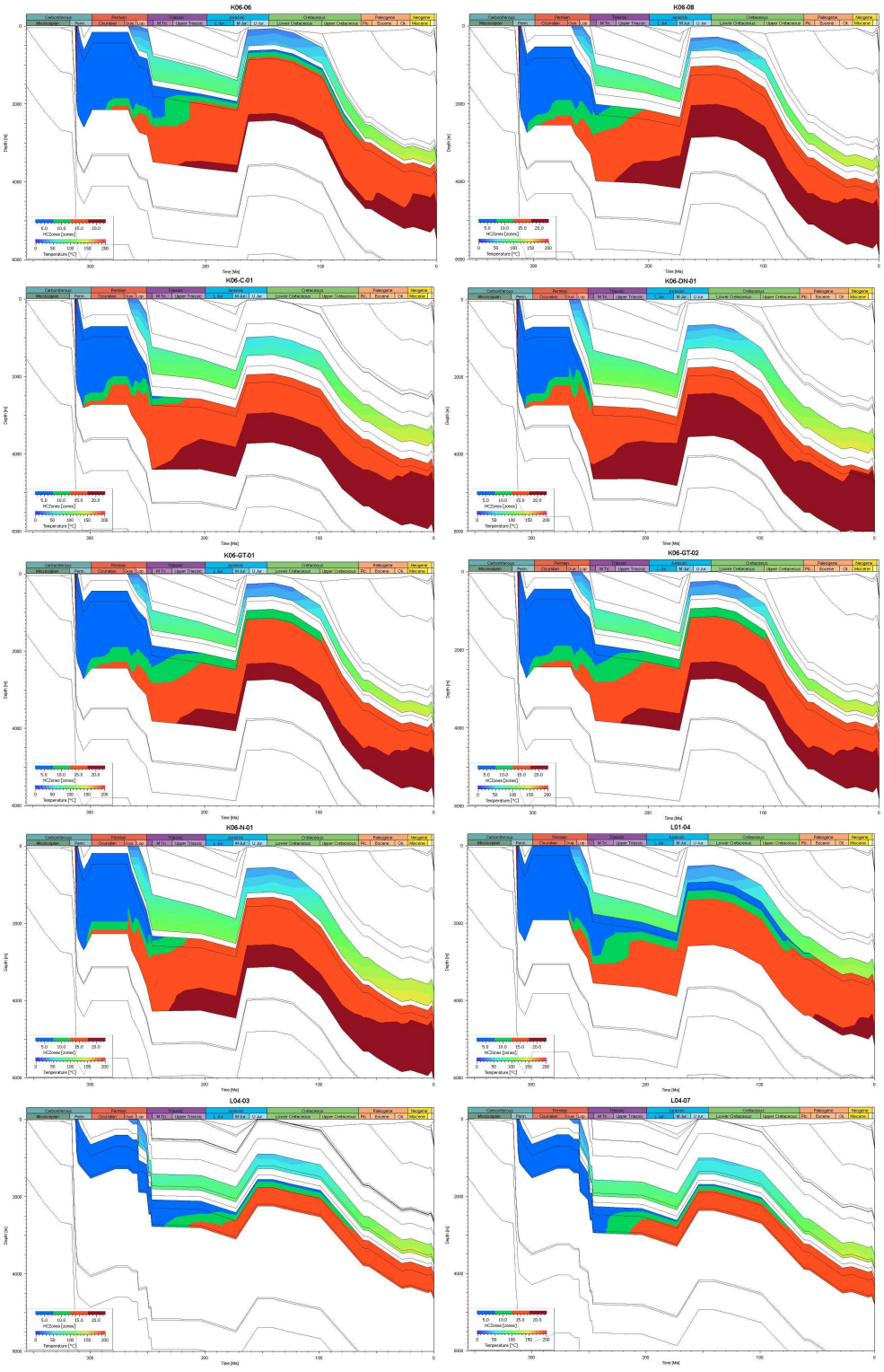
K06-06
K06-08
K06-C-01
K06-DN-01
K06-GT-01
K06-GT-02
K06-N-01
L01-04
L04-03
L04-07

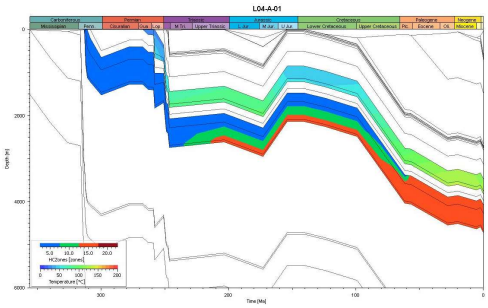

Figure 5-14 1D basin models for single wells in focus area A. The Rotliegend is highlighted by the colour coded thermal evolution with the proposed paragenetic sequences of events below. The Carboniferous source rock maturity is according to Burnham (1989) KIII, blue: immature, green: oil generation, red: gas generation; burgundy: over mature.

Area B has generally a low sulphate content, whereas a few wells in area A have elevated sulphate contents, mainly anhydrite, (Figure 5-12). The comparison to 1D basin models for single wells in Area A indicates that the wells with higher sulphate content were uplifted closer to the surface, whereas the wells with lower content anhydrite experienced less uplift erosion in the late Jurassic and remained deeper buried (Figure 5-12). Area B experienced a lesser degree of uplift and erosion in the late Jurassic (compare Figure 5-3). The exception is well L01-04, which was not elevated as high but has relatively high anhydrite content. Coincidentally, this is the wells that is close to a Zechstein fault, emphasizing the importance of structural juxtapositioning on sulphate cementation.

It is thus likely that locally the Slochteren strata were elevated to a high enough level to begin to interact with the sulphate rich Zechstein or Silverpit deposits due to the renewed meteoric influence. However, for the vertical fluid migration from the Zechstein and/or Silverpit into the Slochteren reservoir a fracture and fault network is required. Although we observe that anhydrite was a fracture-filling cement, these fractures would have had to have been sufficiently large and interconnected. To date, there is no evidence for such a fracture network (Total E&P Netherlands, pers. comm.). This is a conundrum that still requires further investigation.

5.4.2 Silicates (clays and quartz)

Authigenic illite content increases from area A to A2 to B. Authigenic kaolinite is also more abundant in area B. Authigenic quartz is equally distributed in all areas.

Porosity and permeability was compared to authigenic quartz and the clay minerals illite and kaolinite for the focus areas A, A2 and B. Authigenic quartz content did not show any correlation to porosity or permeability in any of the areas. Illite on the other hand was responsible for porosity reduction in area B but due to its low abundance did not have much effect in areas A and A2 (Figure 5-15). Porosity was not affected by illite, mainly due to sufficient microporosity between the illite needles/fibres.

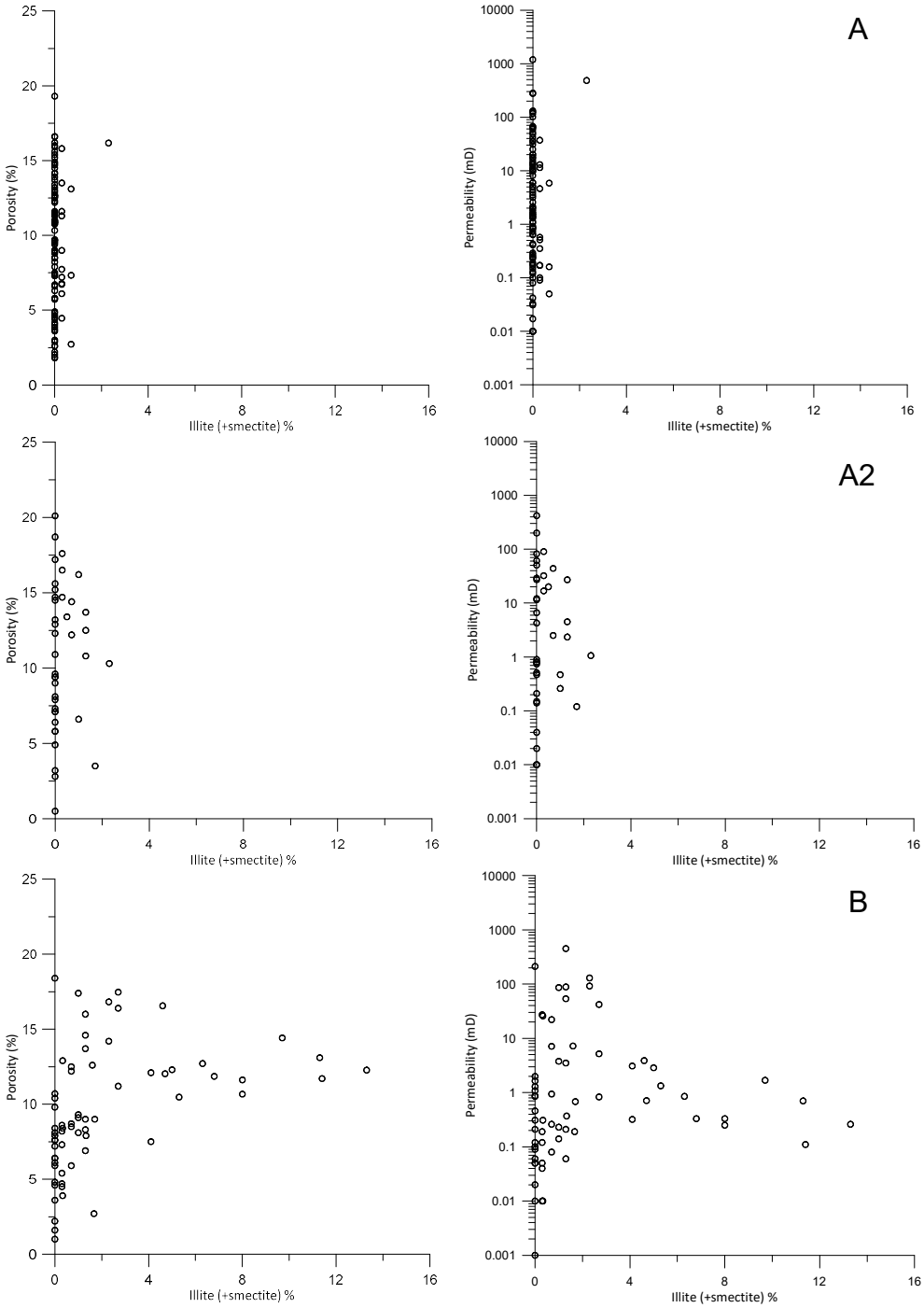

Figure 5-15 Authigenic illite plotted against He-porosity and horizontal permeability in area A, A2 and B.

A closer look at illite types in area B reveals that it is the pore-filling illite that causes the permeability reduction. A good negative correlation is seen between the permeability and the authigenic pore-filling illite (Figure 5-16). Grain rimming illite is also partially responsible for some reservoir quality loss, whereas grain replacive illite does not play much of a role.

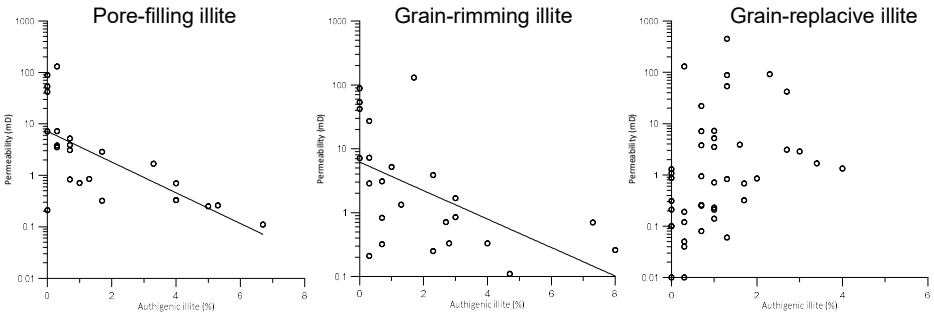

Figure 5-16 Different illite types plotted against horizontal air permeability in area B.

Fibrous pore-filling illite was identified in thin sections and via SEM (Figure 5-17). The illite has grown fibrously into the pore-spaces and pore-throats beginning with an initial grain-rimming phase. Grain-replacive illite merely replaces grains that were mostly pore-free and thus does not further restrain fluid/gas flow pathways.

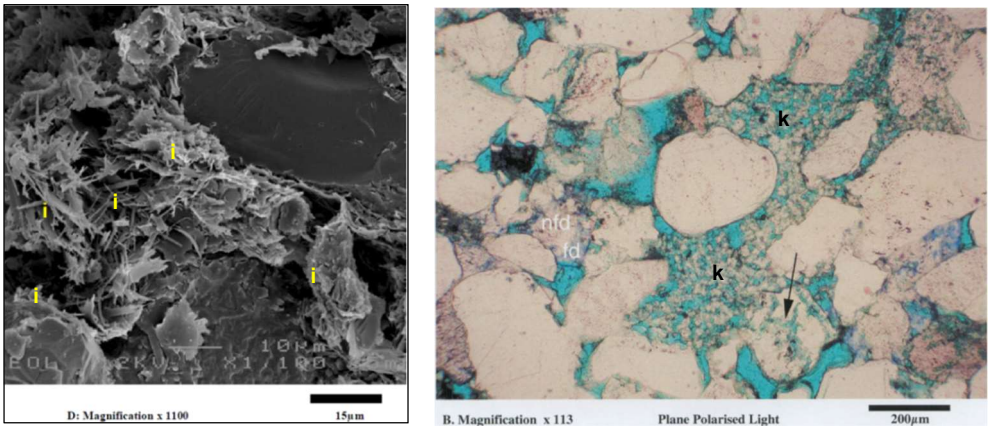

Figure 5-17 Left: SEM image of authigenic fibrous illite growth (i) in pore-spaces between detrital grains in well L06-07, modified after (Pierau, 2010). Right: Thin-section image from well L05-09 displaying kaolinite (k). The blue colour represents open pore-space. Modified after (Rieke, 2003).

Kaolinite has a negligible effect on permeability and porosity. A slight increase in permeability and porosity is indicated in areas A and A2 (Figure 5-18). Kaolinite formed as both grain-replacive and pore-filling cement after detrital grain dissolution. Pore-spaces between the kaolinite crystals or crystal clusters remained open (Figure 5-17) thus not restricting permeability and porosity.

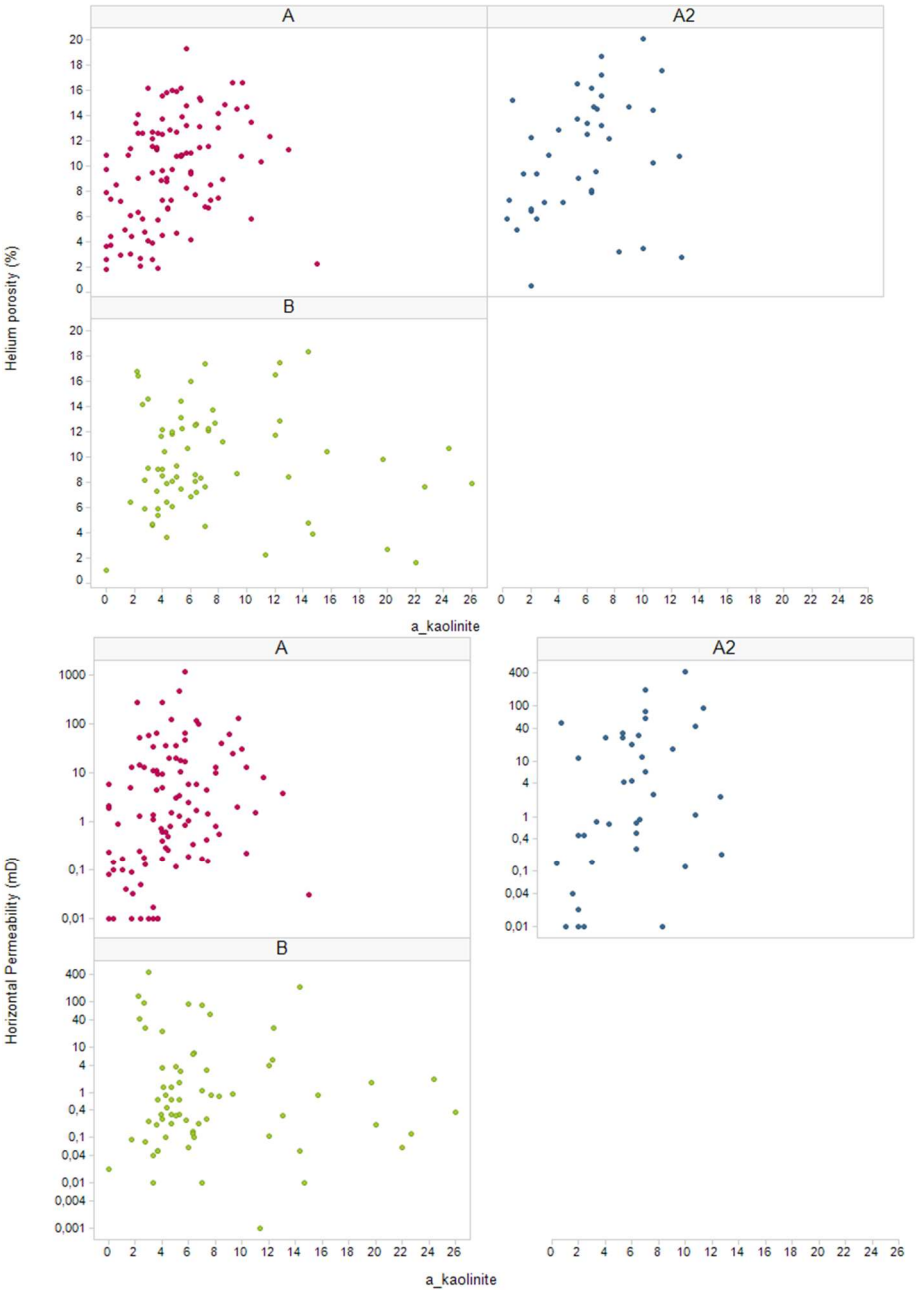

Figure 5-18 Authigenic kaolinite plotted against porosity and permeability for areas A, A2 and B.

Clay minerals such as illite and kaolinite commonly form by recrystallization of detrital clays and grain dissolution (mainly feldspar). The introduction of aluminium and potassium rich fluids from the coal bearing Carboniferous deposits can enhance clay formation (Ehrenberg, 1991). An increase of kaolinite (and authigenic quartz) was observed with progressive proximity to the Carboniferous in the previous chapter. The Carboniferous fluids are generally acidic thus can dissolve detrital grains providing more Al, K^+ and silica for clay (and quartz) formation, creating a favourable environment for these minerals. Aluminium can also be sourced from dissolution of alumosilicates and albitisation of feldspar (Boles, 1982).

The dissolution of K-feldspar in sandstones also enhances the illitisation of illite/smectite mixed-layer minerals (Lynch et al., 1997; Wilkinson et al., 2003). Temperature is assumed to be not the most important factor controlling illite precipitation, instead the growth of (particularly fibrous) illite is limited by nucleation kinetics (Darby et al. 1997; Wilkinson and Haszeldine, 2002).

The distance to the Carboniferous subcrop and kaolinite for both focus areas does not have a relationship with any of the areas or subcrop types (Figure 5-19). Illite tends to increase towards the Rotliegend/Carboniferous boundary in the study area. The increase is seen for the Westphalian B subcrop in area B, that also contains some coal deposits. The coal-bearing Westphalian C, on the other hand, does not have an effect on the illite composition. It is likely but not certain that fluid flow from the Carboniferous may have triggered the formation of illite. According to the paragenetic sequence of area B illite formation was rather early, starting during early diagenesis and continuing to the intermediate diagenesis. The main gas charge was probably during the Jurassic, which would have been preceded by CO_2 rich Carboniferous fluids. The timing of illite formation was likely prior to the Carboniferous fluid charge, which makes the influence of Carboniferous fluids on illite formation less likely.

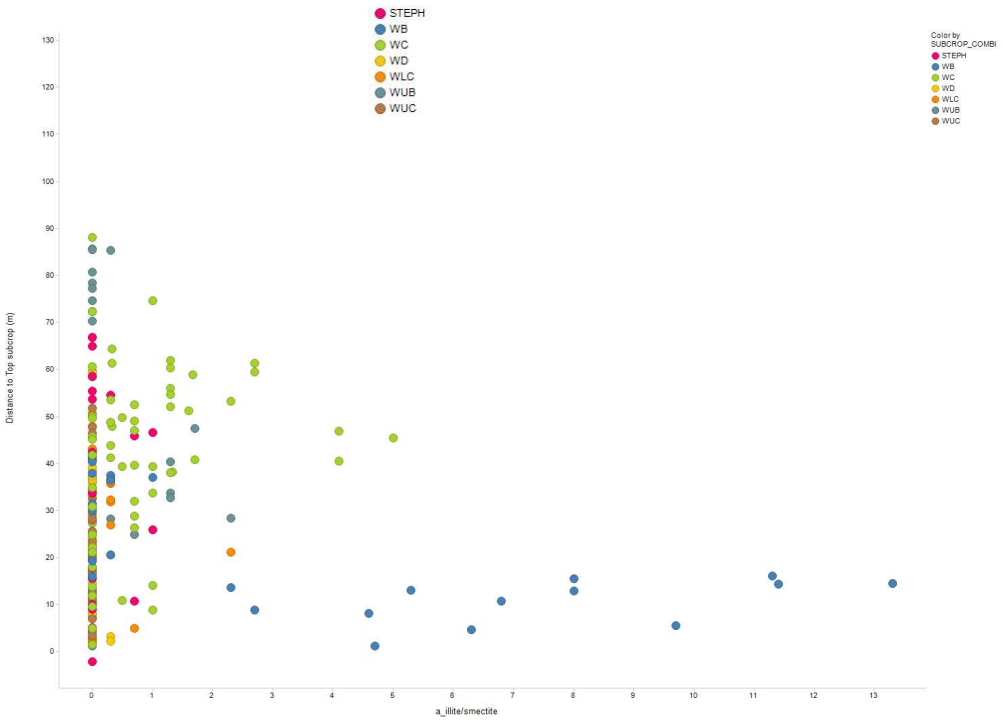

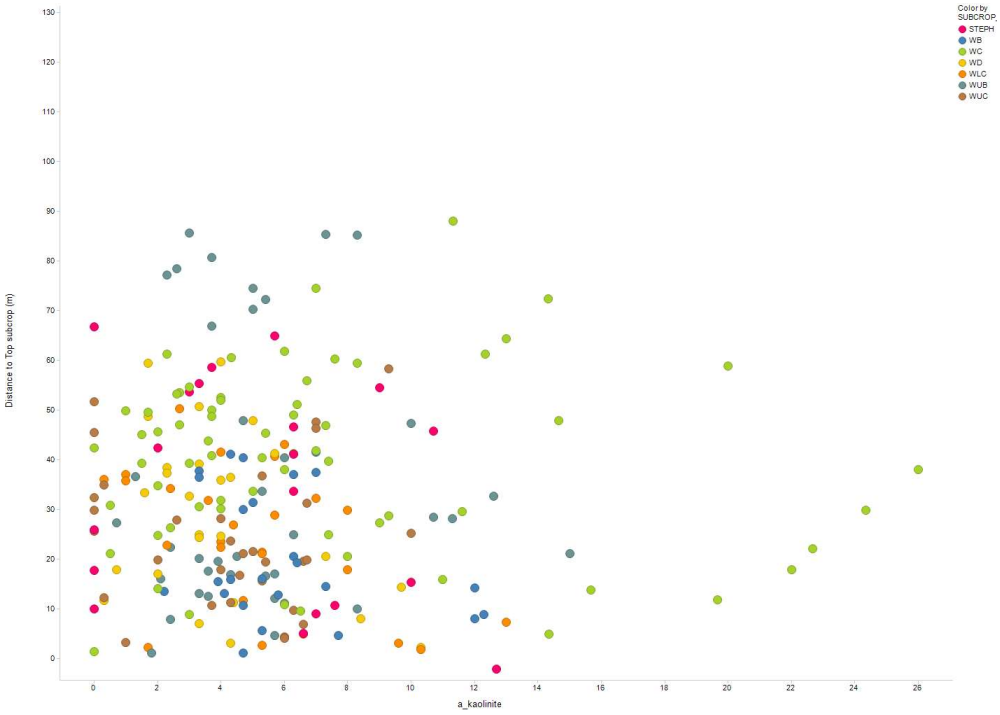

Figure 5-19 Distance to subcrop vs authigenic illite content (top) and kaolinite content (bottom).

As previously discussed in Chapter 4.5, the burial history and structural setting can influence clay formation. Burial of the Rotliegend deposits was substantially deeper in area B (Figure 5-20) and remained at depth longer than in area A (Figure 5-14), which can explain the kinetically driven illite formation under prolonged high temperatures. Illite is inferred to have formed during early and intermediate burial. When considering the mesodiagentic growth of illite the maximum depth of the top Rotliegend before the Middle-Late Jurassic uplift is consistent with the higher illite content in the deeper set area B (Figure 5-21).

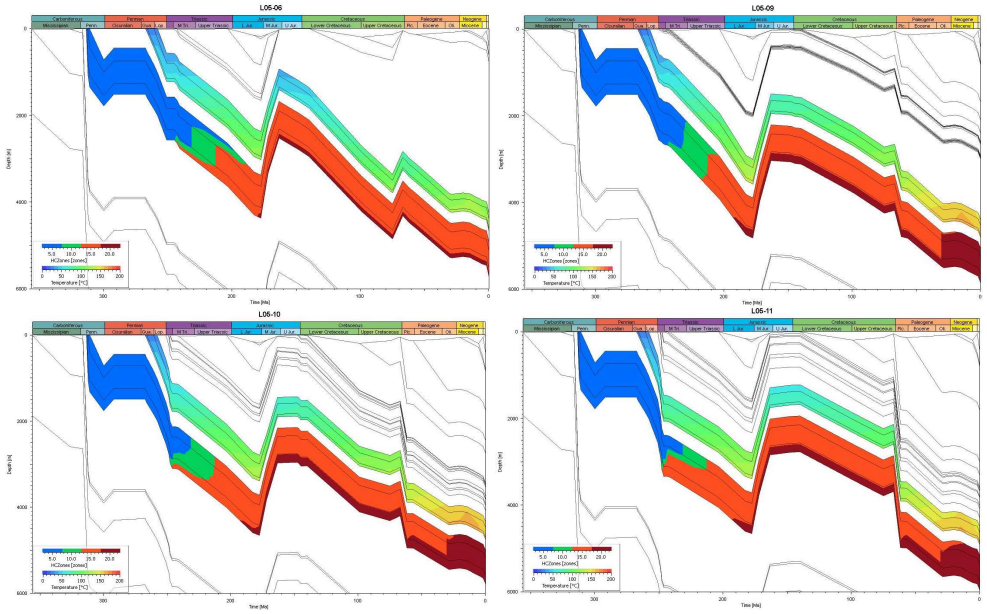

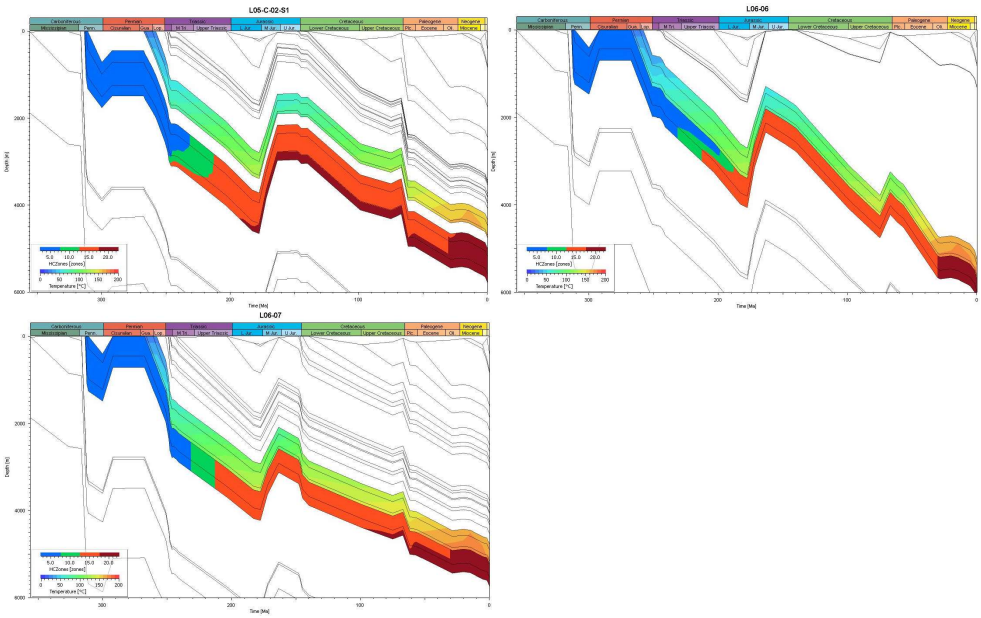

Figure 5-20 1D basin models for single wells in study area B. The Rotliegend is highlighted by the colour coded thermal evolution with the proposed paragenetic sequences of events below. The Carboniferous source rock maturity is according to Burnham (1989) KIII, blue: immature, green: oil generation, red: gas generation; burgundy: over mature.

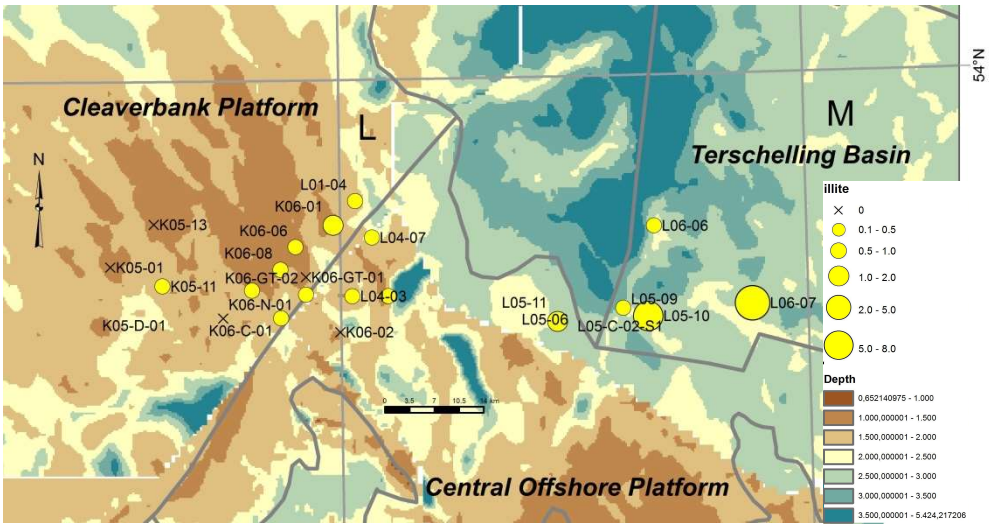

Figure 5-21 Average authigenic illite content per well in the focus areas plotted on maximum depth of the top Rotliegend before the Middle-Late Jurassic uplift phase according to 3D basin modelling and the top Rotliegend depth map. In some wells authigenic illite could not be determined.

If the duration of deep burial was the only driver for illite formation then wells L06-06 and L05-09 should also be illite rich. Strictly speaking, this not the case. Here, depositional environment may play a role. Authigenic Illite is most commonly seen as early cement in fluvial (proximal) overbank and unconfined deposits (Figure 4-16). The sediment samples from wells L05-10, L05-11 and particularly L06-07 were deposited to a large part in this environment (Figure 5-22), whereas samples in wells with lower content of illite content (L06-06 and L05-09) are related to

predominantly fluvial (proximal) channelized and other fluivial and aeolian sub-environments. The early (eodiagenetic) formation of illite (compare Figure 5-5) is coherent with the environmental control we observe in area B.

In summary, illite abundance is dependent on a combination of factors, being depositional environment, duration of deep burial and possibly the influence of the Carboniferous (WB). The combination of all these factors is bound to result in significant illite growth, which effects the permeability in sandstones.

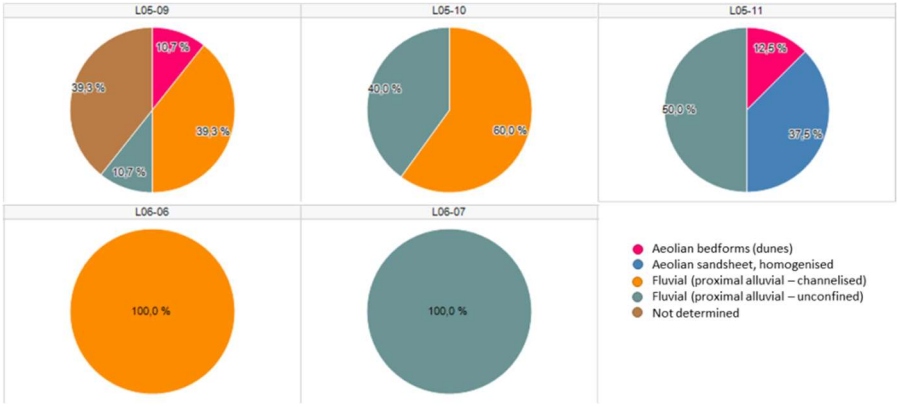

Figure 5-22 Depositional sub-environment per well in area B. In wells L05-06 and L06-C-02-S1 sedimentological data was not provided.

Kaolinite is unrelated to the depositional environment, burial history and the overlying, underlying and adjacent formations in both areas. The grain replacive nature of kaolinite indicates that it is predominately bound to previously dissolved detrital grains. Particularly feldspar grains are prone to dissolution and promote the precipitation of kaolinite (Curtis, 1983; Ziegler, 2006). The (remaining) feldspar content is quite low (< 4%) in the study area but would have been originally higher. The comparison of authigenic kaolinite and detrital feldspars does not show a clear negative correlation (Figure 5-23). Nevertheless, most of the samples with high kaolinite contents do not contain any feldspar. The feldspar could have been dissolved or not deposited. The original feldspar content is related to sediment provenance. We cannot reconstruct the original feldspar content in this study but believe that the feldspar content could have been a driver for kaolinite precipitation in the area.

Quartz is an omnipresent cement (not only in the case study area). Quartz cementation does not follow a particular trend. Several studies point to the reducing effect of early chlorite coatings on quartz (e.g., Taylor et al., 2015). Also clay grain coatings are proposed to decrease quartz overgrowth. However, the dataset does not provide clear evidence for this, possibly because a differentiation between grain-coating clay and other clay was not rigorous and chlorite too rare in the studied dataset to be able to see a relation.

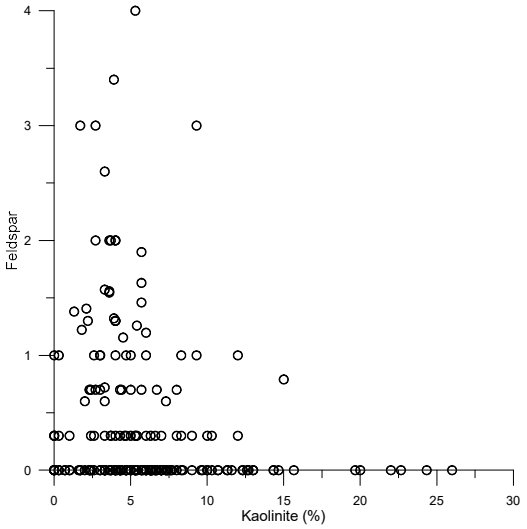

Figure 5-23 Negative envelope of detrital feldspar vs authigenic kaolinite in the focus area.

5.4.3 Carbonates

The carbonate minerals calcite, siderite, dolomite and ankerite were identified in the focus area, with ankerite having the highest and calcite the lowest abundance. The total carbonate content is higher in area A. Ankerite is more abundant in area A and A2 compared to area B. In area A and partially in area A2 ankerite is a porosity and permeability reducing cement (Figure 5-24). Dolomite has also a somewhat negative effect on both porosity and permeability in all areas (Figure 5-25), although the relationship is not as clear as for ankerite.

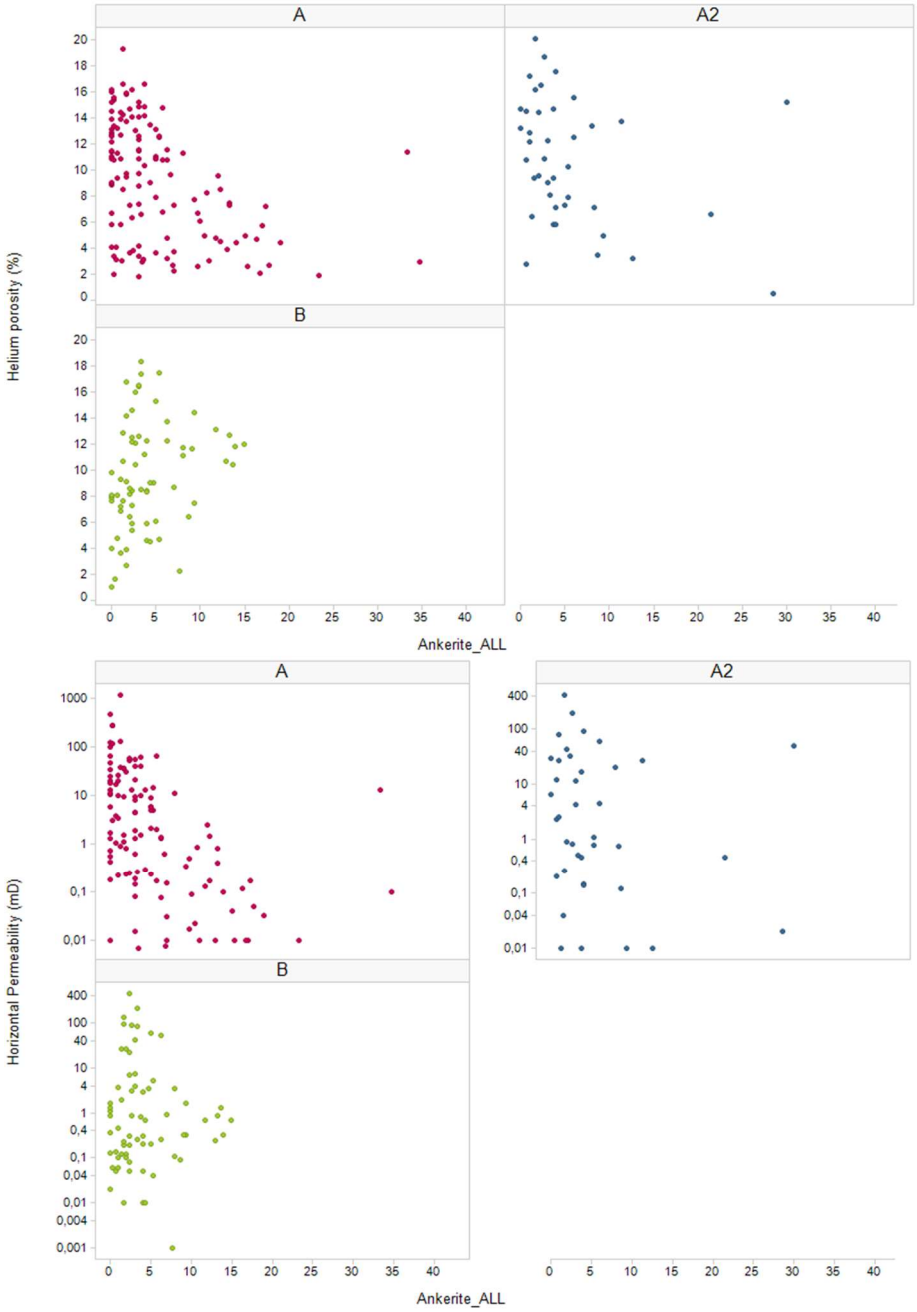

Figure 5-24 Ankerite (%) plotted against He-porosity and horizontal permeability in areas A, A2 and B.

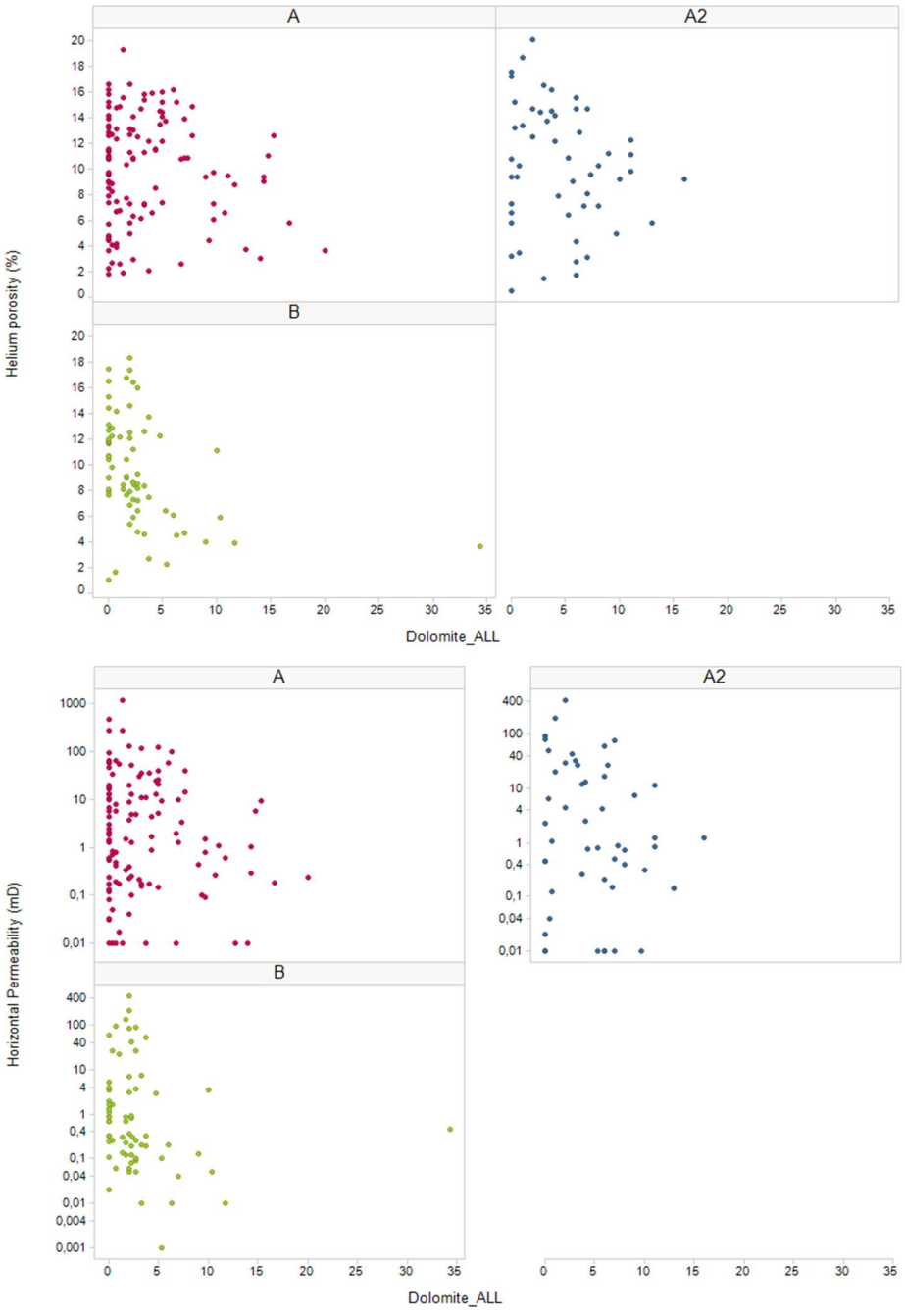

Figure 5-25 Dolomite (%) plotted against He-porosity and horizontal permeability in areas A, A2 and B.

Calcite content was too low to determine a relationship to reservoir quality in the focus area. It is likely to have no effect on porosity and permeability. Siderite has no effect on porosity and permeability in area A. In area B we observe a weak positive effect on porosity and permeability (Figure 5-26).

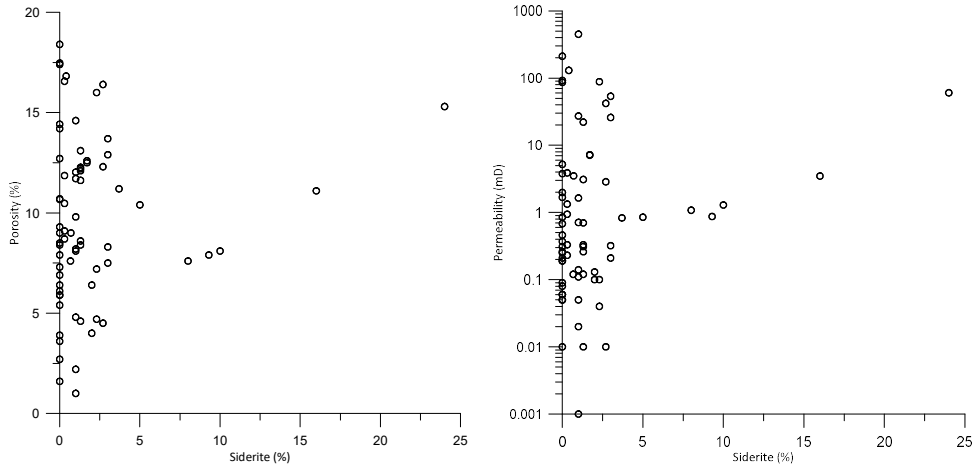

Figure 5-26 Siderite plotted against He-porosity (left) and horizontal permeability (right) in area B.

Because carbonates, particularly ankerite and partially dolomite have a significant effect on the reservoir quality in the focus areas it is important to understand the origin of their formation. There is a clear difference in carbonate cementation within the focus area. Sediments from area A (and A2) have sufficiently more carbonate, particularly ankerite, than those from area B. Dolomite and ankerite formed relatively early in the diagenetic history in area A compared to B (see Figure 5-5) and ankerite continued to form during mesodiagenesis. Siderite precipitated at different stages both at early (area A), intermediate (area A+B) as well as late (area B) diagenesis. The positive correlation of siderite to reservoir quality may be connected to the fact that late diagenetic grain dissolution lead to only minor cementation of mainly siderite. Siderite, as such, does not have a direct reservoir quality enhancing effect.

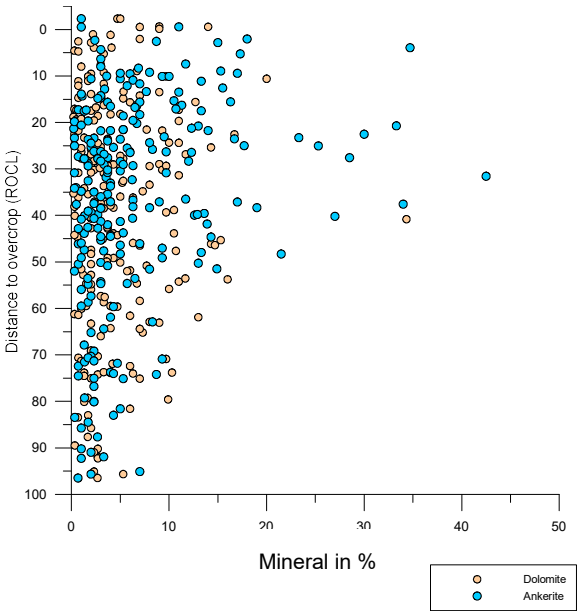

Figure 5-27 Dolomite and ankerite content with distance to the overlying Silverpit Formation.

Ankerite and dolomite cements on the other hand are important to the reservoir quality of the focus area. Early dolomite was seen to be related to the depositional environment, accumulating commonly in proximal fluvial deposits (see chapter 4.6). In the focus area we do not observe an environmental control although dolomite is an early cement in area A. This is possibly because dolomite was dissolved and redistributed at an early stage with additional overprinting in the later diagenesis. When regarding the distance to the overlying Silverpit Formation we observe a slight increase of dolomite and a clear increase of ankerite with proximity to the Silverpit Formation. This indicates that Silverpit fluids may have entered the Rotliegend formation and drove the precipitation of these carbonates. This may have happened during early burial and compaction of the Rotliegend playa shales that released alkaline fluids into the adjacent and underlying sandstones or during the deposition of the Zechstein sediments. In some wells (e.g. L05-09) siderite content also increases with proximity to the Silverpit, which indicated that the fluids may have been Fe-rich. Iron may have been released due to reduction of Fe-oxides.

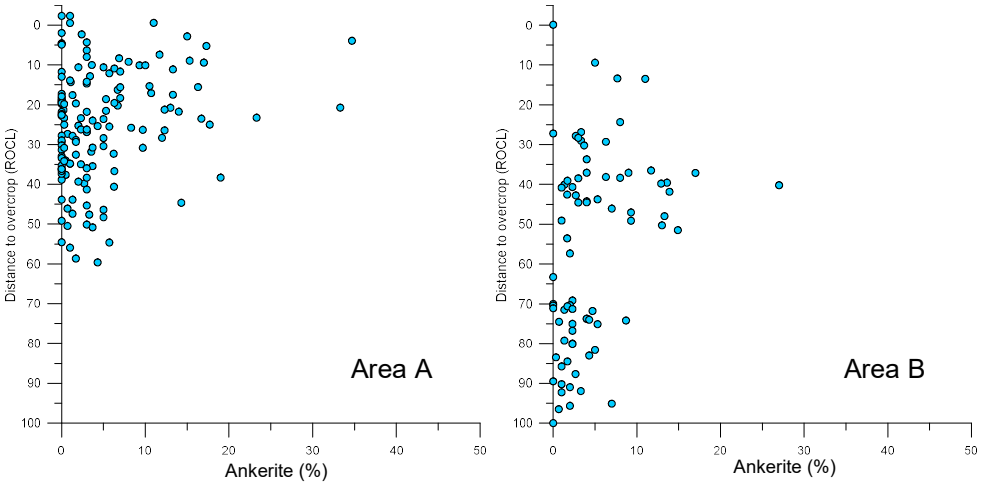

Figure 5-28 Ankerite content plotted against the distance to the overlying Silverpit Formation for area A and A2 (left) and area B (right).

The higher ankerite content and thus also the stronger impregnation on the reservoir quality in area A may be connected to the fact that the samples are closer to the Silverpit Formation in area A, whereas in area B they are further away due to the larger thickness of the formation (Figure 5-28). As the sample density is low within about 20m proximity of the Silverpit Formation in area B it is possible that we are missing the ankerite rich samples and that the process may be equally important in area B.

Fluid flow from adjacent Silverpit, Carboniferous or Zechstein formations due to tectonic juxtapositioning may have also been important for carbonates. Dolomite shows a slight decrease with increasing proximity to the adjacent Silverpit Formation but also to Zechstein and Carboniferous (Figure 5-29). The relationship is however not clear because a few wells that are close to the faults have very low dolomite contents. We do not have any information about whether these or other faults were/are sealing, therefore further speculation is not feasible. Ankerite, on the contrary, seems to decline with distance to Silverpit and Carboniferous juxtaposed strata (Figure 5-29), however this may be a coincidence.

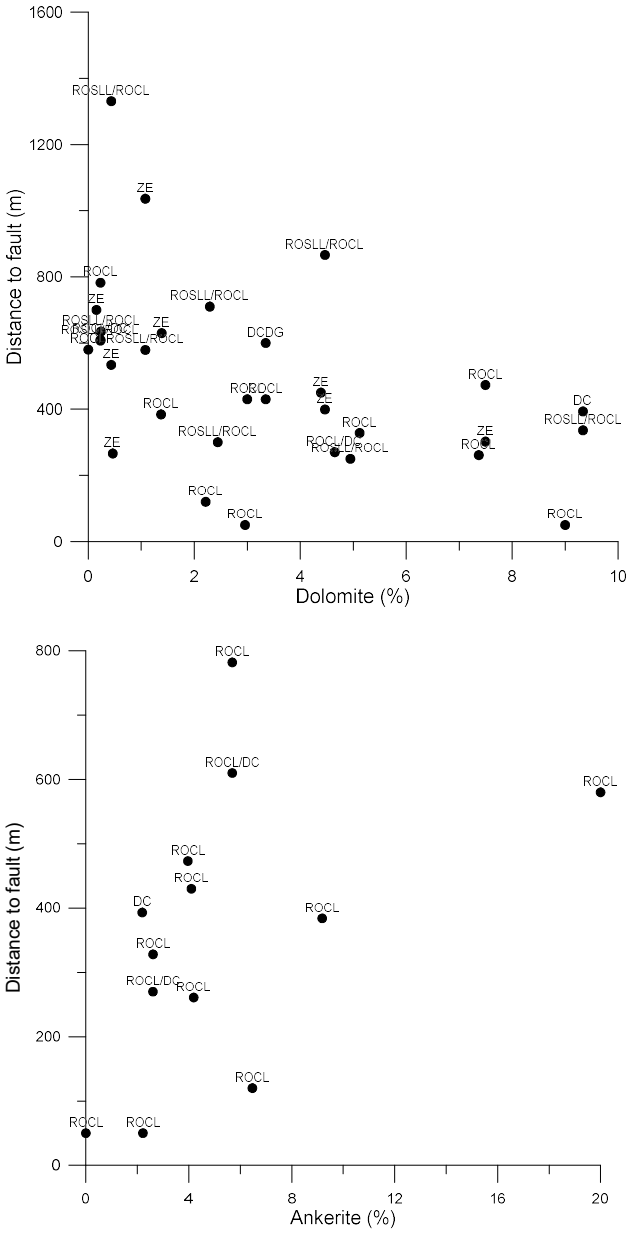

Figure 5-29 Distance to the nearest faults plotted against average composition of dolomite (top figure) and ankerite (bottom figure) per well.

A further cause for carbonate formation was proposed by Miocic (2011) who studied the carbonate mineralogy in well K02-02. In the study dolomite and ankerite cements were proposed to increase with proximity to interbedded mudstones, whereas siderite had no relation. Gerard et al. (2008) noted that in their studied wells (that cover most wells in area A) early dolomite formation was related to the proximity to the desert lake and playa shales and distal fluvial shale deposits.

We compared the clay volume that was derived from wireline logs for a few wells in area A and B (Figure 5-30). In wells K06-GT-01 and K06-GT-02 there is some relation of mostly dolomite to the clay layers. In well K06-01 the connection to clay

layers is not visible. Moving to area A2, we observe a possible but not clear relationship to ankerite/dolomite. In well L05-09 there is no association with the clay layers.

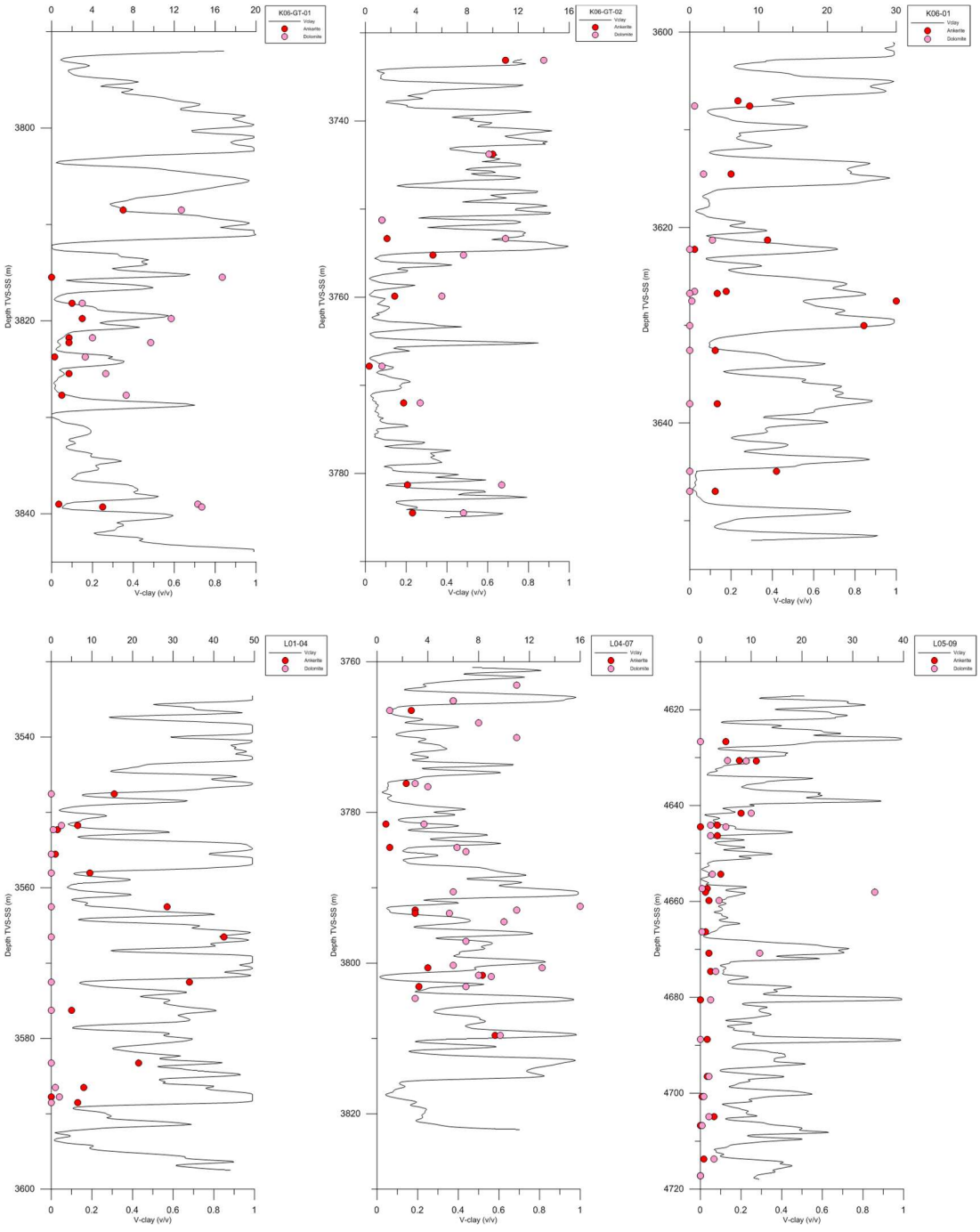

Figure 5-30 Dolomite and ankerite content and Vclay plotted against depth (TVDss) for wells K06-GT-01, K06-GT-02, and K06-06 from area A, wells L01-04 and L04-07 from area A2 and well L05-09 from area B.

It is apparent that intercalated clay layers are related to dolomite and ankerite cements in some wells. However, it is not clear why intercalated shales/mudstones should provide a pathway for carbonate formation.

5.5 Summary

The main reservoir quality reducing cements in the focus area are ankerite, dolomite, illite and locally anhydrite, whereas area A is more prone to carbonate cementation and area B to authigenic illite. Both areas experienced a similar burial sequence of events but to a different degree. The diagenetic mineral emplacement as well as mineral dissolution also varies between the two areas. In area A carbonate minerals are some of the earliest cements, whereas in area B illite precipitated earlier and was more pervasive as a pore-filling mineral. Late diagenesis (telodiagenesis and mesodiagenesis II) is governed by sulphate cements. Interestingly, although mesodiagenesis II resulted in more deeper burial, there does not seem to be much more authigenesis at the stage. One hypothesis may be the introduction of bitumen that may have prohibited further cementation.

Figure 5-31 summarises the factors effecting cementation and reservoir quality in the focus area. Sulphates (mainly anhydrite) are related to the proximity to the Silverpit formation and thus may have precipitated from the ingression of Silverpit fluids. Sulphate cementation were also driven by the degree of Late Jurassic uplift and the connected Zechstein or Silverpit fluid ingression, whereas fluid ingression may have also occurred due to fault related juxtapositioning of Zechstein deposits. A relation to faults is not evident and thus builds a conundrum for the theory.

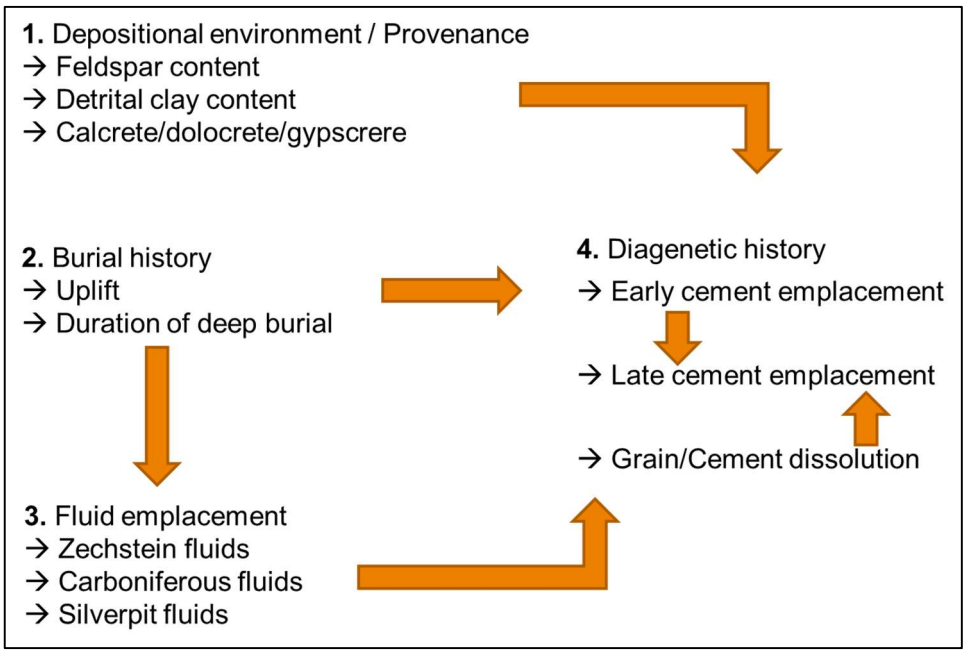

Figure 5-31 Schematic diagram displaying factors influencing cementation and reservoir quality in the focus area. Direction of orange arrows refer to the influence of one factor on another.

Illite abundance is dependent on a combination of factors, being depositional environment, duration of deep burial and possibly the influence of the Carboniferous fluids. Kaolinite may be connected to the original feldspar content.

Carbonate cementation was likely influenced by the Silverpit fluids, particularly observed by the increase of ankerite cement with proximity to the overlying Silverpit formation. There is a possible relation of dolomite cementation with relation to faults, but without certainly. Lastly, intercalated clay layers may be related to both ankerite and dolomite formation but this remains speculative.

6 Conceptual Diagenetic Models

6.1 Introduction

Results from previous chapters suggest that diagenetic processes (or models) can vary from location to location and different strata. Nevertheless, certain cementational trends can be traced throughout the Netherlands. In this chapter the main drivers for cementation are determined. Authigenic minerals are attributed to different sources of cementation. By comparing insights from the focus area with other locations and combining the regional cementational models we aim to establish a conceptual diagenetic model for the Dutch Upper Rotliegend.

It is important to note that for areas outside of the focus area the data density is often poor. The investigation of locations outside of the focus area was not as in-depth as for the focus area.

6.2 Conceptual cement models

6.2.1 Prolonged deep burial (of proximal alluvial unconfined and overbank deposits)

Pore-filling (fibrous) Illite cement was observed to be detrimental for reservoir permeability. Authigenic illite (and smectite) is commonly found in fluvial environments, particularly in proximal alluvial unconfined and overbank deposits. The high detrital clay content in these sediments is converted to authigenic illite, provided suitable growth conditions are met. A primary factor for illite formation is the duration of deep burial, which is prone to deep basinal structural elements. The reason for higher illite contents in deeper set areas is the kinetically driven illite growth with deep burial. The duration of deep burial is thus more important than the present or maximum burial depth. For many areas the initial phase of prolonged deep burial from the Permian to the Early/Mid Jurassic was paramount to illite formation (Figure 6-1).

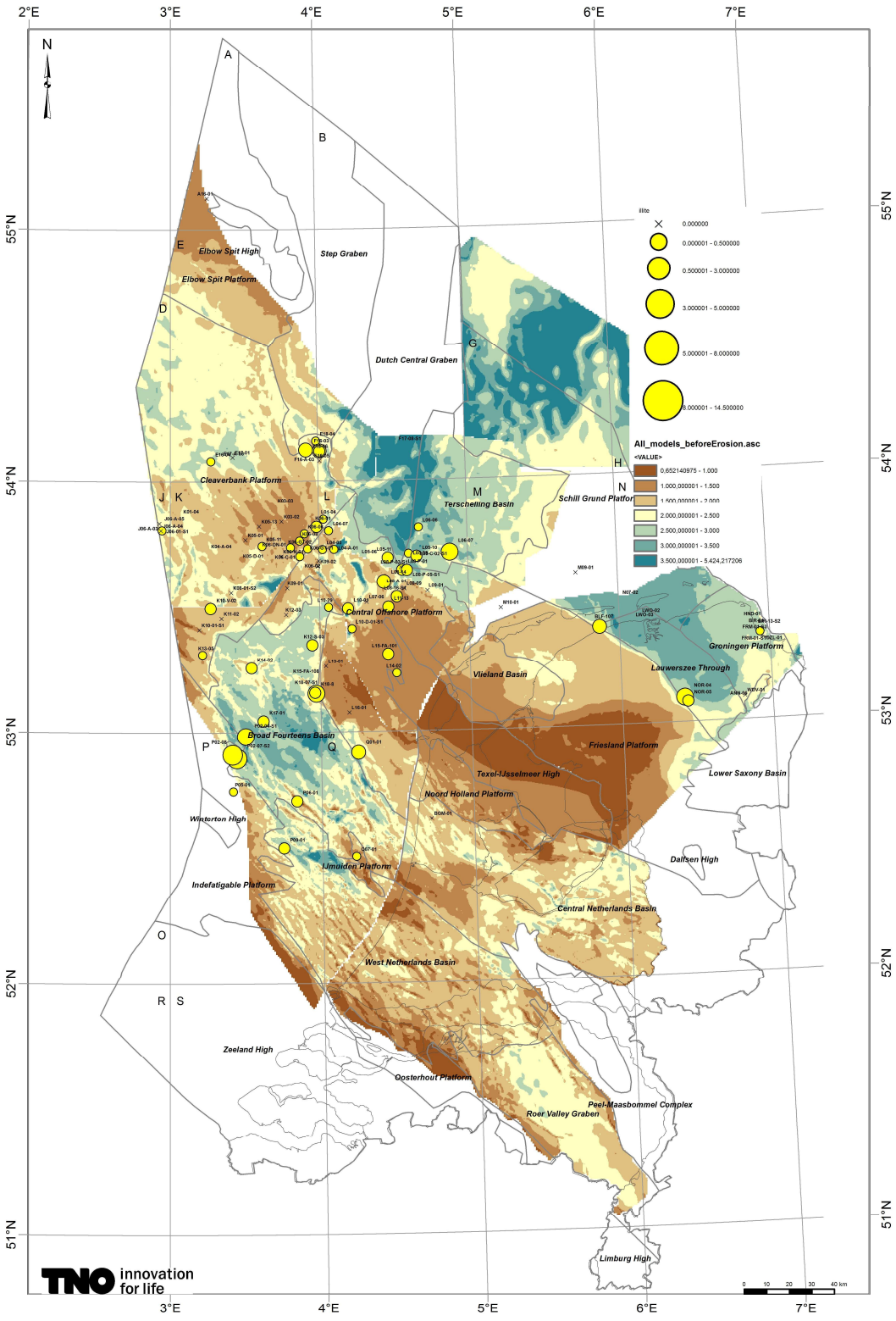

Figure 6-1 Maximum depth of the Top Rotliegend before the Middle-Late Jurassic uplift phase according to 3D basin modelling with average authigenic illite contents per well.

6.2.2 *Influence of Carboniferous fluids (and feldspar)*

Allochthonous fluids can influence illite, kaolinite and quartz precipitation. An increase in authigenic kaolinite and partly authigenic quartz is evident towards the Carboniferous subcrop. The acidic fluids from the coal-bearing Carboniferous strata (DCC) can enhance the dissolution of feldspar and provide an optimal environment for kaolinite precipitation. For this process to occur the original feldspar (and rock fragment) content is also particularly important for the formation of these cements. Feldspar dissolution delivers significant amounts of aluminum and silica that react to form kaolinite and also quartz. The original amount of feldspar depends on the provenance of the detrital components and distance to their source. Areas with high present day feldspar content may indicate a lower level of cementational diagenesis.

The initial environment that the Carboniferous fluids create is possibly more favourable to kaolinite, rather than illite precipitation (e.g. low pH, low K^+ activity) and may be the reason for the opposite trend for kaolinite and illite contents with proximity to the coal-bearing Carboniferous (Figure 6-2). Illite increases away from the Carboniferous. This is a similar trend that can be seen between juxtapositioned Rotliegend and Carboniferous strata. At the contact to the coal-bearing Carboniferous the first layer contains large amounts of kaolinite and the second layer mainly illite (Figure 6-3). In consensus with the general model we observe a thickness of the kaolinite zone at a stratigraphic contact (as opposed to a fault contact) of only a few tens of meters and the illite zone starting at about 100m.

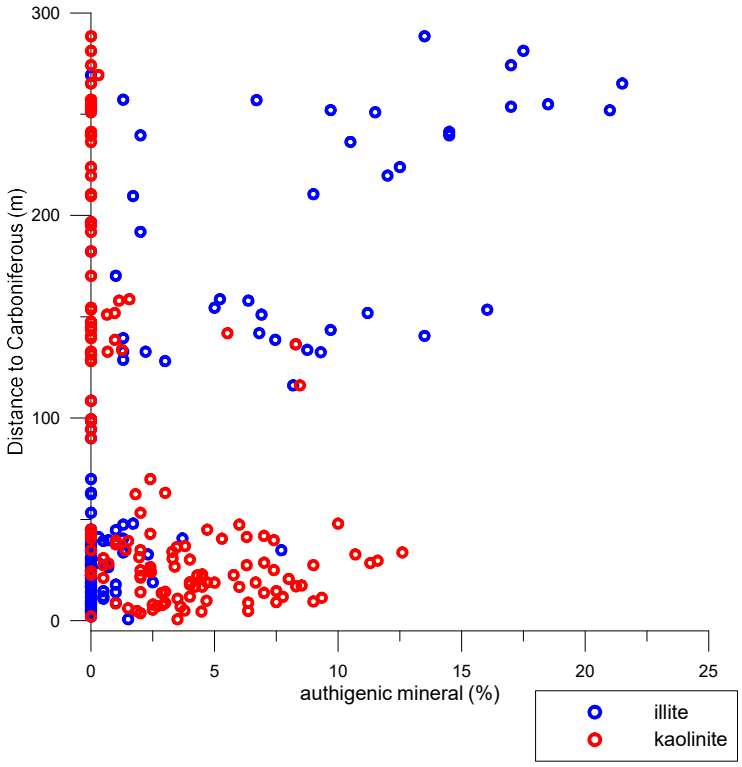

Figure 6-2 Authigenic illite and kaolinite contents versus the distance to the coal-bearing Westphalian C (DCC).

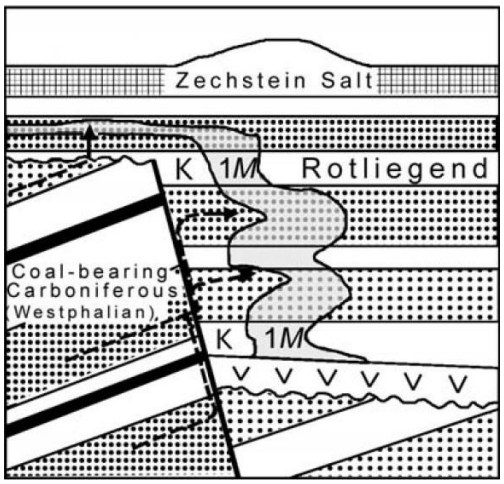

Figure 6-3 Zonation of clay minerals around a contact between Carboniferous Coal Measures and Rotliegend deposits, K = kaolinite, 1M = illite (from Ziegler, 2006).

The reason for this trend is that the reactive elements of the Carboniferous fluids are neutralised the further away they migrate from the BPU. Kaolinite precipitation reduces the pH of the fluid, while the potassium is transferred further into the sandstone leading to illitisation in the next zone. The extent of both kaolinite and illite zones depends on the permeability of the sediments.

Notably, kaolinite does not reduce reservoir quality as opposed to illite, whereas carbonate cements and particularly ankerite reduce both porosity and permeability. Ankerite and siderite are also influenced by the Carboniferous fluids. The migration of CO_2-rich, acidic fluids from the coal-bearing Carboniferous likely dissolved pre-existing carbonate phases, such as calcite and possibly dolomite. Contribution of bicarbonate ions and pH neutralisation by precipitation of other minerals (e.g. kaolinite) lead to the formation of ankerite and siderite. Fe^{2+} contribution for ankerite and siderite is sourced from the leaching of Fe-oxides by the reducing fluids. Ankerite and particularly siderite will not precipitate if Fe^{2+} is insufficient. Particularly siderite and Fe-oxides rarely occur together (Figure 6-5). To some degree the preference of ankerite over dolomite to precipitate at the boarder to the coal-bearing Carboniferous is demonstrated when both minerals are plotted together against the proximity to the Westphallian C (Figure 6-4). The ankerite peak (between ~ 0 and 50m) is followed by a dolomite peak (~ 100m).

The relationship of dolomite, however, to the carboniferous fluids is not as distinct as for ankerite. As previously observed, dolomite precipitation is also bound to the depositional environment. It is not entirely clear whether cross formational fluid flow also affected dolomite during faulting and fracturing periods. A broader fault study would be needed to answer this question. Proximity to intercalated mudstones was also proposed for dolomite, as well as ankerite cementation. This hypothesis was not fully explored in the current study and may deserve further investigation.

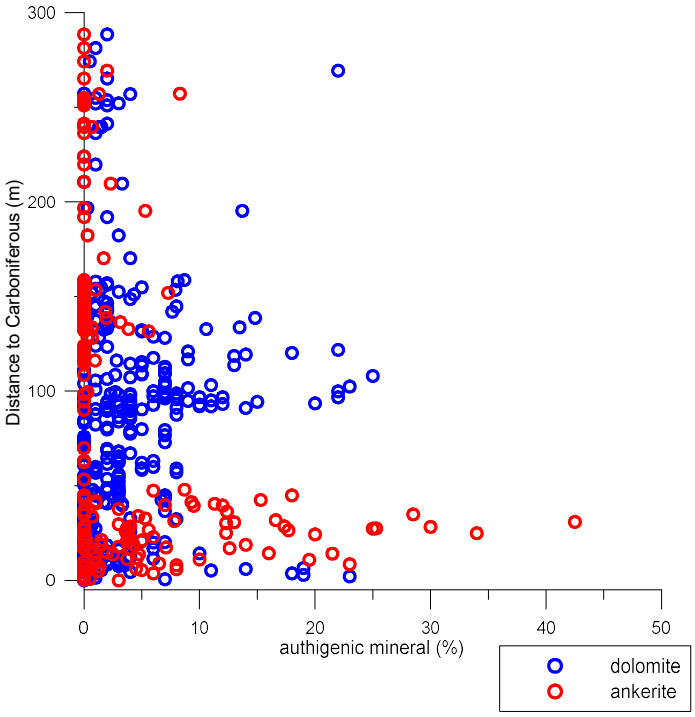

Figure 6-4 Authigenic dolomite and ankerite contents versus the distance to the coal-bearing Westphalian C (DCC).

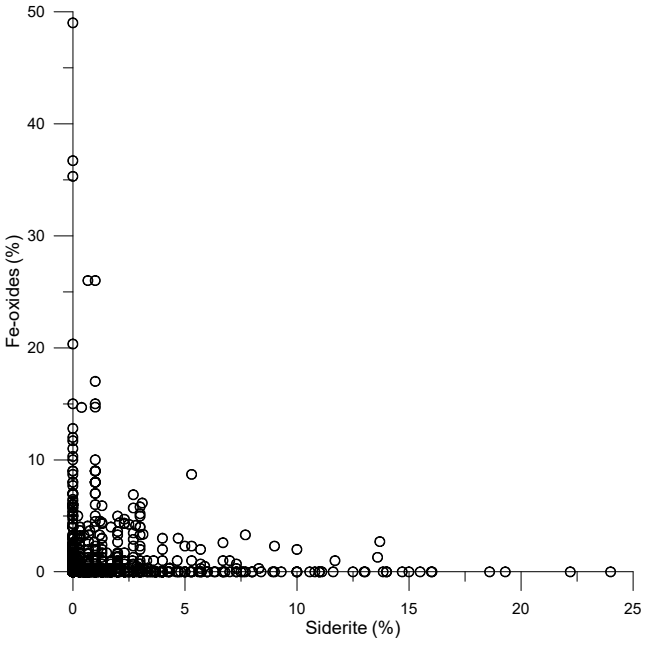

Figure 6-5 Siderite content plotted against Fe-oxides (Whole-rock dataset).

For barite to precipitate, not only sulphate but also sufficient Ba^{2+} contents are required. Ba^{2+} is present in organic matter and also in feldspar. The ingression of Carboniferous fluids delivers both Ba^{2+} (from organic source rocks) and releases it

from feldspars. However sufficient pore-water SO_4^{2-} concentrations are required to precipitate barium. Apparently these conditions are rarely met in the Rotliegend as barium is not a common cement.

It is important to note that the Carboniferous fluid influx into the Rotliegend sandstones can either take place at the Carboniferous/Rotliegend boundary (BPU) or at a fault related to full or cross juxtapositioning of the Rotliegend against the Carboniferous. A thorough investigation of the fault and fracture network is necessary for better prediction of the cementation of the previously mentioned cements.

6.2.3 Evaporitic environments (and early diagenesis)

The Silverpit formation is lithostratigraphically subdivided from the Slochteren. Besides being particularly clay-rich the Silverpit also contains halite and anhydrite deposits, which is the reason why anhydrite, even in sandstone horizons is mainly found in the Silverpit formation (as opposed the Slochteren). The Zechstein strata is predominantly evaporitic.

Both the Silverpit and the Zechstein pore-fluids contain high amounts of total dissolved solids and are mostly saturated with respect to sulphate minerals. With increasing proximity to the Silverpit formation and/or to the Zechstein Group conditions become more evaporitic and the chance of precipitation of gypcretes, calcretes and dolocretes increases. We observe also an increase anhydrite, ankerite, barite and dolomite cements. Upon burial and rising temperature and pressure leads to gypsum dehydration to form anhydrite and calcite is commonly converted to dolomite. Depending on the availability of Fe^{2+} ankerite could be the preferred mineral phase. Both dolomite and ankerite are more stable at high T/P conditions. Alternatively or additionally to the synsedimentary sulphate and carbonate formation, fluids from the Silverpit playa lake were expelled during early burial towards the adjacent Slochteren formation. Transport of their fluids towards the Slochteren sandstones would have resulted in early diagenetic sulphate and carbonate precipitation in the Slochteren sandstones.

Anhydrite is more prominent in the distal aeolean deposits, that are close to the sabhka, whereas ankerite does not show a distinct facies control (Figure 6-6). The lack of correlation with a particular environment for ankerite and to some degree anhydrite is because the cements is also influenced by other diagenetic factors.

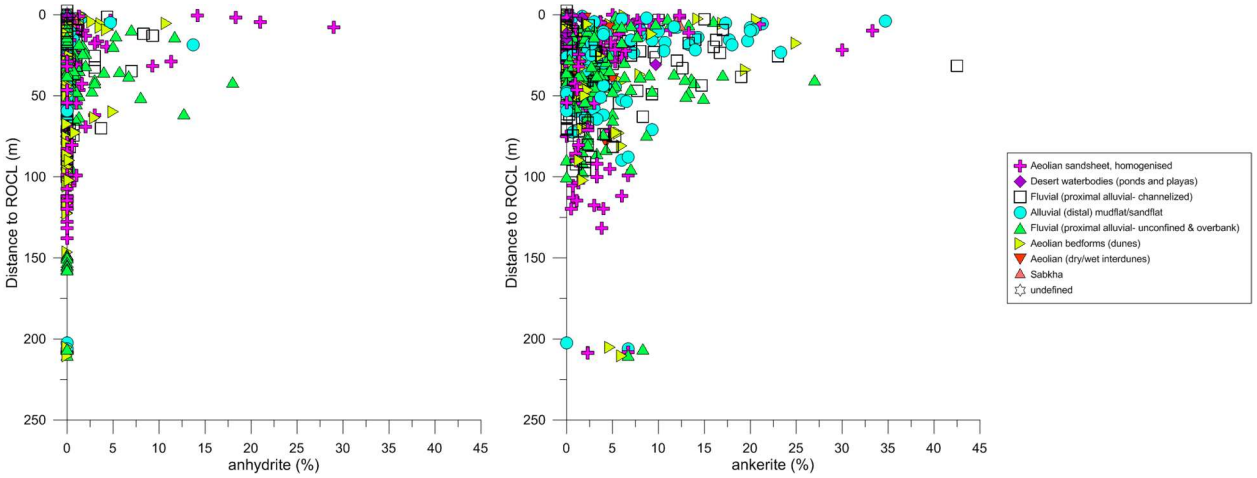

Figure 6-6 Anhydrite and ankerite contents plotted against the distance to the Silverpit formation with indication of the sub-environment.

Generally, these processes occur during early diagenesis. However, in evaporative environments burial results in supersaturation and precipitation of calcite and dolomite. During intermediate to late diagenesis ankerite forms by continuous solid solution from earlier dolomite.

Although precipitation of gypcretes is prone to evaporitic environments the gypsum grains that were deposited near a sabkha can also be wind-blown towards aeoliean sandstones (Henares, 2014). Subsequent burial of the detrital grains will lead to dehydration of gypsum to anhydrite and a possible redistribution within the sandstone.

6.2.4 Late Jurassic inversion (and telodiagenesis)

Zechstein influence on anhydrite cementation in the Rotliegend has often been mentioned in literature. During uplift and erosion in the late Jurassic the Zechstein the Rotliegend deposits were locally lifted towards the ground-water level.
The higher the Slochteren deposits were uplifted the more likely were they to interact with a renewed influx of meteoric fluids. Meteoric fluids can lead to dissolution of anhydrite in overlying or adjacent Zechstein deposits and also in overlying Silverpit deposits and carry the sulphate-rich fluids via density driven flow towards the Slochteren Formation. This can rapidly lead to late diagenetic anhydrite emplacement in sandstones. However, for the fluids to enter the Rotliegend sandstones an open fault and fracture network needs to be in place between the strata. The lack of such a network may be the reason for not seeing a clear trend between the degree of uplift and proximity to the surface in the Late Jurassic/Early Cretaceous (Figure 6-7) and high anhydrite contents. Previous tectonic juxtapositioning with Zechstein or the evaporite-rich Silverpit strata is favourable in such a case and deserves further investigation.

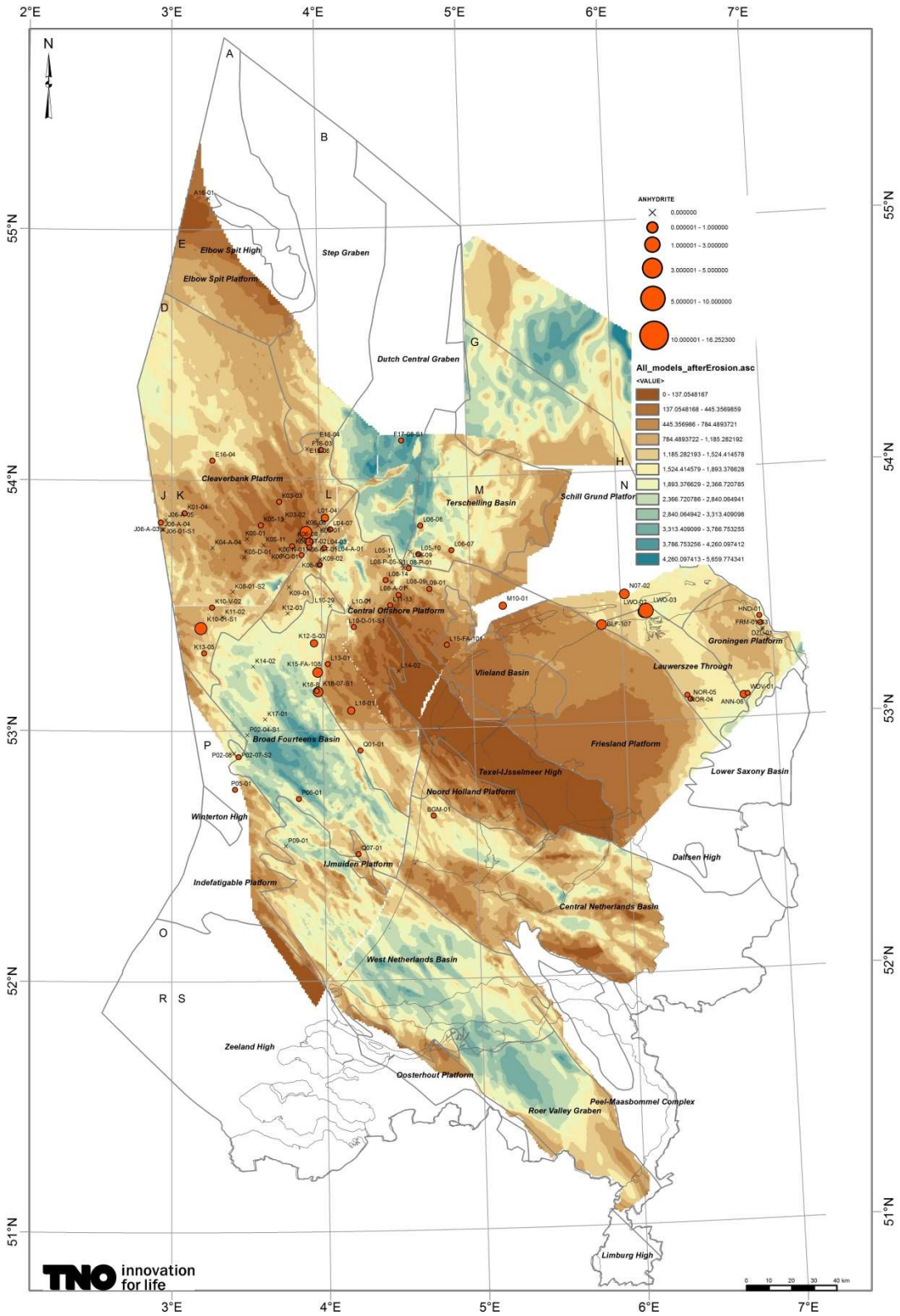

Figure 6-7 Minimum burial depth of the Rotliegend just after the exhumation caused by the erosion phase in the Jurassic (Middle to Late Cimmerian erosion phase according to 3D basin modelling with average anhydrite contents per well. Only wells with Slochteren deposits are shown.

6.2.5 *Combined diagenetic models and timing of minerals emplacement*

The timing of cement emplacement is driven by temperature, pressure and also CO_2/hydrocarbon charge. Burial history, as well as the environment and climate, play a major role in cementation. By combining diagenetic models and burial history one can link mineral precipitation and dissolution to a timeline. Under consideration of the conceptual models we present the (proposed) paragenetic sequences of events for focus areas A and B (Figure 6-8, Figure 6-9).

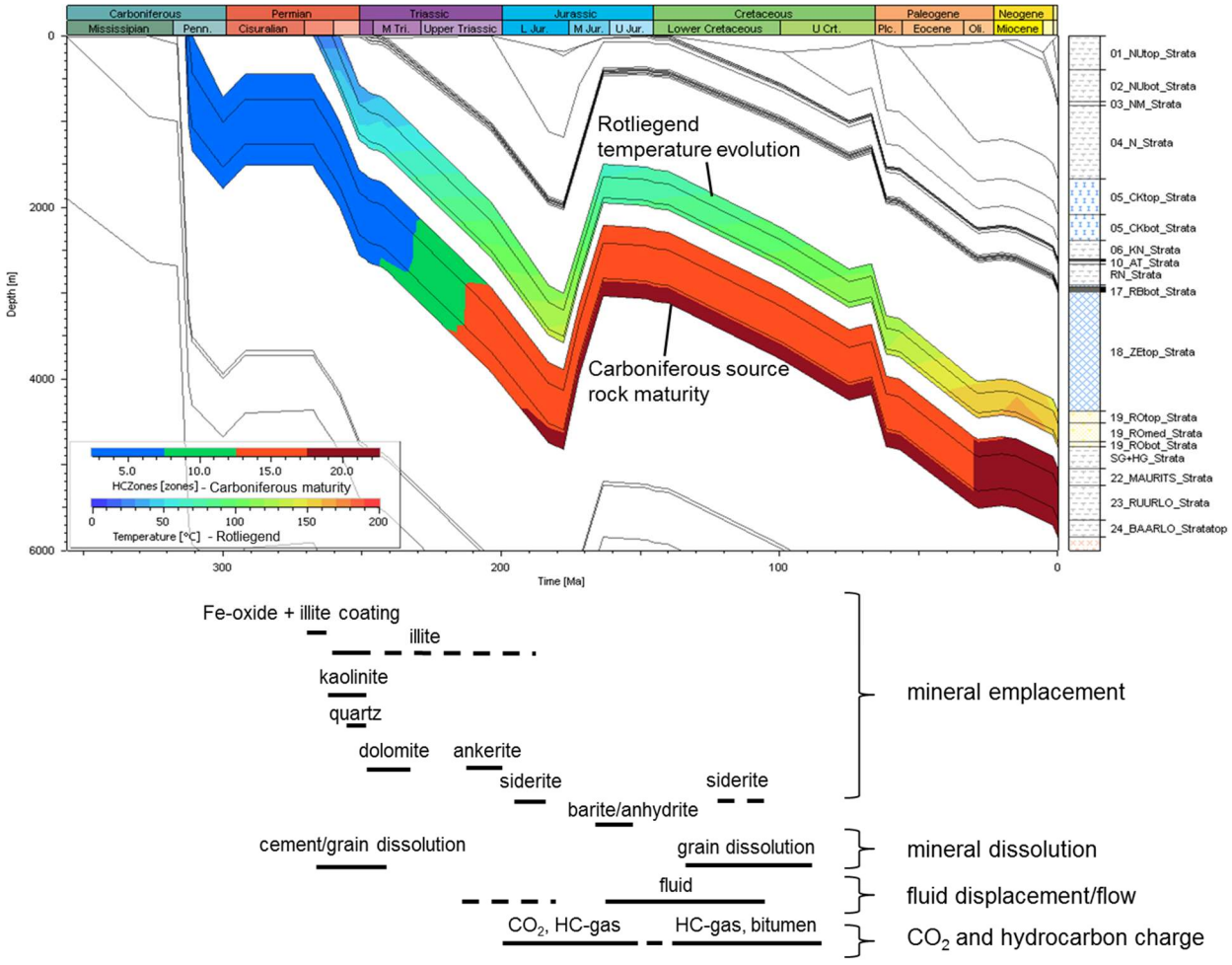

Figure 6-8 Burial and thermal history in focus area B, on example of well L05-09. The Rotliegend is highlighted by the colour coded thermal evolution with the proposed paragenetic sequences of events below. The Carboniferous source rock maturity is according to Burnham (1989) KIII, blue: immature, green: oil generation, red: gas generation; burgundy: over mature. Dashed lines depict uncertain timing of emplacement.

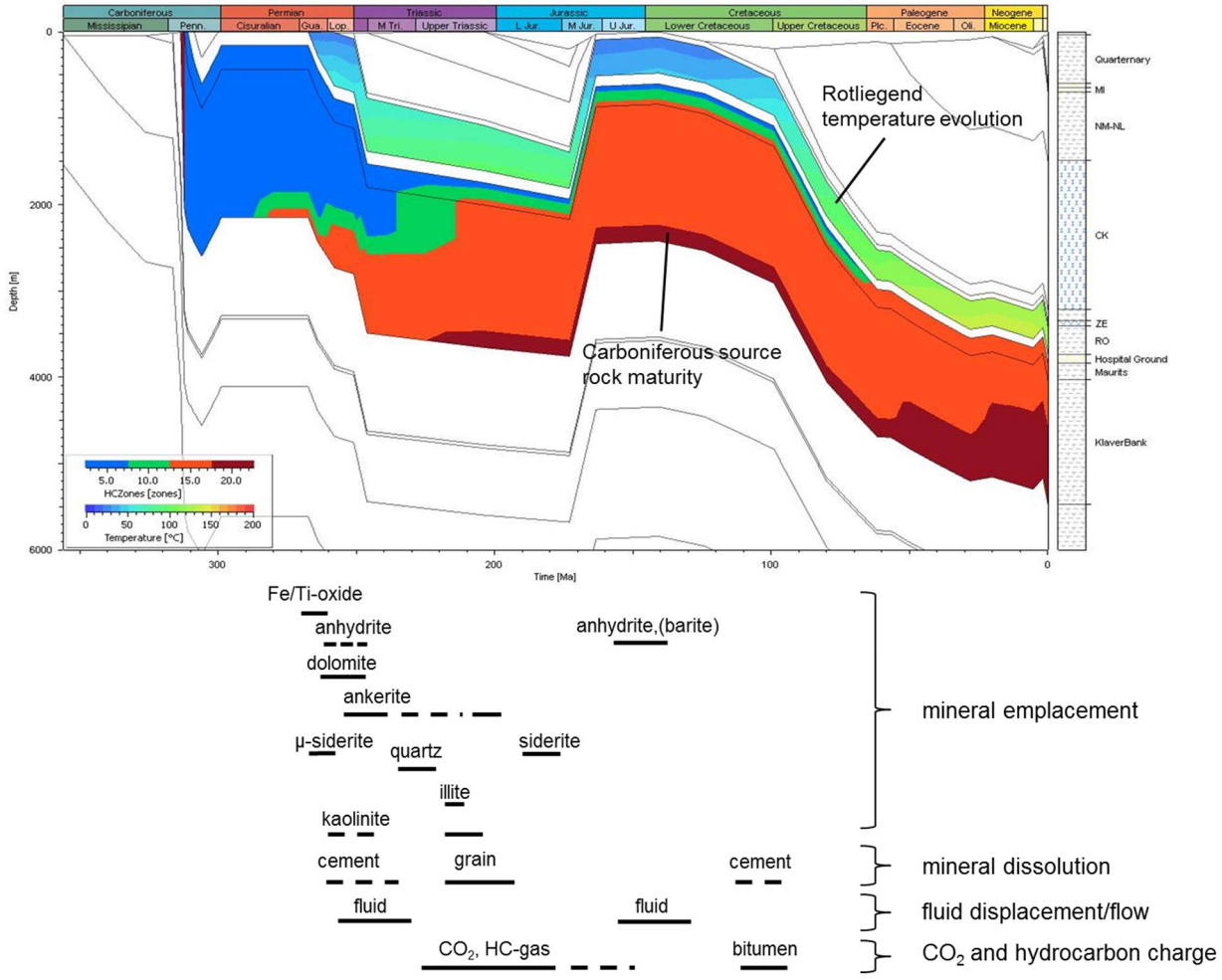

Figure 6-9 Burial and thermal history in focus area A, on example of well L06-06. The Rotliegend is highlighted by the colour coded thermal evolution with the proposed paragenetic sequences of events below. The Carboniferous source rock maturity is according to Burnham (1989) KIII, blue: immature, green: oil generation, red: gas generation; burgundy: over mature. Dashed lines depict uncertain timing of emplacement.

Thin section petrography and SEM imaging does not reveal the whole mineral history. Particularly the early cements can be replaced with late cements. Some of the earliest cements (dolomit/ankerite in area A and illite in area B) were paramount for today's reservoir quality. The deeper and longer burial in area B promoted further growth of pore-filling illite, whereas the inversion and uplift in area A may have re-distributed or introduced anhydrite into the Rotliegend sandstones. Interestingly, during the second deep burial (mesodiagenesis II) cementation basically comes to a halt. It is possible that late bitumen emplacement (Jurassic source?) lined the pores and prevented further cementation. Alternatively, the cessation of further fluid flow in the Paleogene and Neogene prevented further changes in the pore-fluid composition, which remained from that point onwards in equilibrium.

We distinguished particular processes that can lead to extensive cementation. To avoid locations of extensive cementation and target the optimal reservoir quality sweetspots the following actions are recommended, listed in the order of their

importance (note that this is a very general view and it requires a good understanding of the subsurface):

1. Avoid areas of long deep burial of particularly fluvial deposits
2. Target preferably aeolian depositional environments
3. Target sandstones with sufficient distance to the Silverpit deposits
4. Trace the illite zone followed by the kaolinite zone when in contact to Carboniferous (Westphallian B,C) strata.
5. Avoid areas close to major faults and magmatic sills/dykes
6. Target areas with high (present day) feldspar.
7. Avoid areas uplifted close to the surface, followed by burial.

The models we present are conceptual and may differ considerably locally. The following chapter aims to compare and test the concepts in other areas.

6.3 Regional intercomparison

6.3.1 Broad Fourteens Basin

The P, K and Q block wells in the Broad Fourteens Basin are characterised by high authigenic illite contents and high illite/kaolinite ratios. The area experienced prolonged deep burial (see Figure 3-5) that, similar to the focus area B, promoted the growth of illite. This area can be compared to the Terschelling Basin and the Lauwerzee Through, where illite, as well as illite/kaolinite ratios are generally high.

At the eastern edge of the Broad Fourteens Basin high anhydrite contents are evident in wells K12-S-03, K15-FA-08, K18-07-S1 and K18-08. The sediments are situated in a deep graben setting, which negates the possibility of Zechstein fluid ingression. A possible explanation for well K15-FA-08 is that the mineral analyses were performed on cuttings that included caved anhydrite cuttings from the Zechstein (Braunack, 2007). Nevertheless, the neighbouring wells are naturally rich in anhydrite. Zechstein is not in contact with the Slochteren Formation here but the samples are close to the Silverpit Formation (Figure 6-10), which can explain the high anhydrite content.

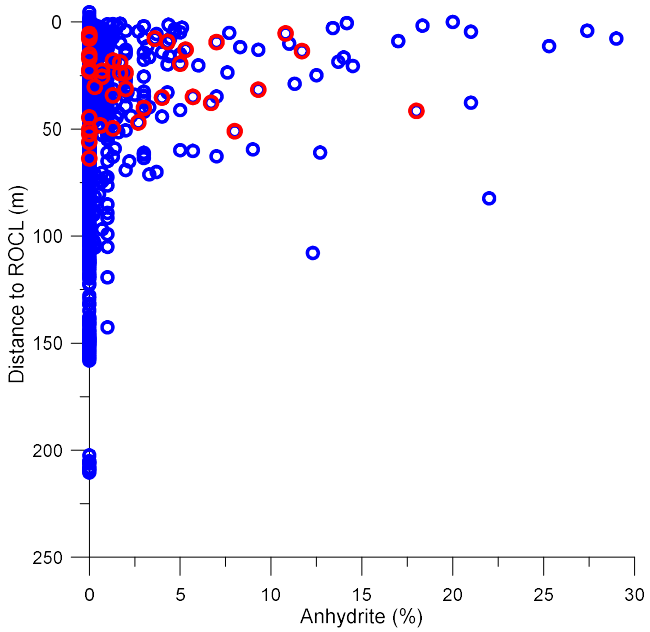

Figure 6-10 Anhydrite plotted against the proximity to the Silverpit formation for all wells with over or underlying Silverpit Formation in blue and wells K12-S-03, K15-FA-08, K18-07-S1 and K18-08 in red.

The wells also lie close to a major fault zone. A further possibility is that the influx of Zechstein fluids may have occurred here during a later basin inversion phase in the Late Cretaceous/Early Paleogene (Figure 6-11). During this period the faults were reactivated and may have been juxtapositioned against the Zechstein.

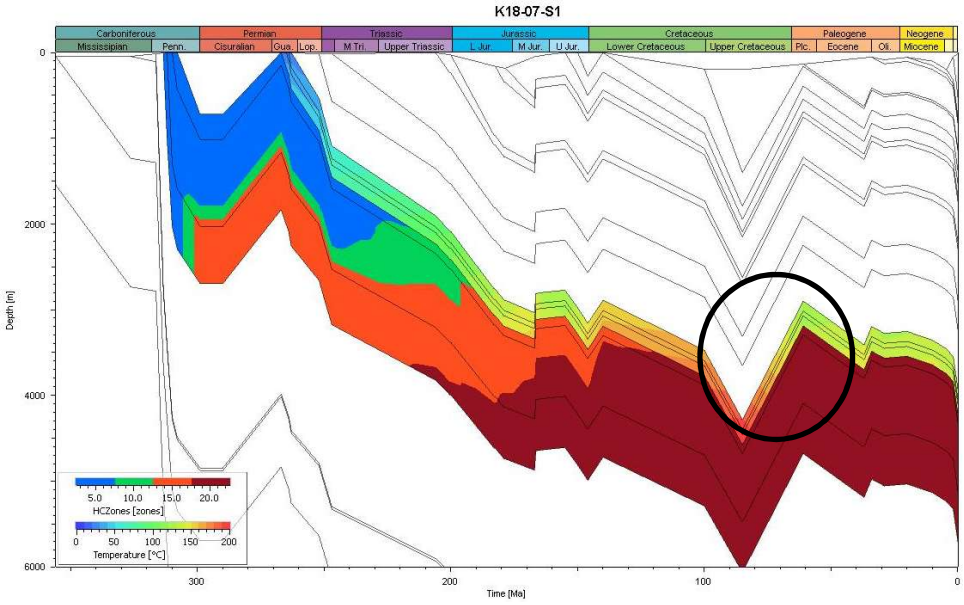

Figure 6-11 1D basin model for well K 18-07-S1. The circle points to the Late Cretaceous inversion.

6.3.2 *Friesland Platform, Lauwerzee Trough and Groningen Platform*

The diagenetic history of the Upper Rotliegend in the northeast of the onshore Netherlands has been studied in great detail in the past due to the presence of the large Groningen Field. Gaupp & Okkerman (2011) give a general overview of the different processes that have been described in the area, Waldmann & Gaupp (2016) and Waldmann (2011) describe several diagenetic sequences for different fields in detail. In addition several reports were published on the petrography of the Upper Rotliegend sediments from wells in the area (e.g., Winters, 1990, de Reuver, 1999, Clelland et al, 1987, Kosters et al., 1991).

In our database the data density for illite (and other cements) in this area is rather poor. For the majority of the wells illite was lumped together with indeterminate clay. Only kaolinite was listed separately. Apparently a great deal of petrographic data was acquired for this area by NAM and others (e.g. Gaupp & Okkerman 2011). Unfortunately this data was not made publically available. The discussion therefore focusses only on wells BLF-107, FRM-01-S3, WDN-01 and NOR-04 and -05.

The authigenic clay fraction in this region, as seen in the database and also described by Gaupp & Okkerman (2011), is highly variable and seemingly does not entirely agree with the assumption that the formation of authigenic illite occurs mainly in deep basins. Sediments from well FRM-01-S3 has low illite contents despite having experienced deep burial. A possible explanation may be the predominance of aeolian deposits in this well that did not contain sufficient clay for illitisation.

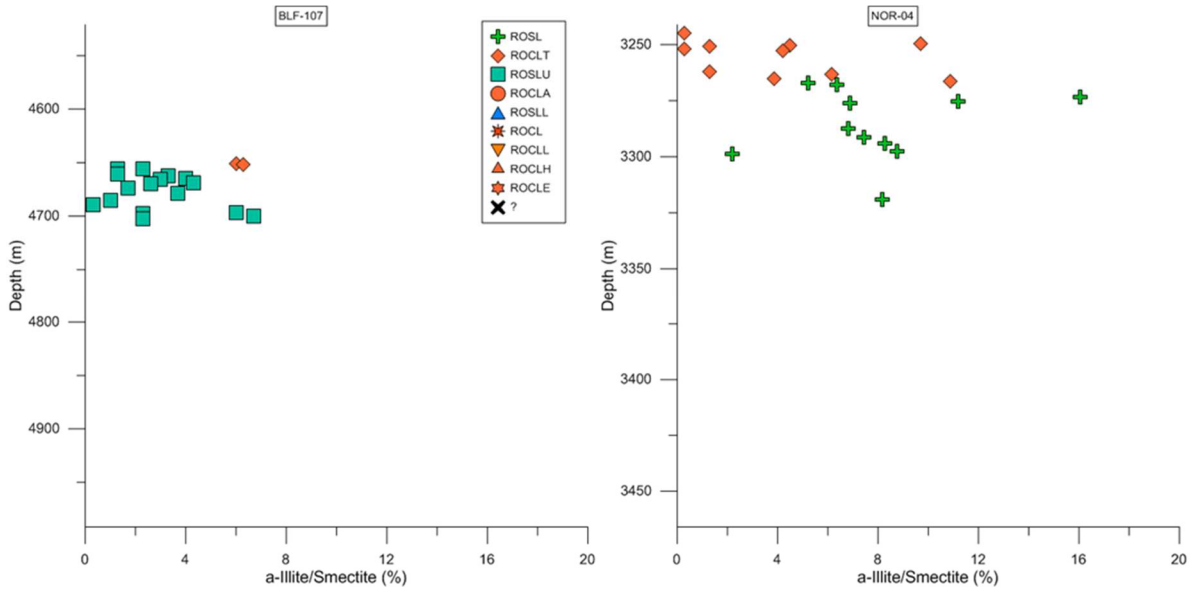

Figure 6-12 Authigenic illite content of wells BLF-107 and NOR-04 plotted against depth and formation.

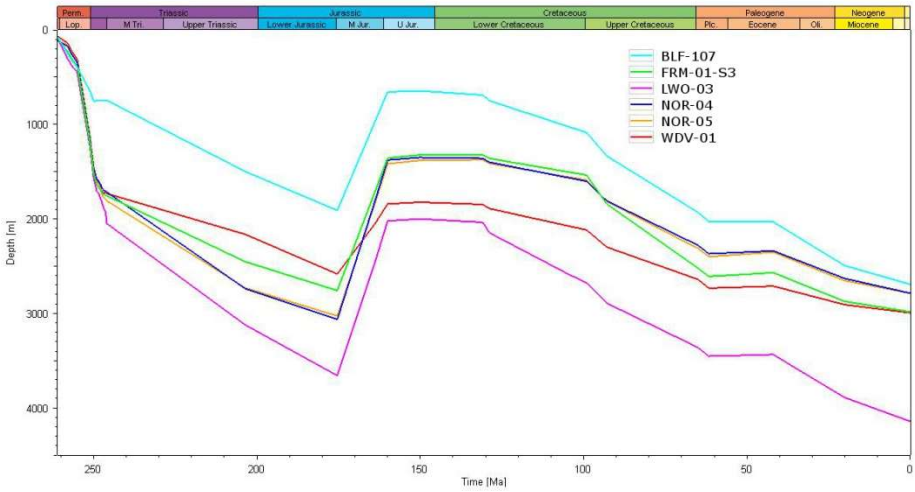

Figure 6-13 Burial depth history of the top of the Rotliegend of 6 wells from the Groningen Platform, Lauwerzee Trough and Friesland Platform.

Wells BLF-107 and NOR-04 and -05 contain significant amounts of illite in the authigenic clay fraction (Figure 6-12). The burial depth before the erosion during the Middle to Late Jurassic for most of the wells in the area is similar to the wells in the L6 blocks of the focus area (Figure 6-13). However, well BLF-107 only reached temperatures of above 100°C during the Neogene and was certainly not buried at high temperatures for a long time. Furthermore, well BLF-107 contains mainly aeolian sandstones (Figure 6-14).

In the case of well BLF-107, the burial history modelling of the area suggests that the Rotliegend reservoir reached temperatures and burial depths similar to the other wells during the Jurassic only in the Paleogene (Figure 6-15). This would suggest of late stage formation of illite.

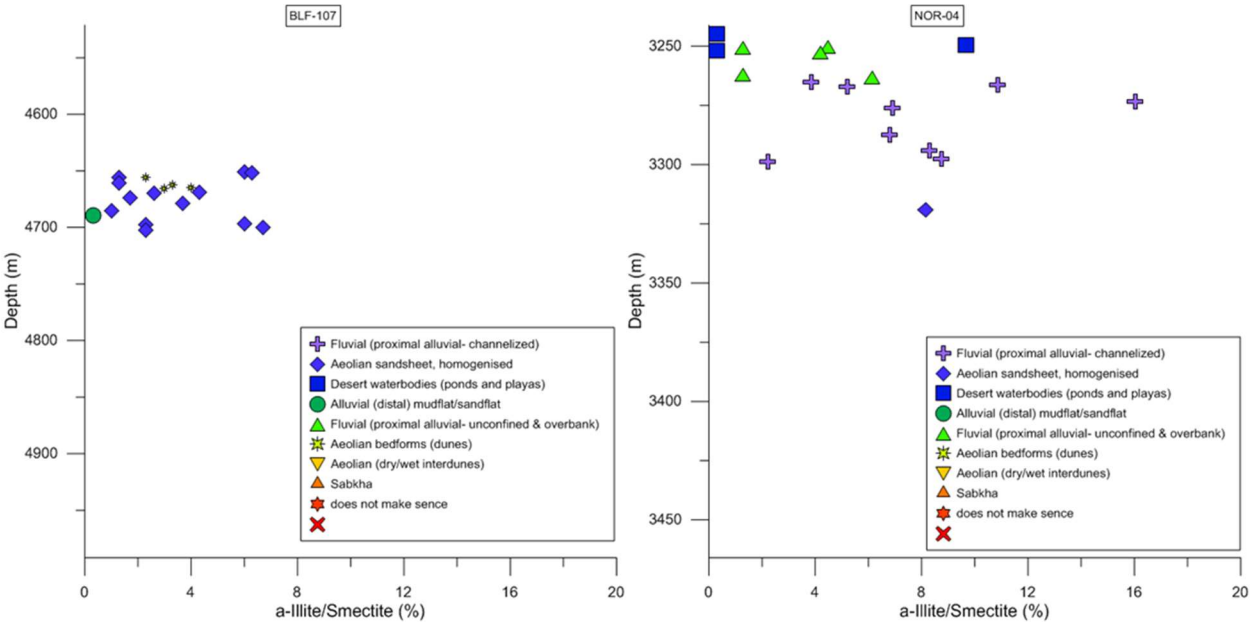

Figure 6-14 Authigenic illite content of wells BLF-107 and NOR-04 plotted against depth and depositional environment.

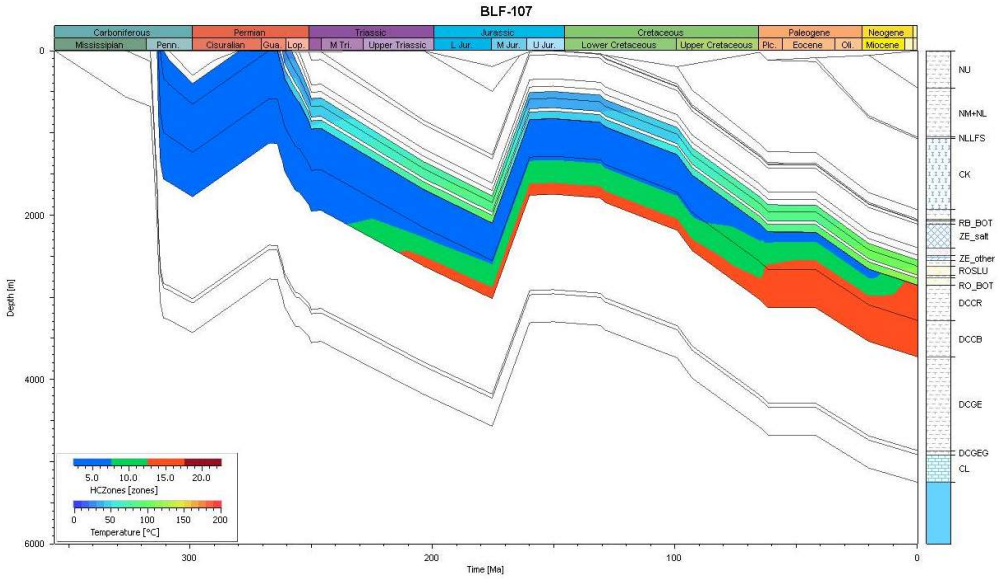

Figure 6-15 Burial history of well BLF-107 with the temperature evolution of the Rotliegend Group and the maturity evolution of the Carboniferous coal bearing layers (according to Burnham TIII, 1989). Blue – immature, green – oil mature, red – gas mature)

The formation age of illites can be measured using the K-Ar age dating method. A compilation of all available K-Ar ages of illites from the Northeast Netherlands is published by Gaupp & Okkerman (2011) and shows a wide spread of formation ages for illites (Figure 6-16). This is in agreement with above postulated theory, that the illite in the shallow areas of the region only formed very late during the latest burial in the Paleogene.

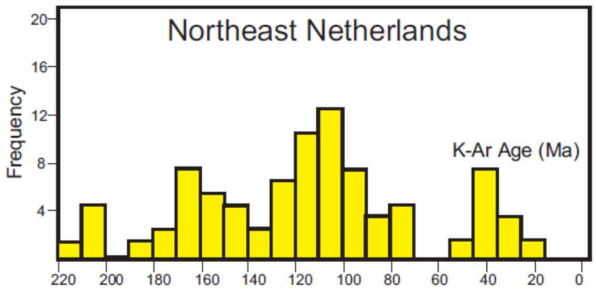

Figure 6-16 Rotliegend illite K-Ar model age distribution from the Northeast of the Netherlands onshore (from Gaupp & Okkerman, 2011).

A further possibility for not only the high illite but also kaolinite in well BLF-107 is its positioning near the Hantum fault zone that was noted to have channelled high temperature hydrothermal fluids.

Anhydrite contents are particularly high in the LWO, BLF and N07 wells. This area was never significantly uplifted (except around well BLF) to experience meteoric interaction later in the diagentic history. The samples with high anhydrite occur at the boarder to the Silverpit Formation, which may be a reason for the early anhydrite cement precipitation. Wells BLF and LWO contain mostly aeolian deposits. Nodular anhydrite was identified in well LWO-02 and LWO-03. Therefore it is also quite likely that anhydrite is of detrital, wind-blown origin (see Henares et al., 2014).

6.3.3 Central part of the Cleaverbank Platform (E18 and F16 blocks)

The illite concentrations in the wells in the E18 and F16 blocks are surprisingly high for their platform setting. According to basin modelling, this area was not buried to great depths before the erosion during the Middle to Late Jurassic and the general burial history is very similar to the K5 and K6 blocks of the focus area (Figure 6-17).

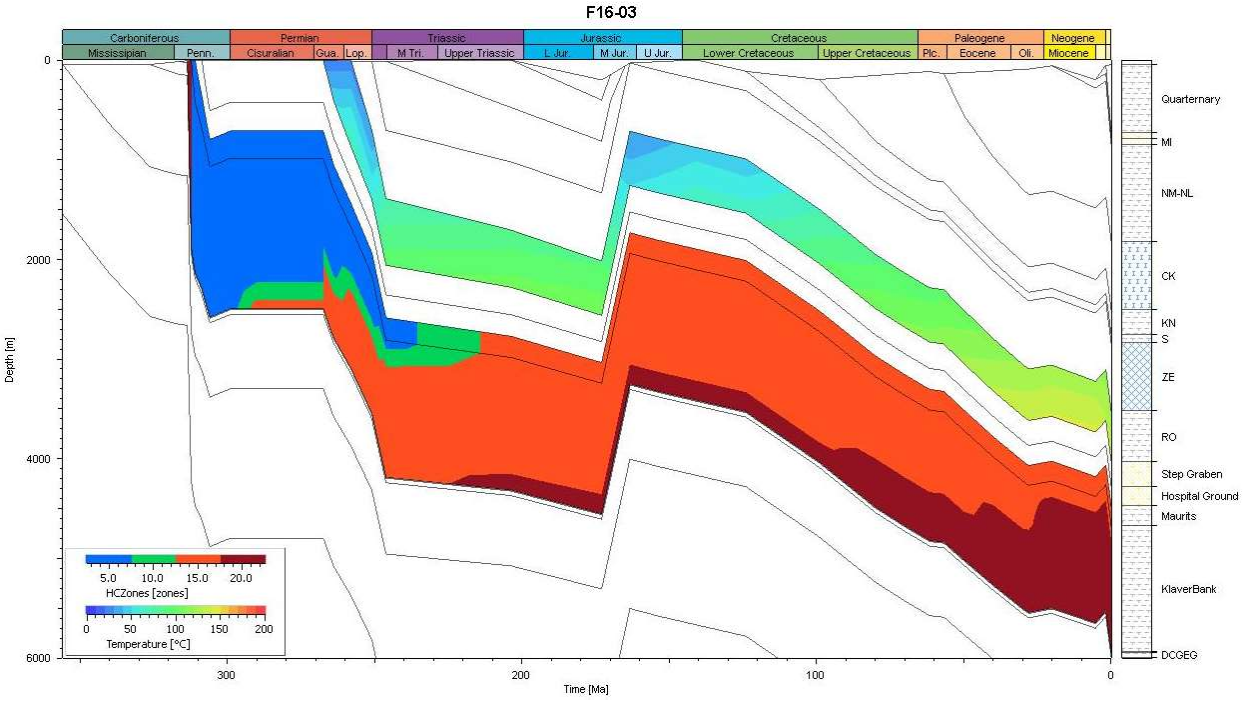

Figure 6-17 Burial history of well F16-03 with the temperature evolution of the Rotliegend Group and the maturity evolution of the Carboniferous coal bearing layers (according to Burnham TIII, 1989). Blue – immature, green – oil mature, red – gas mature, dark red – overmature)

The gas composition of this area shows very distinct compositions as well (Verweij et al. 2016 – confidential report). According to gas composition measurements the fields in this area show very high CO_2 contents that were interpreted to be of magmatic origin. Recent seismic mapping of the area (ter Borgh, personal comment) identified several magmatic sills and dykes, that are a continuation of a Cenozoic dyke swarm that was identified in the UK offshore area (Wall et al. 2010, Hernandez Casado & Underhill, 2013). The high authigenic illite content in these wells could therefore be related to the hot fluids that entered the reservoir at the time of magmatism. The majority of the authigenic illite is classified as replacive and grain rimming. Pore-filling illite is minor, which complies with the generally shallower burial.

7 Conclusion & Recommendations

7.1 Conclusions

High porosity and permeability is favoured in sandstones with high feldspar and low detrital clay and matrix content, provided they were not extensively cemented by carbonates or anhydrite. Statistically, aeolean deposits show better reservoir quality than fluvial and sabka/lacustrine deposits.

Low porosity and permeability in sandstones, on the other hand, is related to high detrital clay and clay matrix/laminae. In general, the lower the grain size, the lower the porosity and permeability. Clay laminae and other ductile grains are reservoir quality reducing, but mainly due to mechanical compaction. Mechanical compaction evidently has a major impact on the reservoir quality, however it was not studied in detail because the focus of the project was on cementation. Carbonate cement (mainly ankerite) is also detrimental to porosity and permeability, whereas high anhydrite contents reduce reservoir quality only locally. High authigenic illite significantly reduces permeability.

One, single diagenetic model cannot be applied for entire Dutch on- and offshore. There are distinct differences in the timing and type of cements locally because mineral authigenesis and reservoir quality have locally different principal drivers. However, general cementational trends can be observed that can be combined to develop predictive trends for cementation.

Dolomite cementation was observed to be higher in fluvial settings and authigenic illite tends to be most abundant in proximal alluvial (unconfined and overbank) environment. Anhydrite is most common in aeolian homogenized sheetsands. The Silverpit formation contains more sulphate (mainly anhydrite) than the Slochteren Formation. Anhydrite, ankerite and partly dolomite cement contents increase towards Silverpit Formation. Anhydrite increases also towards the Zechstein Group. Proximity to the coal-bearing Carboniferous has a growth-enhancing effect on authigenic kaolinite, ankerite, siderite, barite and quartz. Authigenic quartz also has a tendency to increase towards the Carboniferous.

The illite/kaolinite ratio does not increase with depth, as previously assumed. An important factor for high illite content is the duration of deep burial, which is found in deep basinal structural elements. This is likely due to kinetically controlled illite formation during prolonged deep burial. Kaolinite may be connected to the original feldspar content. The acidic fluids from the coal-bearing Carboniferous strata enhance the dissolution of feldspar and provide an optimal environment for kaolinite precipitation.

Statistical cluster analysis indicated that sediments with high feldspar contents have on average low kaolinite and authigenic quartz (particularly in NE Netherlands). The original feldspar (and rock fragment) content is particularly important for kaolinite formation and partly for quartz cementation. The dissolution of feldspar delivers significant amounts of Al^{3+} and Si for kaolinite and a quartz formation and is probably central to their formation in some areas.

Locally, where the Slochteren sandstones are in contact with either Silverpit or Zechstein strata, the Silverpit and Zechstein brines promoted the formation of anhydrite. The fluids from the Silverpit lake may have been expelled during the early diagenesis leading to preferentially more early anhydrite in the near playa lake deposits. A later telodiagentic interaction with meteoric fluids may have led to dissolution of sulphates in the overlying Silverpit deposits, that reprecipitated in the Slochteren Formation. A similar process can be assumed with Zechstein fluids. However, if Zechstein is not directly overlying the Slochteren sandstones either a fracture network or tectonic juxtapositioning with Zechstein is required.

A further local process for anhydrite formation that occurs near Sabkha in aeolian deposits is the deposition (and redistribution) of detrital, wind-blown gypsum and anhydrite grains. Barite formation was influenced mainly by Carboniferous fluids that may have come in contact with sulphate rich, possibly Silverpit, brine.

Silverpit fluids also contributed to the cementation of ankerite and dolomite cements. They would have contained high amounts of total dissolved solids, resulting in supersaturation and precipitation of dolomite upon burial. During the intermediate to late diagenesis preferential precipitation of ankerite followed by continuous solid solution. Ankerite (and siderite) formation was further influenced by migration Carboniferous fluids. Fe^{2+} contribution for ankerite and siderite would have sourced from the leaching of Fe-oxides by the reducing fluids. Increase of dolomite and ankerite cements with proximity to intercalated mudstones is possible but needs further investigation.

Locally, juxta positioning of other strata against the Slochteren lead to intense cementation. In this sense, anhydrite cementation would have been driven by fluid ingression during juxtapositioning of Zechstein deposits. Interaction of juxtapositioned Rotliegend and coal-bearing Carboniferous strata can lead to large amounts of kaolinite cement followed by illite cement. Other cements may also have been effected. Notably, fluid flow and cementation was depended on whether the faults represented conduits or barriers for fluid flow. A more thorough fault study is necessary to identify the relationships.

Regional effects on cementation are related to complex structural evolution (as proposed for the north-eastern Broad Fourteens Basin), differences in burial history and hydrocarbon emplacement (example of Groningen Platform and Lauwerszee Through) and magmatic intrusions, as seen in the E18 and F16 blocks.

Lastly, this study demonstrates that the compilation of multi-vintage and multi-source petrographic data can provide insight into cementational processes. Integrating these findings with burial history studies led to a better insight into diagenetic mechanisms, which when applied eventually may become predictive. However, more data (either existing or new) is required as well as better mineral dating. The conceptual models will only become predictive if they are incorporated into a well-researched and constructed geological subsurface model. This model will require a rigorous study of facies and environmental interpretation.

7.2 Recommendations

- The study could be greatly improved by more petrographic data, including new analyses on already existing but not yet petrographically analysed core material.
- To be able to reconstruct the paragenetic sequences a good cement dating procedure is required. Particularly of the carbonate and sulphate minerals can be dated well with isotope thermometry, including clumped isotopes. Fluid inclusion thermometry is helpful for a number of cements as well.
- Facies and sub-environment interpretation needs to be improved and extended, as it may provide more information than revealed in this study.
- Gas charge history may be a critical factor for cementation. There is a need for better understanding of CO_2 and hydrocarbon emplacement.
- A good geological model is required to trace fluid flow pathways. Particularly compartmentalisation is crucial to understand fluid flow. In this regard the fault study should be strengthened and broadened to other areas.
- Extend the database with more general description, for example colour of core samples.
- Connect cementational to compactional (mechanical) reservoir quality loss. Consider using Touchstone modelling.
- Further investigation into dolomite and ankerite cementation in relation to intercalated mudstone layers.

7.3 Acknowledgment

We like to thank our partners from EBN and Total E&P Nederland; Jan Lutgert, Paul Segers, José van Koppen and Veerle Palmaers, in this project for their constructive input during the project.
The project has been executed with subsidy of the Ministry of Economic Affairs, National regulations EA-subsidies, Top sector Energy performed by the “Rijksdienst voor Ondernemend Nederland”.

8 References

Abdul Fattah, R., Verweij, J.M., Witmans, N., ten Veen, J.H. (2012) Reconstruction of burial history, temperature, source rock maturity and hydrocarbon generation in the northwestern Dutch offshore. Netherlands Journal of Geosciences – Geologie en Mijnbouw, 91(4), 535-554.

Abdul Fattah, R., Verweij, J.M., Witmans, N. (2010) Reconstruction of burial history, temperature, source rock maturity and hydrocarbon generation for the NCP-2D area, Dutch Offshore. TNO report TNO-034-UT-2010-0223, 72 p.

Adelmann, D., 2004. Sedimentology, petrography and reservoir quality of cores 1 and 2 (Lower Slochteren Sandstone) in well L5-10 and Petrography of cuttings samples from the Carboniferous in well L5-10. Panterra Report G464.

Ajdukiewicz J.M. and Lander R.H. (2010). Sandstone reservoir quality prediction: The state of the art. AAPG Bulletin 94, no. 8, 1083-1091.

Bertier, P., Swennen, R., Laenen, B., Lagrou, D. and Dreesen, R., 2006, Experimental identificationof CO2-water-rock interactions caused by sequestration of CO2 in Westphalian and Buntsandstein sandstones of the Campine Basin (NE-Belgium). Journal of Geochemical Exploration, 89, pp. 10-14.

Bjørlykke, K., Ramm, M. and Saigal, G.C., 1989, Sandstone Diagenesis and Porosity Modification during Basin Evolution. Geologische Rundschau, 78, pp. 243-268.

Boles, J.R., 1982, Active Albitization of Plagioclase, Gulf-Coast Tertiary. American Journal of Science, 282, pp. 165-180.

Braunack, C. (2007) Petrographical investigation of 15 cuttings samples – Slochteren Formation well: K15-FA-108 (offshore – the netherlands). Panterra report g601.

Brouwer, G.C. (1972): “The Rotliegend in the Netherlands”, in Falke, H. : Rotliegend, Essays on European Lower Permian, p. 34-42.

Buggenum, J.M., den Hartog Jager, D.G. (2007) Silesian. In: Geology of the Netherlands. S. Wong, D.A.J. Batjes and J. de Jager (Eds.) (Royal Netherlands Academy of Arts and Sciences), 43-62.

Burnham [1989]. A simple kinetic model of petroleum formation and cracking. Lawrence Livermoore National Laboratory Report UCID 21665, pp. 11.

Clelland, W.D., Kantorowicz, J.D., Nicolls, C.A., de Weerd, J., de Gier, F.A.M. (1987) Pilot study into the diagenesis of the northern Groningen wells: Stedum-1, Uithuizermeeden-1 and Delfzijl-1, onshore Netherlands. NAM report RKTR.87.282.

Curtis, C.D., 1967, Diagenetic Iron Minerals in Some British Carboniferous Sediments. Geochimica Et Cosmochimica Acta, 31, pp. 2109-2123.

Curtis, C.D., 1983, Link between Aluminum Mobility and Destruction of Secondary Porosity. American Association of Petroleum Geologists Bulletin, 67, pp. 380-384.

Darby, D., Wilkinson, M., Fallick, A.E. and Haszeldine, R.S., 1997, Illite dates record deep fluid movements in petroleum basins. Petroleum Geoscience 3, 133-140.

de Jager, J. & Geluk, M.C. (2007) Petroleum Geology, 241–264. In: Geology of the Netherlands. S. Wong, D.A.J. Batjes and J. de Jager (Eds.) (Royal Netherlands Academy of Arts and Sciences).

de Reuver, F. (1999) Sedimentology, reservoir quality and petrography of core 1 from the Upper Slochteren Sandstone in well Blija Ferweradeel (BLF)-107. Panterra report No. G275-2

Dixon, S.A., Summers, D.M. and Surdam, R.C., 1989, Diagenesis and Preservation of Porosity in Norphlet Formation (Upper Jurassic), Southern Alabama. American Association of Petroleum Geologists Bulletin, 73, pp. 707-728.

Doornebal H., Stevenson, 2010. Petroleum Geological Atlas of the Southern Permian Basin. EAGE Publications.

Drong, H.J., 1979, Diagenetische Veränderungen in den Rotliegend Sandsteinen im NWDeutschen Becken. Geologische Rundschau, 68, pp. 1172-1183.

Ehrenberg, S.N., 1993. Preservation and anomalously high porosity in deeply buried sandstones by grain-rimming chlorite: examples from the Norwegian continental shelf. American Association of Petroleum Geologists Bulletin 77, 1260-1286.

Gast, R.E., Dusar, M., Breitkreuz, C., et al., 2010, Rotliegend. in Doornenbal, J.C. and Stevenson, A.G., eds., Petroleum Geological Atlas of the Southern Permian Basin: Houten, EAGE, p.101-121.

Gaupp and Okkerman 2011 Reservoir quality of Rotliegend sandstones in the northern Netherlands - A review. In The Permian Rotliegend of the Netherlands, J. Grötsch and R. Gaupp (Eds.), pp. 193-228 (Tulsa, Oklahoma: SEPM Special Publication).

Gaupp, R., Moeller, P., Luders, V., di Promio, R., Littke, R. (2008) Fluids in sedimentary basins: an overview. In: Littke,R., Bayer, U., Gajewski, D., Nelskamp, S. (eds) Dynamics of Complex Intracontinental Basins - The Central European Basin System, 345-359, Springer-Verlag, Berlin-Heidelberg.

Gaupp, R., 1996, Diagenesis types and their application in diagenesis mapping. Zentralblatt für Geologie und Paläontologie, 1994, pp. 1183-1199.

Gaupp, R., Matter, A., Platt, J., Ramseyer, K. and Walzebuck, J., 1993, Diagenesis and Fluid Evolution of Deeply Buried Permian (Rotliegende) Gas-Reservoirs, Northwest Germany. American Association of Petroleum Geologists Bulletin, 77, pp. 1111-1128.

Geluk, M., 2005, Stratigraphy and tectonics of Permo-Triassic basins in the Netherlands and surrounding areas. Dissertation, Utrecht, Netherlands.

Geluk, M., Dusar, M. and de Vos, W., 2007, Pre-Silesian. In Geology of the Nerherlands, S. Wong, D.A.J. Batjes and J. de Jager (Eds.) (Royal Netherlands Academy of Arts and Sciences).

Girard, JP., Kluska, JM., Walgenwitz, F., 2008. Block Diagenesis of the Lower Slochteren Sandstones and impact on reservoir properties. TOTAL internal report No. DGEP/GSR/TG/ISS/CLAS R08-095.

Glennie, K.W., 1983, Early Permian (Rotliegendes) Paleowinds of the North-Sea. Sedimentary Geology, 34, pp. 245-265.

Glennie, K.W., 1997, Recent advances in understanding the southern North Sea Basin: a summary: Geological Society, London, Special Publications, v. 123, no. 1, p. 17-29.

Glennie, K.W., 1998, Lower Permian – Rotliegend. In Petroleum Geology of the North Sea, K.W. Glennie (Ed.), pp. 137-174 (Oxford: Blackwell Science).

Glennie, K.W., Mudd, G.C. and Nagtegaal, P.J.C., 1978, Depositional environment and diagenesis of Permian Rotliegend sandstones in Leman bank and Sole Pit areas of the UK southern North Sea. Journal of the Geological Society of London, 135, pp. 25-34.

Heim, S., Lutz, R., Nelskamp, S., Hanneke Verweij, H., Kaufmann, D., Lutz Reinhardt, L., 2013. Geological Evolution of the North Sea: Cross-border Basin Modeling Study on the Schillground High. Energy Procedia 40, 222–231.

Henares S., Bloemsma M.R., Donselaar M.E., Mijnlieff H.F., Redjosentono A.E. Veldkamp H.G., Weltje, G.J. (2014). The role of detrital anhydrite in diagenesis of aeolian sandstones (Upper Rotliegend, The Netherlands): Implications for reservoir-quality prediction. Sedimentary Geology 314, 60–74.

Hernandez Casado, J., Underhill, J.R. 2013 Consequences of Intrusions for Sub-salt, Sub-basalt Exploration and Development. Abstract for 75th EAGE Conference & Exhibition, London, UK, 10-13 June.

Hiller, S. (2003) Quantitative analysis of clay and other minerals in sandstones by X-ray powder diffraction (XRPD). Int. Ass. Sedimentol. Spec. Publ. 34, 213-251.

Kombrink, H., Doornenbal, J.C., Duin, E.J.T., den Dulk, M., van Gessel, S.F., ten Veen, J.H., Witmans, N. (2012) New insights into the geological structure of the Netherlands; results of a detailed mapping project. Netherlands Journal of Geosciences 91 (4), 419-446.

Kosters, M., Schöbel, M., Winters, C.G. (1991) Sedimentology and petrography of core from well NORG-04. Core Laboratories report NRG 90115.

Lee, M., Aronson, J.L. and Savin, S.M., 1989, Timing and conditions of Permian Rotliegende Sandstone Diagenesis, Southern North Sea: K/Ar and Oxygen Isotopic Data. American Association of Petroleum Geology Bulletin, 73, pp. 195-213.

Lynch, F.L., Mack, L.E. and Land, L.S., 1997, Burial diagenesis of illite/smectite in shales and the origins of authigenic quartz and secondary porosity in sandstones. Geochimica Et Cosmochimica Acta 61, 1995-2006.

McKinley, J.M., Worden, R.H. and Ruffell, A.H., 2003, Smectite in sandstones: a review of the controls on occurence and behaviour during diagenesis. In Clay Mineral Cements in Sandstones, R.H. Worden and S. Morad (Eds.), pp. 109-128 (Special Publication of the International Association of Sedimentologists).

Mijnlieff H.F. et al. (1999). The Petrographic Description System of clastic sedimentary rocks: a proposal for standardized petrographic data storage. In: Mededelingen Nederlands Instituut voor Toegepaste Geowetenschappen TNO Nr. 62.

Mijnlieff H.F. et al. (2014) The Permian Rotliegend Reservoir Architecture of the Dutch Koekoekspolder Geothermal Doublet. EAGE conference paper, Amsterdam.Miocic (2011)

Morad, S. (1998). Carbonate cementation in sandstones: distribution patterns and geochemical evolution. Spec. Publs. Int. Ass. Sediment. 26, 1-26.

Nelskamp, S., Verweij, J.M, (2012) The role of salt tectonics and overburden in the generation of overpressure in the Dutch North Sea area. Netherlands Journal of Geosciences – Geologie en Mijnbouw 91 (4), 517-534.

Nguyen et al. 2013. The role of fluid pressure and diagenetic cements for porosity preservation in Triassic fluvial reservoirs of the Central Graben, North Sea. AAPG Bulletin, v. 97, no. 8, 1273–1302.

van Ojik K., Böhm, A.R., Cremer, H., Geluk, M.C., De Jong, M.G.G., Mijnlieff, H.F. Djin Nio, S. (2011) The Rationale for an Integrated Stratigraphic Framework of the Upper Rotliegend II Depositional System in the Netherlands. In: The Permian Rotliegend of the Netherlands, J. Grötsch and R. Gaupp (Eds.), pp. 193-228 (Tulsa, Oklahoma: SEPM Special Publication).

Pierau, P., 2010. Sedimentology, Petrography and Reservoir Properties of Core 1 and 2 from Well L6-7, Dutch Offshore. Panterra Report No. G762

Platt, J.D., 1994, Geochemical Evolution of Pore Waters in the Rotliegend (Early Permian) of Northern Germany. Marine and Petroleum Geology, 11, pp. 66-78.

Purvis, K., 1992. Lower Permian Rotliegend sandstones, southern North Sea: a case study of sandstone diagenesis in evaporite-associated sequences. Sedimentary Geology, 77, 155-171.

Rieke, H., 2003. Sedimentology, Petrography and Reservoir Quality of Cores 1 To 6 (Lower Slochteren Sandstone and Carboniferous) in Well L5-9. Panterra Report No. G425.

Saigal, G.C. and Bjørlykke, K., 1987, Carbonate cements in clastic reservoir rocks from offshore Norway - relationship between isotopic composition, textural development and burial depth. In Diagenesis of sedimentary sequences, J.D. Marshall (Ed.), pp. 313-324 (London: Geological Society of London Special Publication).

Stahl, S. (2011). Local and regional distribution of the primary and diagenetic mineralogical components within the Rotliegend, Diploma Thesis, University of Cologne.

SULLIVAN M.D., HASZELD1NE R.S., BOYCE A.J., ROGERS G., FALLIC, A.E. (1994) Late anhydrite cements mark basin inversion: isotopic and formation water evidence, Rotliegend Sandstone, North Sea. Mar. Petrol. Geol. 11/1, 46-54.

Taylor T. R., Kittridge, M.G., Winefield, P., Bryndzia, L.T., Bonnell L.M. (2015). Reservoir Quality and Rock Properties Modeling Results – Jurassic and Triassic Sandstones: Greater Shearwater (HPHT) Area, UK Central North Sea. Search and Discovery Article #20320.

Taylor, T. R., M. R. Giles, L. A. Hathon, T. N. Diggs, N. R. Braunsdorf,G.V. Birbiglia,M.G.Kittridge,C. I.Macaulay, and I. S. Espejo, 2010, Sandstone diagenesis and reservoir quality prediction:Models,myths, and reality. AAPG Bulletin, v. 94, p. 1093–1132

Van Bergen, M.J. Sissingh, W. (2007) Magmatism in the Netherlands: expression of the north-west European rifting history. In: Geology of the Netherlands. S. Wong,

D.A.J. Batjes and J. de Jager (Eds.) (Royal Netherlands Academy of Arts and Sciences), 197-221.

Van den Belt, F.J.G., and Van Hulten, F.F.N., 2011, Sedimentary architecture and paleogeography of Lower Slochteren aeolian cycles from the Rotliegend desert-lake margin (Permian), the Markham area, Southern North Sea. in Grotsch, J. and Gaupp, R., eds., The Permian Rotliegend of the Netherlands 98, p.161-176.

Van Kempen, B., van der Molen, J., Mijnlieff H. (2016). Reservoir properties revisited: results of datamining in the Dutch Oil and Gas Portal www.nlog.nl.

Verdier, J.P., 1996, The Rotliegend sedimentation history of the southern North Sea and adjacent countries. in Rondeel, H.E., Batjes, D.A.J. and Nieuwenhuijs, W.H., eds., Geology of Gas and Oil under the Netherlands: Dordrecht, Kluwer Academic Publishers, p.45-56

Verweij, J.M., Souto Carneiro Echternach, M., Witmans, N. (2009) Terschelling Basin and southern Dutch Central Graben – Burial history, temperature, source rock maturity and hydrocarbon generation – Area 2A. TNO report TNO-0.34-UT-2009-02065, 46 p.

Verweij, J.M., Simmelink, H.J., Underschultz, J., Witmans, N. (2012) Pressure and fluid dynamic characterisation of the Dutch subsurface. Netherlands Journal of Geosciences – Geologie en Mijnbouw 91 (4), 465-490.

Verweij, J.M., Nelskamp, S., Hegen, D. (2016) Geochemical composition and origin of natural gas in onshore and offshore Netherlands – Confidential TNO report

Verweij, J.M., Souto Carneiro Echternach, M., Witmans, N. (2010) Central Offshore Platform – Area NCP2E; burial history, temperature, source rock maturity and hydrocarbon generation. TNO report TNO-034-UT-2010-01298/A, 70 p.

Waldmann S., & Gaupp, R. (2016) Grain-rimming kaolinite in Permian Rotliegend reservoir rocks. Sedimentary Geology,

Waldmann, S. (2011) Geological and mineralogical investigation of Rotliegend gas reservoirs in the Netherlands and their potential for CO2 storage. PhD Thesis, University Jena.

Walker, T.R., 1967, Formation of Red Beds in Modern and Ancient Deserts. Geological Society of America Bulletin, 78, pp. 353-368.

Wall, M., Cartwright, J., Davies, R., McGrandle, A. 2010 3D seismic imaging of a Tertiary Dyke Swarm in the Southern North Sea, UK. Basin Research 22, 181-194

Wilkinson, M., Haszeldine, R.S. and Milliken, K.L., 2003, Cross-formational flux of aluminium and potassium in Gulf Coast (USA) sediments. In Clay Mineral Cements in Sandstones, R.H. Worden and S. Morad (Eds.), Special Publication of the International Association of Sedimentologists, pp. 147-160.

Wilkinson, M. and Haszeldine, R.S., 2002, Fibrous illite in oilfield sandstones - a nucleation kinetic theory of growth. Terra Nova 14, 56-60.

Wilson, M.D., 1992, Inherited grain-rimming clays in sandstones from eolian and shelf environments: Their origin and control on reservoir properties. In Origin, diagenesis and petrophysics of clay minerals in sandstones, D.W. Houseknecht and E.D. Pittman (Eds.), pp. 209-225 (Tulsa: SEPM - Special Publication).

Winters, C.G. (1990) Petrological review of lithofacies of the Rotliegend Slochteren Sandstone member from well Bierum-13B. Core Laboratories report NRG 89031A.

Worden R.H. & Burley, S.D., (2003). Sandstone diagenesis: the evolution of sand to stone. In: Sandstone diagenesis: Recent and Ancient, (Eds) Burley & Worden, International Association of Sedimentologists, 4-44.

Worden, R.H. and Morad, S., 2003, Clay minerals in sandstones: controls on formation, distribution and evolution. In Clay Mineral Cements in Sandstones, R.H. Worden and S. Morad (Eds.), pp. 3-42 (Special Publication of the International Association of Sedimentologists).

Ziegler, K., 2006, Clay minerals of the Permian Rotliegend Group in the North Sea and adjacent areas. Clay Minerals, 41, pp. 355-393.

9 Signature

Utrecht, April the 25th 2017 TNO

Philippe Steeghs
Head of department

Tanya Goldberg
Authors